TECHNO-ECONOMIC ASSESSMENT FOR THE ROGUN HYDROELECTRIC CONSTRUCTION PROJECT

PHASE II: PROJECT DEFINITION OPTIONS

Volume 2: Basic Data

Chapter 4: Seismicity

August 2014

Report No. P.002378. RP 33 rev G

Revision	Date	Subject of revision	Drafted	Checked	Approved
G	19/08/2014	Final – August 2014	BRGM	LBO	LBO
F	31/03/2014	Final	BRGM	NSA	NSA
E	20/12/2013	4th set of comments addressed	BRGM	TWI	NSA
D	30/09/2013	3rd set of comments addressed	BRGM	TWI	NSA
C	10/09/2013	2nd set of comments addressed	BRGM	TWI	NSA
B	10/07/2013	1st set of comments addressed	BRGM	TWI	NSA
0	11/01/2013	First Emission	BRGM	TWI	NSA

CONTENTS

1 Introduction 3

2 Global Tectonic Framework 4

3 Regional Geologic Context 5

4 Geological structure in the dam surroundings 7

5 Geological structure at the dam site 10

5.1 Crustal deep faults: Guissar and Vakhsh 14

5.2 Upper crustal levels 15

6 Seismicity 17

6.1 Regional seismicity 17

6.2 Connection of major historical earthquakes with major faults in the surroundings of the dam site 19

6.2.1 Significant seismicity associated with the Guissar Fault 21

6.2.2 Significant seismicity associated with the Vakhsh fault 26

6.2.3 Significant seismicity associated with the Tajkikistan fold-and-thrust belt (in particular Ionaksh and Gulizindan faults) 28

6.2.4 Tavil Dara earthquake in 1937 28

7 Assumptions for DSHA 31

8 Seismic hazard Assessment 33

8.1 Introduction 33

8.2 Estimate of the Maximum Credible Earthquake (MCE) 33

8.3 Response spectrum at the dam site 36

8.4 Co-seismic displacements potentially affecting the dam foundation 38

8.4.1 For the Guissar fault system: 38

8.4.2 For the Vakhsh thrust system: 38

8.4.3 For the Ionakhsh ramps: 38

8.4.4 For the Gulizindan ramp: 39

8.4.5 Dam foundation between Ionakhsh and Gulizindan ramps 39

9 Reservoir Triggered Seismicity 40

9.1 Potential induced seismicity linked to the dam 40

9.2 Previous examples of reservoir-triggered/induced seismicity 40

10 Proposed Seismic Monitoring 43

11 Recommendations for PSHA 44

12 References 45

12.1 Reports 45

12.1 Articles 45

1 INTRODUCTION

The present study presents an independent Deterministic Seismic Hazard Assessment (DSHA) for the Rogun Hydro Power Project (HPP), with the aim of defining preliminary design parameters for the different dam alternatives that could be developed.

It should be noted that as per the Scope of Services, at this phase of the study, the purpose of this report is **not to precisely define the seismic hazard for the site but to derive representative parameters against which safety of each dam alternative should be ensured**. The design parameters presented in this study are, therefore, used as input parameters in the design of the different alternatives in the Report on Embankment Dam Stability.

The present assessment also provides recommendations to restore the existing seismic network in the project area and ensure proper monitoring of seismicity near the site before, during and after construction.

The report ends with recommendations to be included in the next phase of the study, namely a comprehensive seismic hazard assessment dedicated to the selected dam alternative. This study shall be in the form of a state-of-the-art Probabilistic Seismic Hazard Assessment (PSHA), for which Terms of Reference have been laid down by the TEAS[1] Consultant for further reference.

The present report is organized thus:

- the seismotectonics assessment and the derived assumptions on active deformation characteristics at all scales from plate tectonics to the dam abutments of the Rogun site;
- the review of the significant seismicity associated with the faults contributing most to the seismic hazard at the site;
- the definition of the Maximum Credible Earthquake (MCE) based on a DSHA;
- the assessment of co-seismic displacements along identified critical capable faults;
- a general synthesis of seismicity associated with large reservoirs and general recommendations for seismic monitoring; and, finally,
- some recommendations on PSHA that will need to be conducted to define the design criteria.

[1] *TEAS = Techno-Economic Assessment Studies*

2 GLOBAL TECTONIC FRAMEWORK

The Rogun hydroelectric scheme project is located within the region of the India-Asia collision and more accurately north of the western syntax of the Himalayan range (Tajikistan) in an exceptionally complex tectonic area. This collision results in spectacular tectonics giving rise to the planet's highest mountain ranges, intense seismic activity, and faults that can extend more than a thousand kilometres (e.g., Molnar and Tapponnier, 1975; Burtman and Molnar, 1993; Lukk et al., 1995).

The current rapid convergence between India and Eurasia at an average rate of 5 cm per year is made possible by broadly distributed deformation deep inside the Asian continent (Figure 1). The most spectacular effect of the collision of the Indian and Asian continents is undoubtedly the enormous mass of high ground standing over the low Indus-Ganges plain. This high ground includes not only the high Himalaya range but also, further north, Tibet, a zone some 1000 km wide at an average altitude close to 5,000 m. In fact, as a result of the cumulative post-collisional northward drift, the Himalayan-Tibet system must have accommodated over 2000 km of shortening (Figure 1) through a combination of: (i) subduction of continental India under Asia, (ii) thickening of the leading edge of India by thrusting, (iii) homogeneous thickening of Tibet and regions to the north, (iv) successive lateral eastward extrusions of Sundaland (from 50 to 17 Million years B.P.) then Tibet (from probably 5 Million years B.P. to present) continental blocks along the large conjugate strike-slip faults in the lithosphere, and (v) lateral westward extrusion towards the Makran subduction zone of the Afghanistan blocks along the Chaman fault system (Figures 1 and 2)

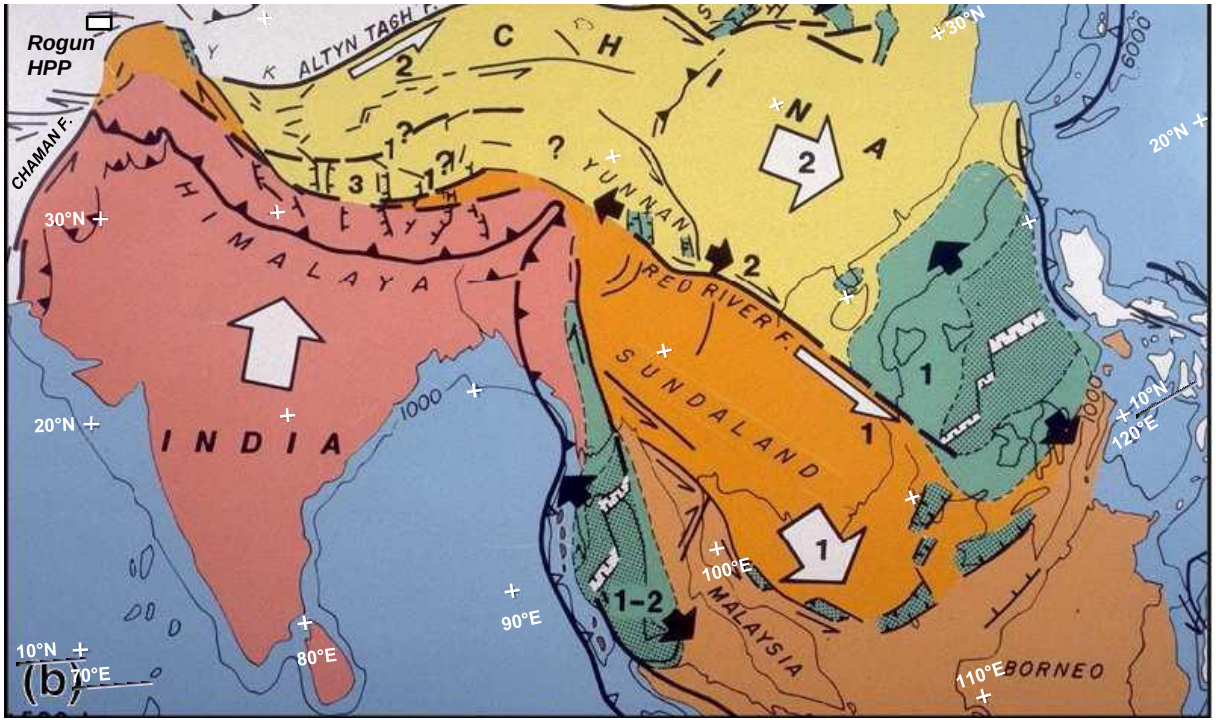

Figure 1 – India-Asia collision and induced deformation within Eurasia (from Tapponnier et al., 1982). White square shows the Rogun dam site.

3 REGIONAL GEOLOGIC CONTEXT

The Rogun dam site and reservoir are located in the upper Vaksh valley and its tributaries of the Obikhingo and Surkhob rivers. It is located within the Tajik Depression, more precisely within Vakhsh Range (Figures 2 and 3), which is a portion of the active deformation zone resulting from the Cenozoic collision between the Indian and Eurasian plates (Figure 2). Crustal shortening between the Pamir and Tien Shan is an important consequence of this India-Eurasia convergence (Burtman and Molnar, 1993).

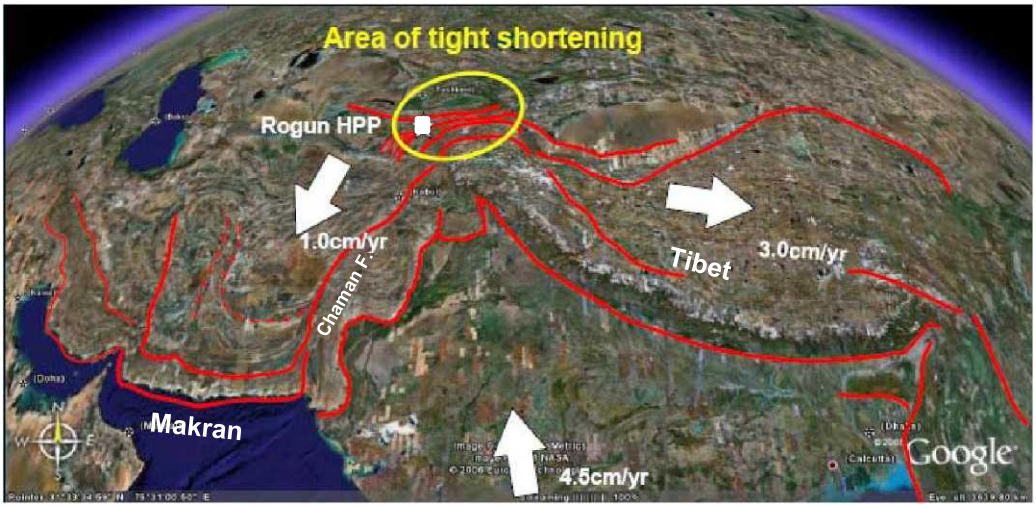

Figure 2 - India-Asia collision and induced deformation within Eurasia. Note that the Rogun HPP is located within the western syntax of the Himalaya, which is characterized by intensive shortening. White square shows the Rogun dam site.

This region is dominated by the interaction of three major tectonic units, namely the Tien Shan mountain range in the north and northwest, the Tajik Depression in the centre and the Pamir mountain ranges in the southeast (Figure 3). This area is thus composed of a complex mosaic of geologic units (Kravchenko, 1979; Zonenshain et al., 1990), which includes a Precambrian basement massif (the south-western Pamir), a reactivated Paleozoic orogen (the Tien Shan range), a deeply subsided Mesozoic-Cenozoic sedimentary basin (the Tajik Depression), and a complex island arc/active continental margin of Paleozoic to earliest Cenozoic age (the central and northern Pamir).

These mountain blocks are bounded by complex systems of active faults, including the North Pamir and Darvaz-Karakul faults (bounding the Pamirs to the north and west), the Guissar fault system (bounding the Tien Shan to the south), and the Talas-Fergana fault (separating the western and eastern Tien Shan).

Recent northward convergence between the Pamir and the Tien Shan ranges is documented by paleomagnetic observations (Bazhenov and Burtman, 1982), by compressional focal mechanisms (Molnar et al., 1973; Shirokova, 1974, 1979; Ni, 1978; Nelson et al., 1987; Lukk et al., 1980; Lukk and Yunga, 1988), and by geodetic observations near Garm (Pevnev et al., 1975; Lukk et al., 1980; Guseva et al., 1983). The convergence between the Pamir and Tien Shan has also resulted in compressive fold-and-thrust deformation of the Tadjik Depression, whose style ranges from open folding in the western Tadjik Depression to tight folds and northward-verging thrusts approaching the Vakhsh and the Peter First Ranges (Leith and Alvarez, 1985; Lukk and Shevchenko, 1986).

The Tajik Depression unit consists of Mesozoic-Tertiary continental and marine sedimentary cover overlying the Paleozoic basement. The thrust-and-fold system appears to have started in the Early to Mid-Miocene since strata of this age truncate some of the early folding and thrusting (Makhamov et al., 1985). The fold- and thrust belt appears to be controlled by décollement above Jurassic salt. The anticlines and synclines tend to be broader and more separated to the south and west and change northward and eastwards into more compressed faulted anticlines and synclines. They are bounded by, and pass into, dominantly

eastward-dipping thrusts, which root into a décollement surface in the Upper Jurassic salt deposits (Bekker, 1996). According to balanced cross-sections proposed by Burtmann (2000), this décollement (Jurassic salt) lies at a depth of about 10 km beneath the Tajik depression. Westward displacements of up to 20 km can be demonstrated in some fold-thrust sections. The arcuate folds are limited by major outcropping strike-slip faults along their northern contact with the Tien Shan and also by buried strike-slip faults to the south. Geomorphic observations in this area provide evidence for significant Quaternary activity along these faults (Skobolev and Florensky, 1974; Trifonov, 1978; Leonov and Nikonov, 1988).

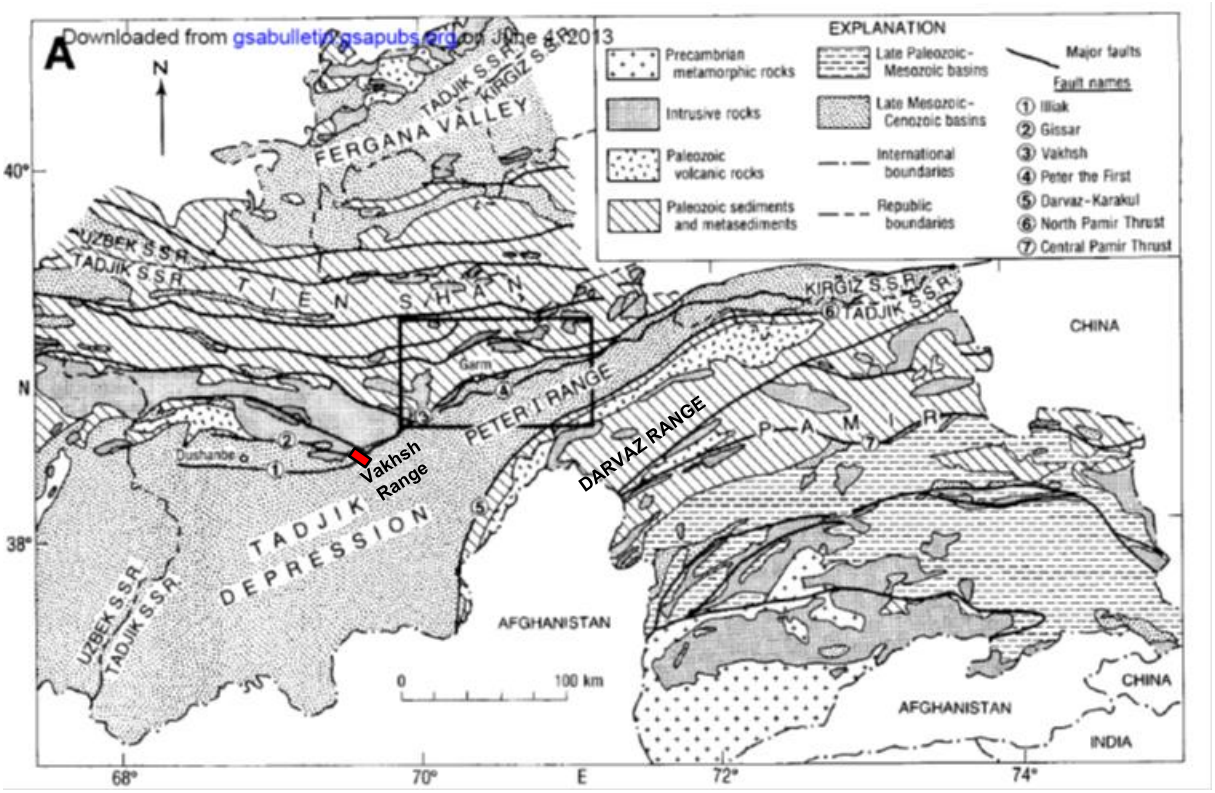

Figure 3 - Regional geology of the Garm region (from Hamburger et al., 1992). Simplified geology, adapted from Loziyev (1968) and Zakharov et al. (1968). The Tadjik Depression sediments are intensely deformed by convergence between the Tien Shan and Pamir blocks. The Peter I Range, located immediately south of Garm, consists of folded and faulted Mesozoic/Cenozoic basin sediments. Rectangle shows location of detailed geological map presented in Figure 4a. Red rectangle indicates the Rogun dam site.

4 GEOLOGICAL STRUCTURE IN THE DAM SURROUNDINGS

As mentioned above, the Rogun hydroelectric scheme is located within the Vakhsh valley, where Paleozoic formations of the Tien-Shan mountain ranges converge with the Vakhsh Range, formed of the tightly folded Mesozoic-Cenozoic sediments of the Tajik Depression.

In general, the Cretaceous rocks exposed in the northern margin of the Vakhsh Range are greatly shortened, with deformation characterized by kilometre-scale, isoclinal, upright to overturned folds and major thrusts that duplicate portions of the Cretaceous section. These thrust faults emerge at the northern edge of the Vakhsh Range, and mark the active boundary with the Tien Shan to the north. Evaporitic rocks of probable Jurassic age are exposed along many of the major thrust faults of the Vakhsh Range , suggesting that these evaporites may provide a regional décollement surface beneath the range. Exposures along the southern portion of the Vakhsh Range are dominated by Neogene strata that are folded but generally young toward the south, forming a synclinorium between structural highs in the Vakhsh Range and Darvaz Range (Figure 3). The Neogene rocks concordantly overlie the Jurassic to Paleogene strata, suggesting that much of the deformation of the Vakhsh Range strata postdates the deposition of the Mio-Pliocene molasse.

Because 1:200 000 scale geological maps (J-42-XI (1965) and J2-42-XI (1964)) and associated cross-sections do not allow the derivation of both fault geometries and mechanisms of deformation at an adequate resolution in the close surroundings of the dam site, and because the northern edge of the Tajik Depression appears quite cylindrical from the Vakhsh Range to the Peter First Range (PFR), we used the works of Hamburger et al. (1992) on the northern edge of the PFR to understand the regional geological structure and more specifically the involved mechanisms of active deformation.

Based on a field survey along the Obi-Khingou River (Figure 4a), Hamburger et al. (1992) have proposed two contrasting structural models of the north-western border of the PFR 30 kilometres upstream from the Rogun dam site (Figure 4b). These interpretations fit the surface geological observations but they are based on different assumptions on basement configuration. Due to both the relative cylindrical geometry of the folds and the strike of the thrusts, it can be assumed that the geological structure proposed by Hamburger et al. (1992) may be applied to the Rogun dam site located 30 kilometres downstream from the Obi-Khingou confluence.

The upper section (Model A) is consistent with the interpretation of the Tadjik Depression as a former passive continental margin (Leith, 1982; 1985) or thinned back-arc basin (Tapponnier et al., 1981). This model is based on the assumption that most of the sediments in the PFR have ramped onto the normal-faulted Jurassic-Paleogene continental margin located at the edge of the Tien Shan. In this model, the hinge line of this rifted continental margin coincides with the frontal thrust of the PFR and explains the sudden change in thickness of Cretaceous strata across the Surkhob River. It must be noted that in Model A, the Vakhsh fault may be interpreted as a crustal pre-existing normal fault re-activated as a thrust and affecting the PFR décollement.

The alternate reconstruction (Model B) is consistent with the model of the Tadjik Depression as a relatively shallow foreland basin that rests primarily on unstretched continental crust. In this case, the marked change in stratigraphy at the northern edge of the PFR would not reflect syndepositional thickening at a structural hinge line, but structural juxtaposition of thin basin-marginal and thick basin-interior facies by major thrusting along the frontal thrust of the PFR. It must be noted that in Model B, the Vakhsh thrust is a typical ramp-flat geometry with the décollement localized in evaporites within the PFR, which would cut down-section to the south to account for the increased stratigraphic section within a large hanging-wall anticline (Pavlis and Hamburger, 1990).

Even if Hamburger et al. (1992) favour model B, they admit that available evidence cannot directly prove or contradict either of the models. The occurrence of seismicity deeper than the décollement supports the presence of crustal faults beneath the décollement (model A). This model is assumed to be representative of mechanisms of active deformation at the Rogun site and it is adopted for the present diagnosis.

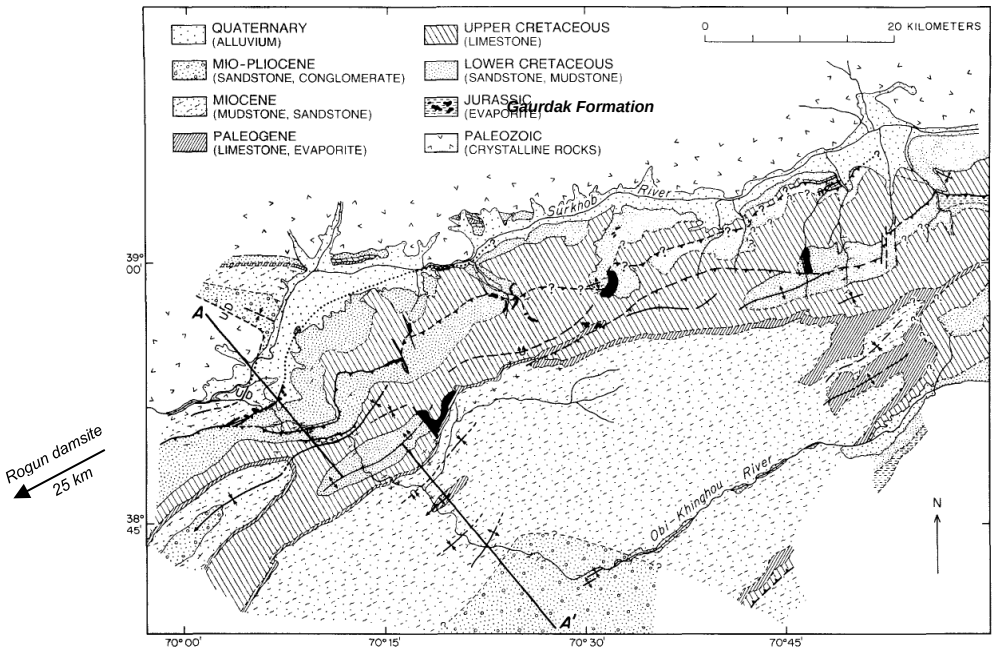

Figure 4a - Reconnaissance geological map of the Garm region (from Hamburger et al., 1992). Contacts and structures are shown in solid symbols where they are well constrained by field observation or imagery interpretation, dashed where they are approximate, queried where uncertain, and dotted where inferred. Heavy dot-dash line indicates drainage network of the Surkhob and Obi-Khingou Rivers. Black areas indicate exposures of Jurassic evaporites, primarily gypsum. Heavy solid line labelled A-A' indicates position of geological cross section shown in Figure 4b. The section is offset along an anticlinal axis. Note that because of distortion in the satellite imagery base maps, geographic coordinates are approximate.

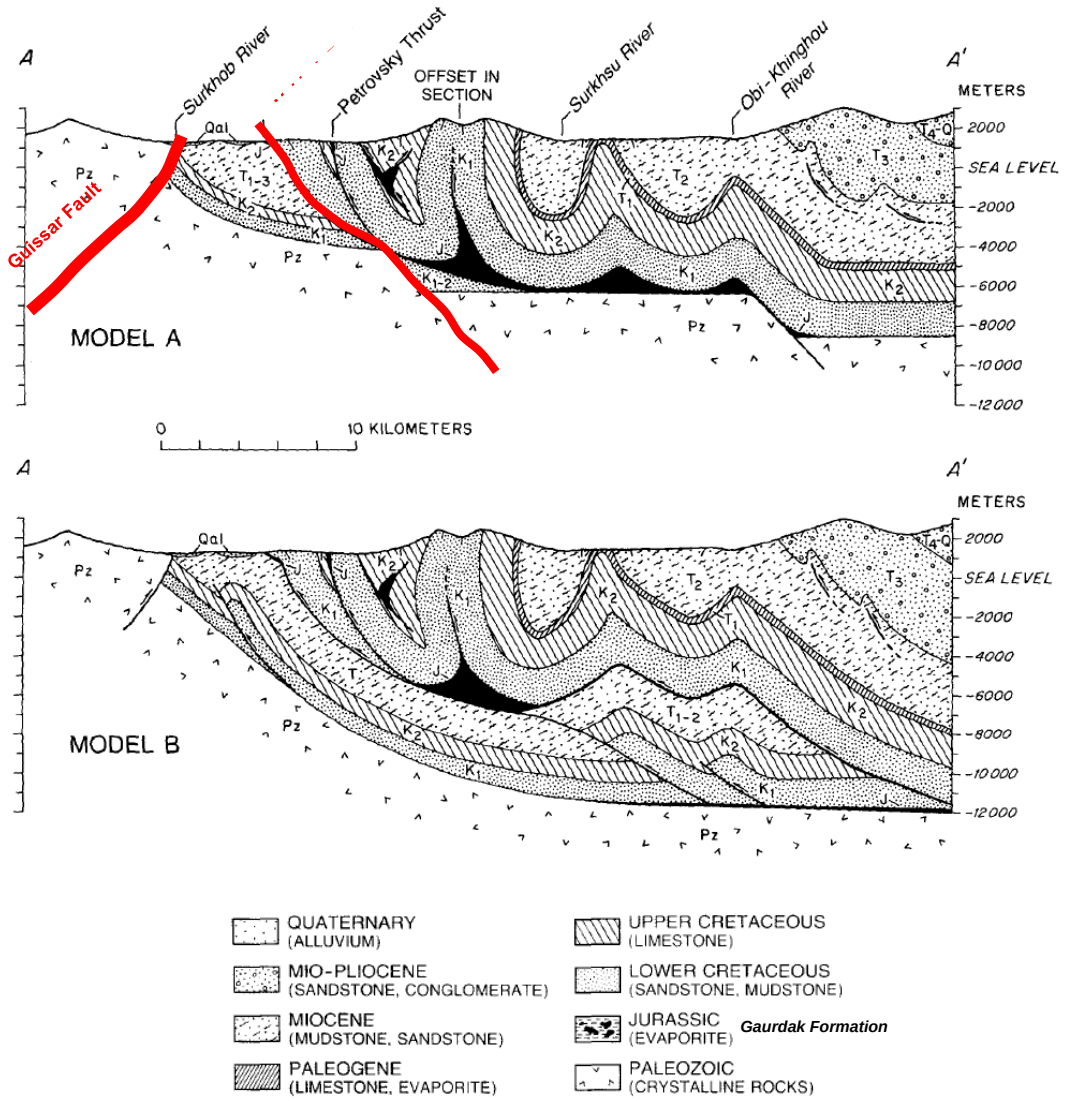

Figure 4b - Alternate interpretations of subsurface geological structure in the PFR (from Hamburger et al., 1992). Both sections are balanced and show no vertical exaggeration. Model A following Leith (1985), assumes that the rapid thickening of Mesozoic strata at the northern edge of the PFR is associated with the hinge line of a normal-faulted former passive continental margin. Guissar and Vakhsh faults are reported in red. Model B assumes that the apparent thickening of Mesozoic strata is caused by structural telescoping of the basin, bringing mid-basin facies into juxtaposition with basin-margin facies. This model implies significantly more Cenozoic shortening in the range than that required by Model A. Location of the section is shown in Figure 4a.

5 GEOLOGICAL STRUCTURE AT THE DAM SITE

The southern slopes of Tien Shan form much of the right bank of the Vakhsh River and of the future reservoir, roughly starting upstream of the Obi-Djushon tributary near the city of Rogun. Within the project area, the hill slopes rise up to 2,500-3,000 m, with variable slope angles. Highly eroded and incised deeply by several major right-hand tributaries of the Vakhsh River, this flank shows a rather irregular slope pattern (Figure 5).

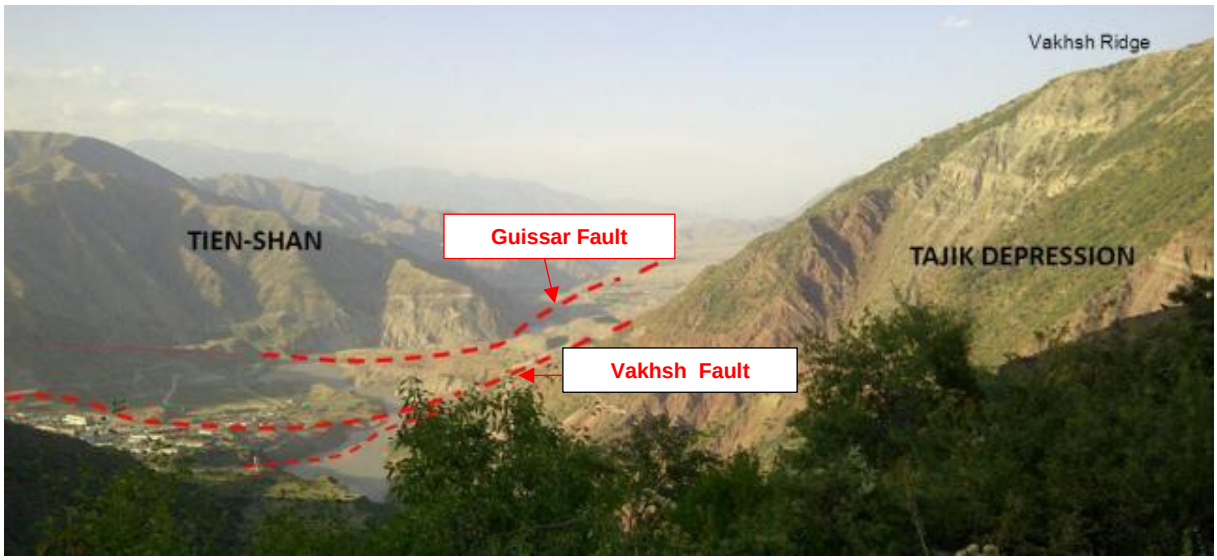

Figure 5 - View upstream from the right bank of the dam site. Location on Figure 10.

The main structural elements are also highlighted on Figures 5, 6, 7 and 8. They will be described in the following paragraphs.

In the project area, the left bank of the Vakhsh River, called in the dam site area the Vakhsh Ridge, shows rather regular slopes of the order of 1.5:1 to 1:1, rising up to 3200 m (Figure 6). The homogenous slopes are likely related with the on-going activity of the Vakhsh regional thrust fault, which carries in its hanging wall the Vakhsh Ridge.

As showed on figure 6b, evaporite rock masses form peculiar morphological features at the toe of the Vakhsh Ridge. Aligned on the fault zone, they are detached from the main slope owing to a high rate of extrusion and to differential erosion. The outcropping part principally comprises gypsum. The presence of salt at deeper levels along the fault or below the alluvial and colluvial cover cannot be discarded. A closer look shows numerous sinkholes, resulting from dissolution (Figure 7a and b).

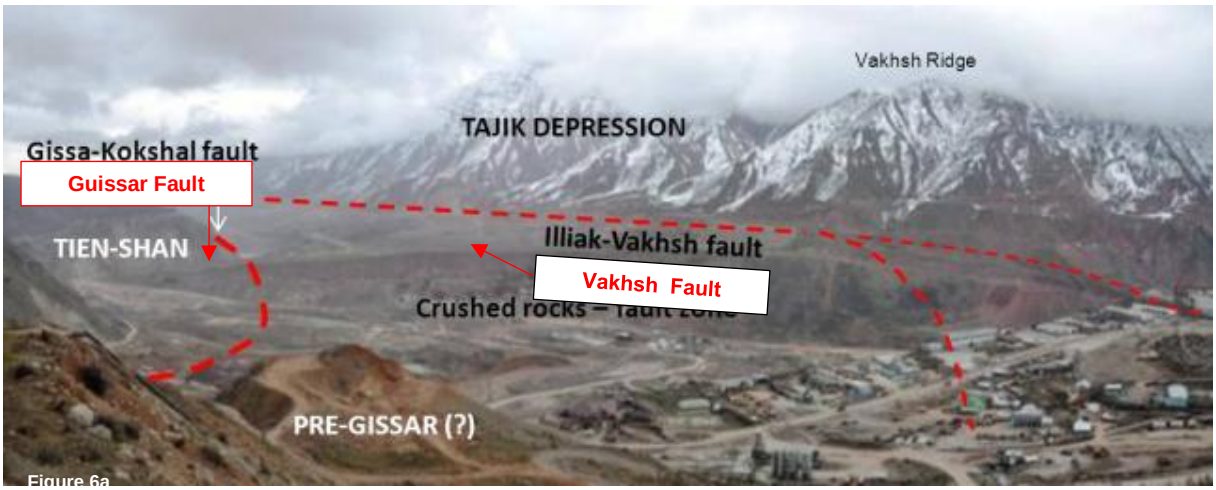

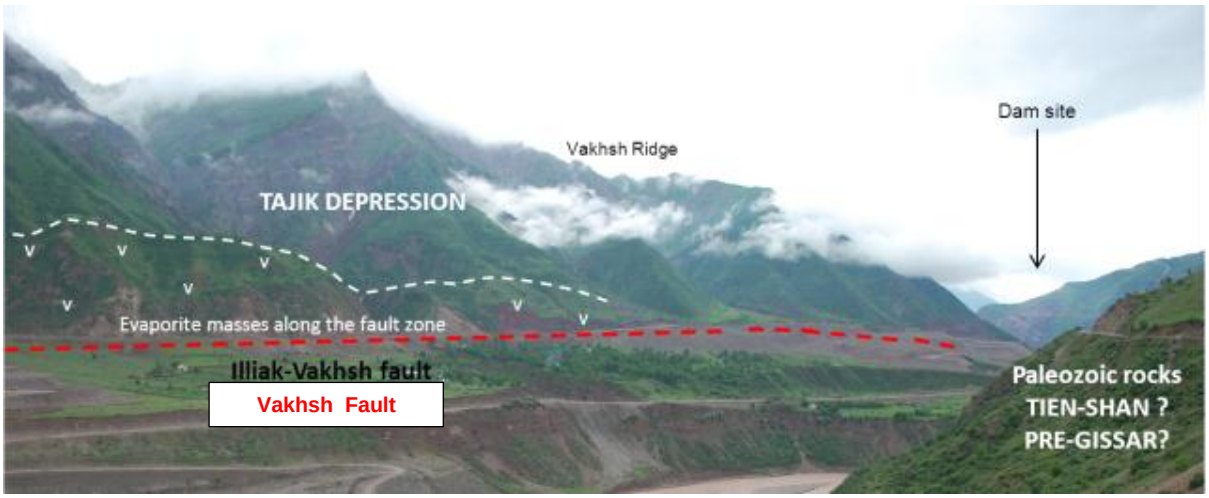

Figure 6a and b - Left bank of Vakhsh River near the dam site, from downstream (a) and from upstream (b). Location on Figure 10.

Figure 7a and b - Detail of gypsum tectonic lenses and sinkholes at the toe of the Vakhsh Ridge. Location on figure 10.

The presence of thick evaporitic layers is an important element in regional tectonics and also, specifically, at the HPP site. The most conspicuous of these is the salt layer of Upper Jurassic Gaurdak Formation, credited with a thickness of around 400 m. At the regional scale, it constitutes the base décollement level for internal deformation within the Tajik Depression. At the dam site, it is found as a thin wedge along the Ionaksh Fault (Figure 9 and 10) and it is the object of detailed studies.

As mentioned above, the dam site lies on the northern boundary of the structural domain of the Tajik Depression (Figure 3). Just upstream from the dam site, the Tajik Depression and Tien Shan are separated by a narrow tectonic unit known as the Pre-Gissaro (or Fore-Gissaro) Downfold. This is a down-thrown bloc composed of Paleozoic sediments and Neogene molasses. However, in the reaches of the dam site, the distance between the Tajik Depression and the Tien-Shan unit is reduced to about 1 km. At this location, at the surface, the zones of influence with mylonites and crushed rocks of Guissar and Vakhsh fault zones could practically touch each other, which results in the formation of a wide fault zone. Figures 5 and 6 show the narrow space between the two structural domains. Figure 8 shows a very wide zone of crushed and weathered rock in the interval between the Vakhsh faults, just upstream from the canyon. It is in this same zone that the Vakhsh Fault is assumed to form a sharp bend to the north, then to the west and then to cross the Vakhsh River.

Figure 8 - Wide zone of crushed rock between two major faults: Guissar (left) and Vakhsh (right). Location on figure 10.

Figures 9 and 10 show the main faults in the project area.

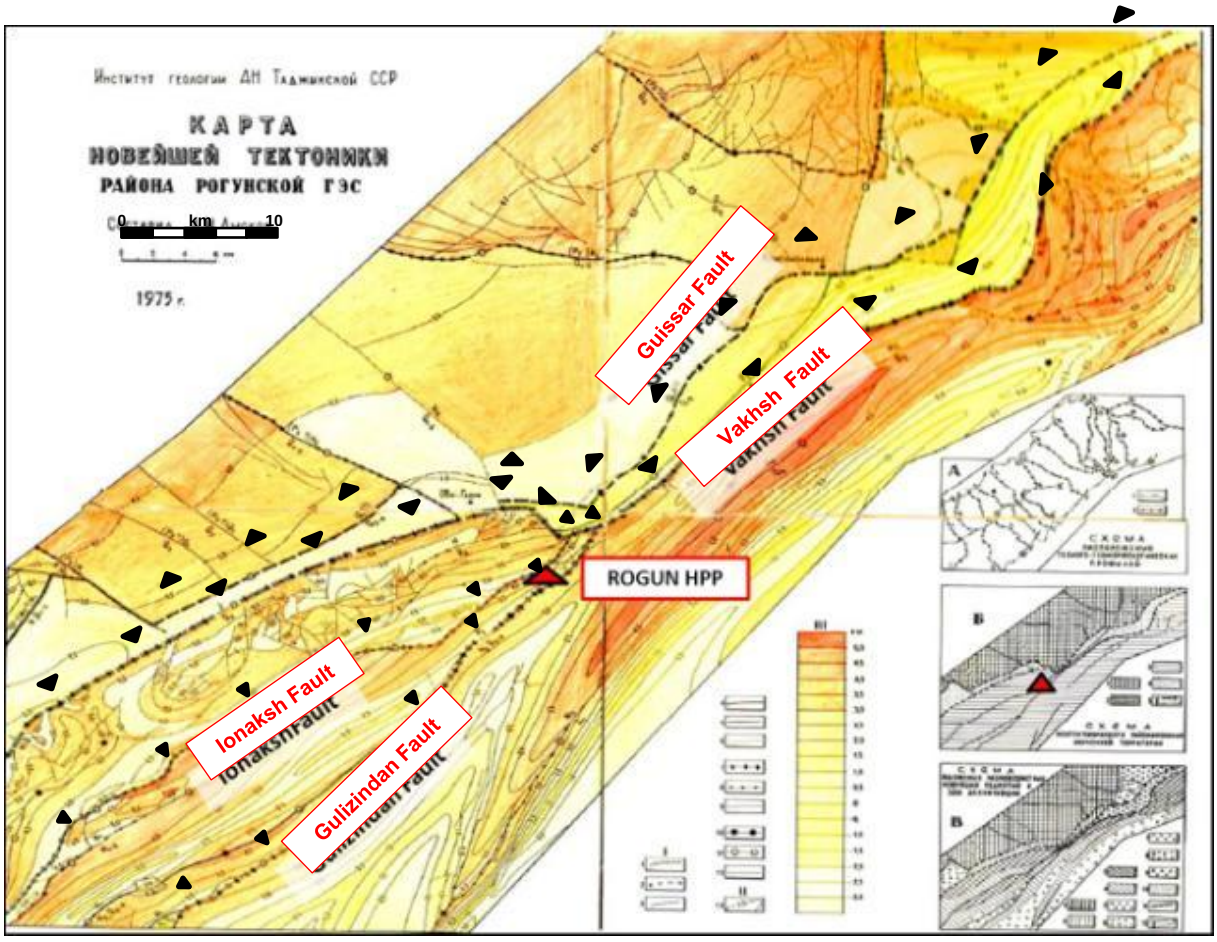

Figure 9 - Map of Neogene tectonic movements in the Rogun HPP area, 1975 (report - Bankable Feasibility for Stage 1 Construction Completion. Vol.3C - Geology, Geotechnics and Seismic Characteristics. LI, 2006). Red triangle shows the dam site.

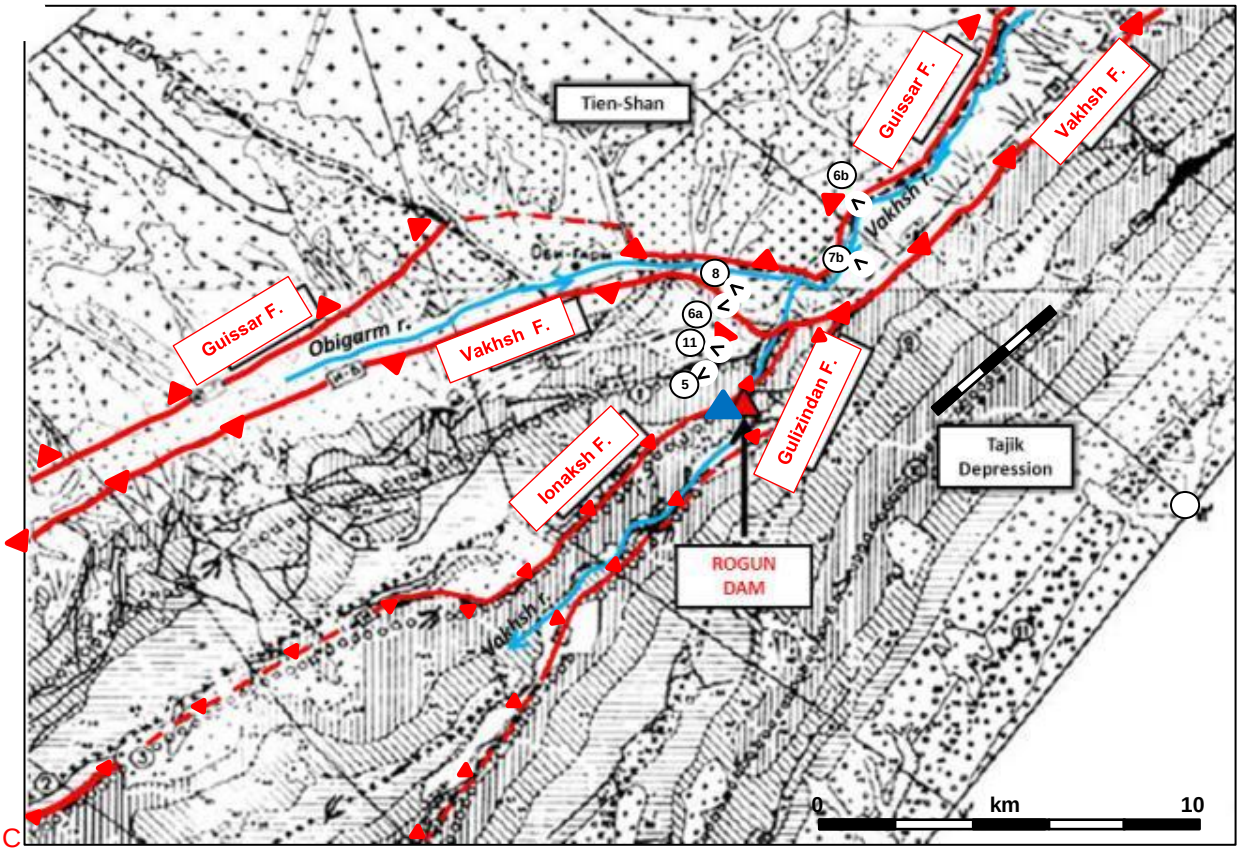

Figure 10 - Main faults near the project area. Background: extract of structural geology map of Rogun HPP (1975). Blue triangle shows the dam site. Circles with numbers locate Figures 5, 6, 7, 8 and 11.

A critical point may be highlighted from these two presented structural maps. In fact, the Vakhsh Fault abruptly cuts the SE-dipping Ionaksh and Gulizindan thrusts which lie, respectively, upstream and downstream from the dam site. This geometric framework suggests a deeper character of the Vakhsh Fault and probably a younger and/or faster activity and tends to support the model A proposed by Hamburger et al. (1992) (Figure 4).

5.1 Crustal deep faults: Guissar and Vakhsh

In the project area, the present-day tectonic stresses related to global geodynamics are largely accommodated by intense shortening along the major fault systems of Guissar and Vakhsh. Both these crustal-scale faults may be followed over dozens of kilometres. The Guissar Fault dips north-north-west and the Vakhsh Fault to the south-south-east, so that they diverge at depth. As discussed above, the faults are difficult to distinguish in the zone of the river bend near the dam site. Figures 9 and 10 show sharp changes of strike of these major faults and the narrow gap between them.

5.2 Upper crustal levels

The following summarizes the faults in the area.

- ✓ Regional thrust faults within the Tajik Depression: Ionaksh and Gulizindan

  As a consequence of the intense shortening, the Mesozoic sedimentary sequence located in the hanging wall of the Vakhsh Fault has been uplifted and is now exposed at the surface. The considerable shortening of the sedimentary cover in response to compressive stresses is mainly accommodated by a series of steep folds and thrusts with NW vergence. The main base décollement level where the thrusts root is the thick Jurassic salt layer a few kilometres deep identified as the Gaurdak Formation. Taking into account the wavelength of the associated folds and the thickness of the sedimentary sequence above the Gaurdak salt layer, these thrust faults must be rooted not deeper than 5 to 8 km.

  The Rogun HPP scheme lies between two of these regional thrust faults: Ionaksh Fault, at the upstream side, and Gulizindan Fault, downstream (Figure 9 and 10). They dip south-east and their length is of several tens of km. To the north-east, few kilometres upstream from the dam site, they are cut by the Vakhsh Fault. The width of the fault zones with crushed rocks reaches generally 10 to 20 m.

  According to the technical report Gidroproyekt (1978), based on monitoring of recent deformation, slip rates along these faults are 0.5-1.8 mm/year for Ionaksh Fault and 1.0 mm/year for the Gulizindan Fault.

  Taking into account the above-documented disconnection between the Vakhsh Fault and upper fold and thrust system rooted in Gaurdak salt layer, a moderate seismogenic capability has, however, to be ascribed to the Ionaksh and Gulizindan (see below).

- ✓ Local faults: F#35 and F#70

  Numerous minor faults participate to the general stress relaxation. Among these, Fault#35 and Fault#70 are directly involved in the dam foundation (Figure 11). Dipping north-west, they seem to branch out from the Ionaksh Fault, which dips south-east, within a few tens to hundreds of meters from the surface. Fault#35 was identified at the surface between Ionaksh and Gulizindan Faults. It exhibits an outstanding crushed zone in the left bank at the dam site. However, its morphological print is more discreet in the right bank and it even becomes untraceable just downstream from the dam site. Such rapid damping suggests a secondary role and a low displacement rate.

Figure 11 - Faults #35 and #70 in the upper Left Abutment. Location on Figure 10.

✓ Second order décollement levels

Above the Gaurdak salt layer, other thick gypsum layers of Upper Cretaceous and Tertiary age form décollement levels for spectacular bubble-wrap folding, likely contributing in this way to the general release of tectonic stresses.

6 SEISMICITY

6.1 Regional seismicity

The Rogun site area is situated on the north-western edge of the Vakhsh Overthrust, which marks the edge of deformation associated with the continental collision (Pavlis et al., 1997; Skobelev, 1977; Burtman and Molnar, 1993; Figure 1). The Surkhob River follows the thrust zone and fluvial erosion by the Surkhob may be an important component of the thrusting mechanism (Lukk et al., 1995; Pavlis et al., 1997).

Pamir and Tien Shan are marked by significant seismicity (Figure12) (Gubin, 1960; Leith and Simpson, 1986; Burtman and Molnar, 1993; Hamburger et al., 1992; Rautian and Leith, 2002). Crustal earthquakes are concentrated near the edges of the Pamir and Tien-Shan mountain belts (Leith and Simpson, 1986). East of a longitude of about 70°20' E, the Tien-Shan boundary zone (Guissar fault zone) and the Pamir boundary zone (Darvaz fault zone) coalesce into a single highly active belt of seismicity that includes the rupture zones of several large historical earthquakes (Kristy and Simpson, 1980). In between the mountain-bounding fault systems, a dense concentration of moderate to small-magnitude activity is observed within the thick sedimentary fill of the Tadjik Depression fold-thrust belt.

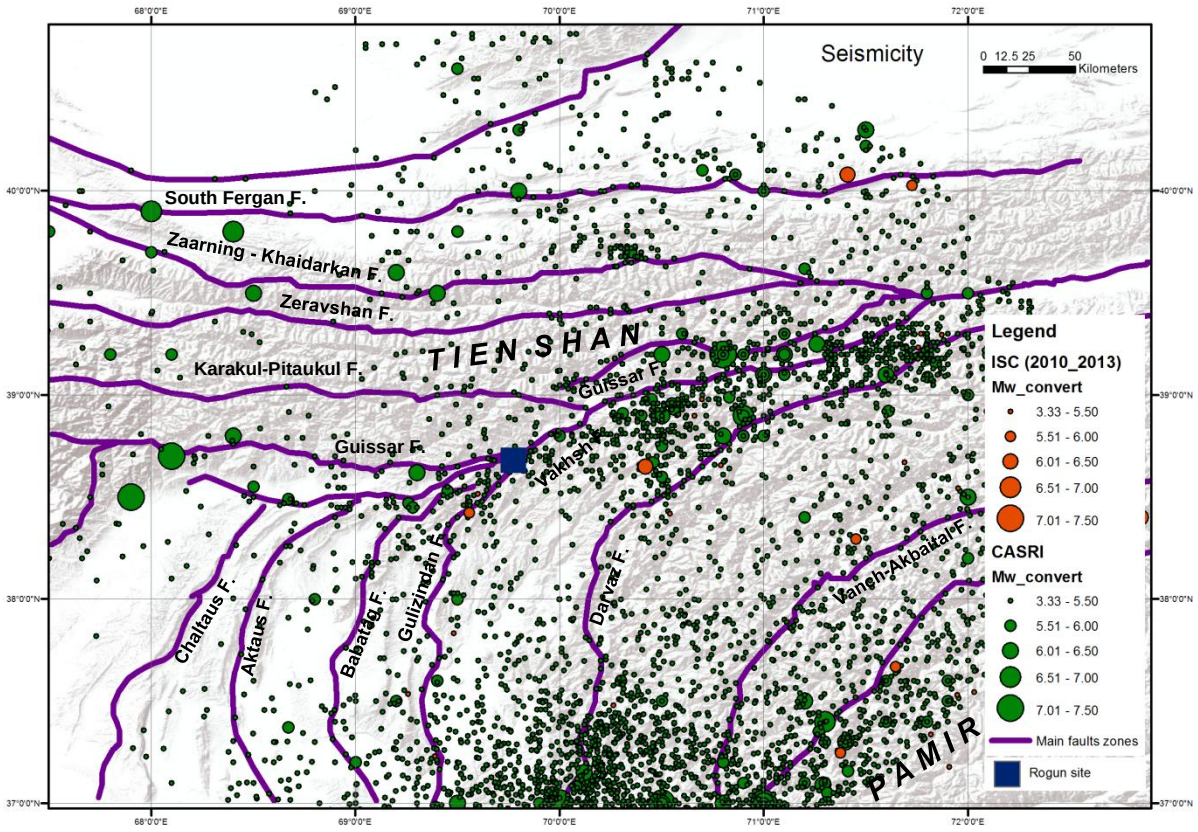

Figure 12 - Epicentres of earthquakes for the period 1895-2013 in an area of 230 km around the Rogun dam site. Magnitudes of the CASRI catalogues (1895-2009) and ISC catalogue (2010-2013) have been converted into homogenous Mw magnitudes (see §6.2).

Central Asian is also unusual for the remarkable concentration of intermediate-depth earthquakes located beneath the Pamir and Hindu Kush ranges. This vigorous intermediate-depth seismicity occurs from 70 to 250km depth in this intra-continental setting. In a map view, this seismicity forms a narrow S-shaped band roughly 450km long from the Hindu Kush in north-eastern Afghanistan to the eastern Pamir (Figure 13). The hypocentres of these mantle earthquakes form two separated Wadati–Benioff zones, one beneath the Pamir

and one beneath the Hindu Kush (Figure 14) (Burtman and Molnar, 1993; Fan et al., 1994; Negredo et al., 2007; Pegler and Das, 1998).

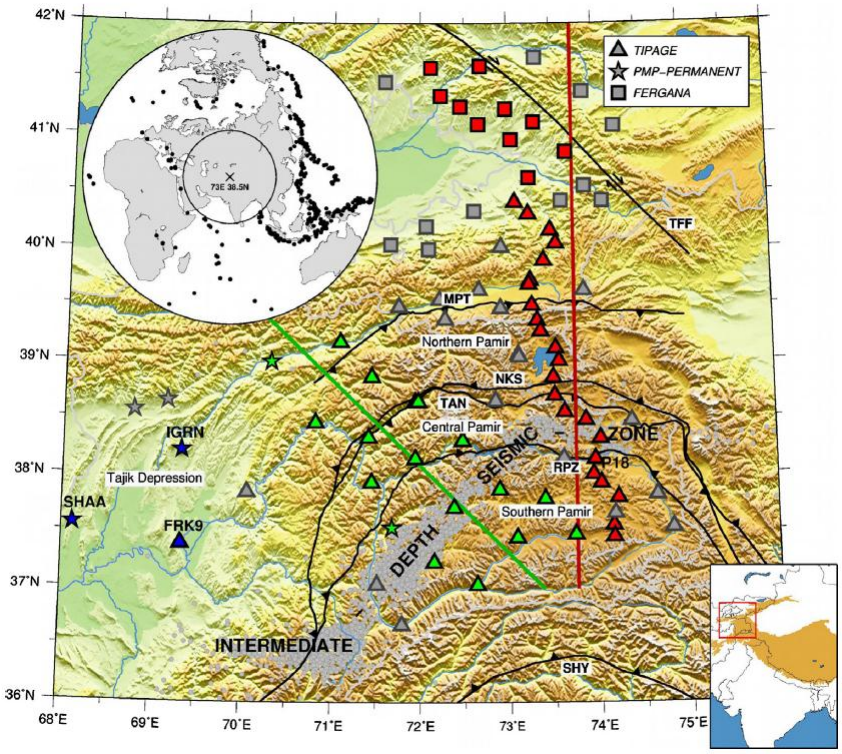

Figure 13: Map of the Pamir with, in grey, the narrow S-shaped band of intermediate-depth seismicity (from Schneider et al., 2013). Major tectonic features such as sutures and faults marked in the map are (from north to south): Talas Fergana fault (TFF), Main Pamir thrust (MPT), Northern Pamir / Kunlun Suture (NKS), Tanymas Suture (TAN), Rushan Pshart Zone (RPZ), and Shyok suture (SHY). Symbol indicate seismic stations used in the study of Schneider et al. (2013): red and green triangles highlighted stations used for the construction of the N–S and the NW–SE depth sections, respectively.

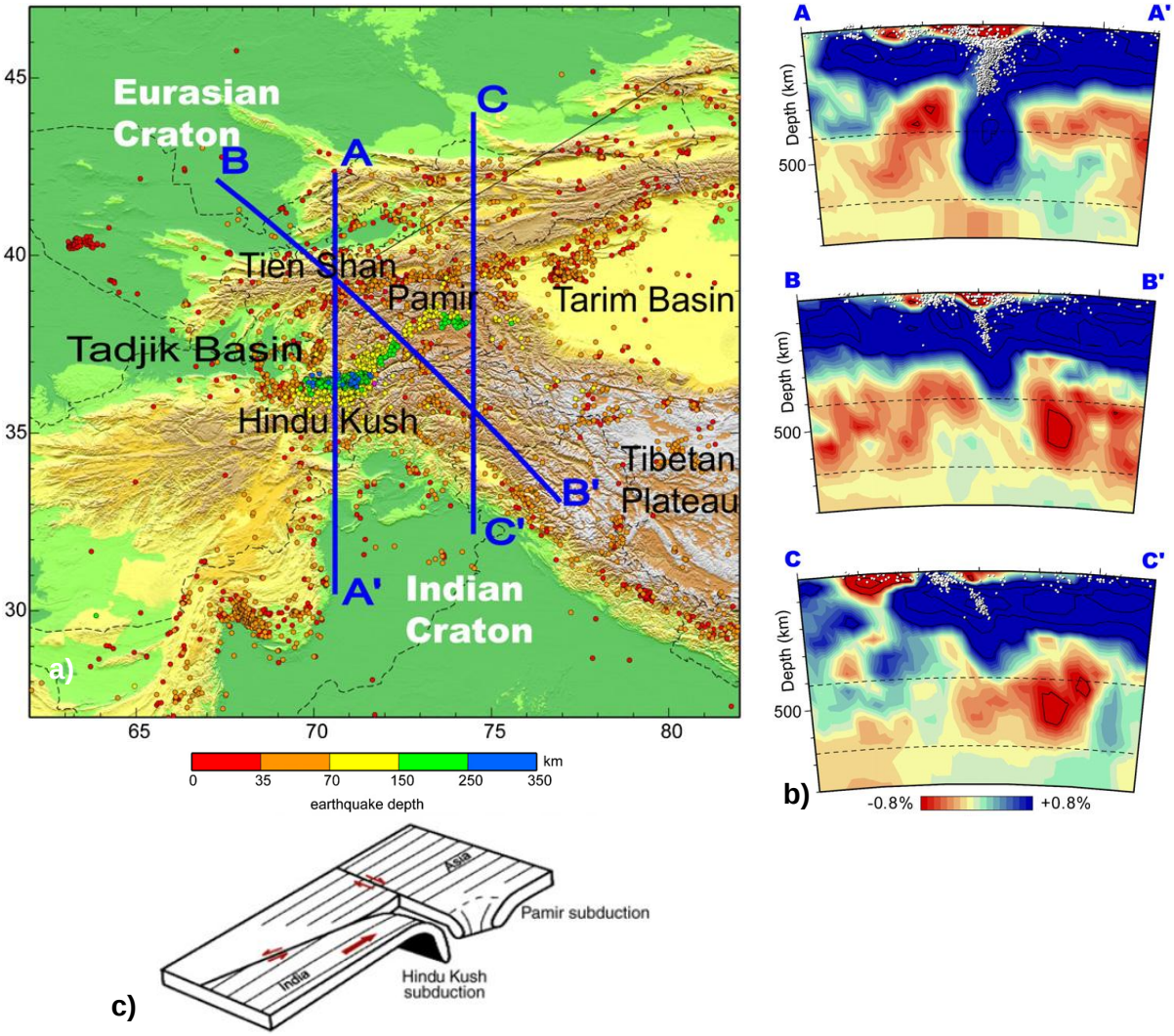

Figure 14 - a) Earthquakes that occurred in the time period 1964–2002 (ISC catalogue) and vertical cross-sections through the Hindu Kush and Pamir regions. Only earthquakes with formal uncertainties in epicentre smaller than 15 km are shown. b) Vertical cross-sections of the global P-wave tomographic model of Villaseñor et al. (2003) through the Hindu Kush and Pamir regions. See a) for location. The contour interval is 1%. c) The inset at the bottom illustrates the multi-subduction 3-D geometry in the region (from Negredo et al., 2007).

There is a long standing debate about whether the geometry of the seismic zone results from a single originally-northward-dipping subduction interface, which was contorted and overturned under the eastern Pamir (Billington et al., 1977; Pegler and Das, 1998; Pavlis and Das, 2000), or if it is the result of two subduction zones, one dipping to the north beneath the Hindu Kush and one dipping to the south beneath the Pamir (Burtman and Molnar, 1993; Chatelain et al., 1980; Fan et al., 1994; Negredo et al., 2007).

6.2 Connection of major historical earthquakes with major faults in the surroundings of the dam site

The analysis of past earthquakes (Figure 14) has been based on:

- the extensive report of Babaev et al. (2005) entitled “Seismic Conditions on the Territory of Tajikistan”;
- the Hydrospecproject technical report n°2360-BTK2-001 (2005); and
- the CASRI earthquake catalogue (1895-2009), provided by the Institute of Earthquake Engineering and Seismology of Dushanbe and including a unified magnitude scale Mw;
- the catalogue of ISC (International Seismological Center) for the period 2010-2013 (July). For the period January 1 2010 to March 1 2011 this catalogue has been reviewed by ISC. For the remaining period the catalogue has not been reviewed by ISC analysts and it includes locations and magnitudes from global networks, such as the NEIC (National Earthquake Information Center of the U.S. Geological Survey).

It has been checked that earthquake parameters of the CASRI earthquake catalogue are consistent with the parameters indicated in the reviewed ISC catalogue for 1964-2010 period. **The CASRI catalogue has been then used as a reference** in order to estimate reference earthquake parameters (see Appendix 1).

In order to homogenize the catalogue, all the magnitudes indicated in the 2010-2013 catalogue have been converted into moment magnitudes (Mw). For instance ISC mb magnitudes have been converted into Mw magnitudes using the relation of Scordilis (2006).

Finally, the earthquakes with Mw>5.5 in this homogeneous catalogue are represented on the Figure 15 with respect to the main faults, for up to 230 km from the dam site of Rogun.

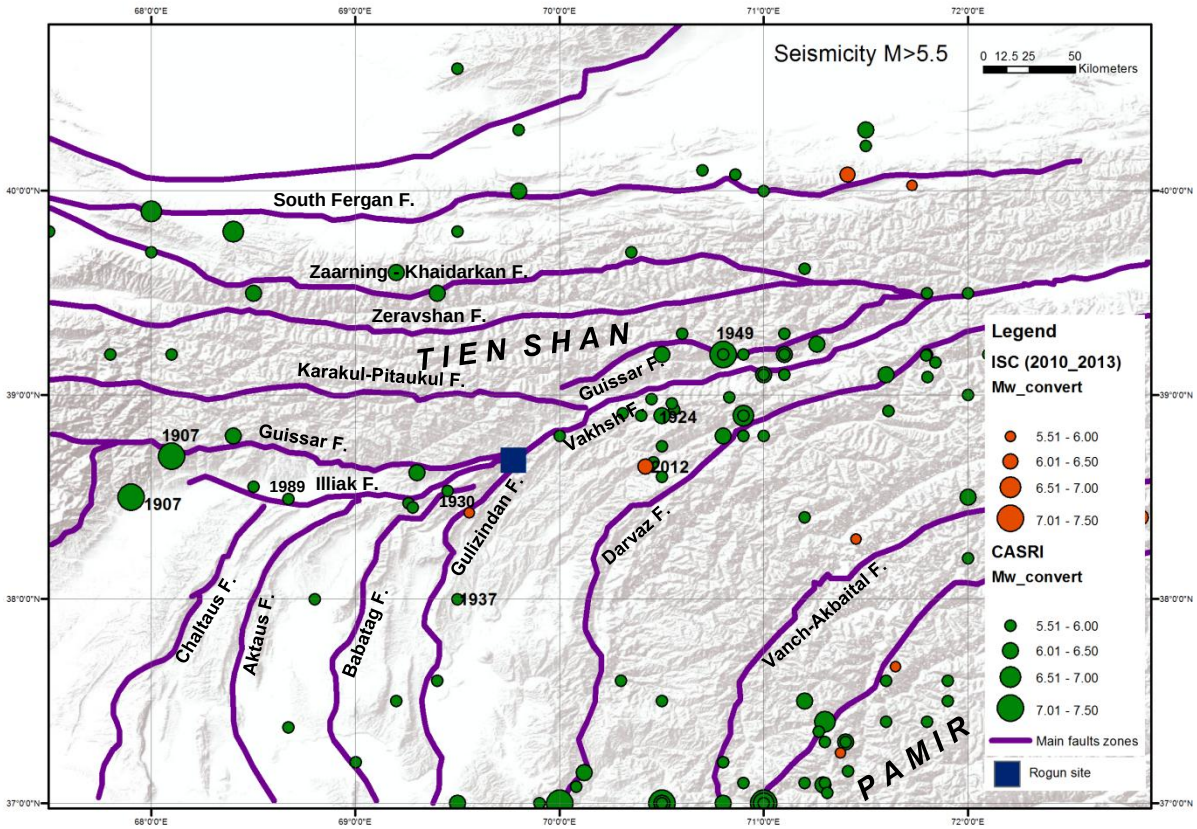

Figure 15 - Map of Tajikistan showing epicentres of earthquakes with Mw>5.5 for the period 1895-2013. Magnitudes of the CASRI catalogues (1895-2009) and ISC catalogue (2010-2013) have been converted into homogenous Mw magnitudes.

6.2.1 Significant seismicity associated with the Guissar Fault

The Guissar fault system is the most active in Tajikistan. Several crustal earthquakes with magnitude greater than 5.5 are reported along this structure. They are listed below in order of decreasing magnitude (Table 1) (CASRI catalogue).

Among them, two major earthquakes occurred along the western (Karatag earthquake in 1907) and eastern (Khait earthquake in 1949) fault segments. It must be noted that depths up to 10 km are assigned to these earthquakes.

Year	Month	Day	Lat	Long	Depth	Mw
1907	10	21	38.5	67.9	35	7.4
1949	7	10	39.2	70.8	16	7.4
1907	10	21	38.7	68.1	24	7.3
1941	4	20	39.2	70.5	8	6.4
1984	10	26	39.25	71.26	15	6.3
1907	10	27	38.8	68.4	24	6.2
1935	7	5	38.3	67.4	18	6.2
1949	7	10	39.2	71.1	19	6.2
1949	7	10	39.1	71	14	6.2
1941	5	6	39.3	70.6	10	5.8
1949	7	8	39.2	70.8	18	5.8
1941	4	26	39.3	70.6	10	5.7
1942	2	28	39.2	70.9	10	5.7
1949	7	10	39.2	71.1	10	5.7
1949	8	23	39.2	71.1	25	5.6
1934	9	23	39.3	71.1	10	5.6

Table 1: Significant earthquakes associated with the Guissar Fault (from CASRI catalogues (1895-2009) and ISC catalogue (2010-2013).

6.2.1.1 Karatag earthquakes in 1907

According to Gubin's assessment (1960) macroseismic intensity in this sequence of earthquakes reached IX to X on the MSK-64 scale. This sequence consisted of the following two principal earthquakes (Table 2) (CASRI catalogue).

Year	Month	Day	Lat	Long	Depth	Mw
1907	10	21	38.5	67.9	35	7.4
1907	10	21	38.7	68.1	24	7.3

Table 2: Main shocks of the 1907 Karatag seismic sequence (from CASRI catalogue 1895-2009).

According to Babaev et al. (2005), the southern boundary of the Hissar range was affected by strong tremors (see Figure 16). The strongly affected area had an area of about 400 km^2 and was located 40 km to the north-east of Dushanbe. 150 villages, including the highly-populated area of Karatag, were destroyed. More than 1,500 people were killed. The earthquake was accompanied by landslides and rock slides that aggravated the destructive effects of the earthquake.

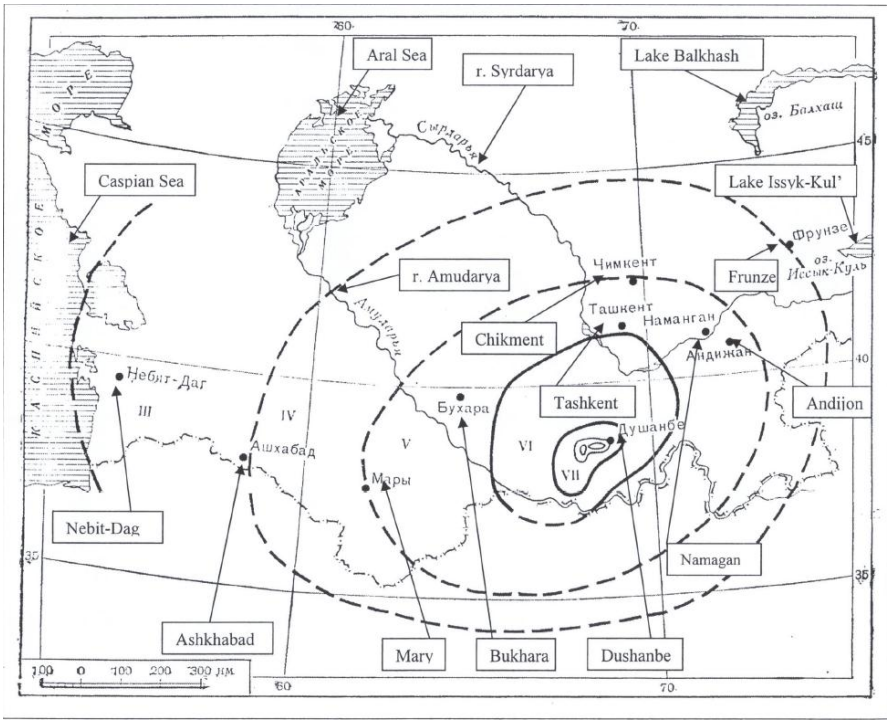

Figure 16 - Isoseismal lines of the Karatag earthquakes, 1907 (Shebalin, 1974).

According to the CASRI earthquake catalogue, a magnitude of Mw 7.4 is ascribed to the Karatag earthquake. This earthquake is assumed to have occurred on the Guissar Fault.

6.2.1.2 Khait earthquake in 1949

This earthquake occurred on July 10 1949 in the area of the village of Khait along the Karategin mountain range (Table 3) (CASRI catalogue).

Year	Month	Day	Lat	Long	Depth	Mw
1949	7	10	39.2	70.8	16	7.4

Table 3: the Khait earthquake in 1949 (from CASRI catalogue 1895-2009).

The macroseismic intensity of shaking in the epicentral zone reached IX to X on the MSK-64 scale (Figure 17).

According to Babaev et al. (2005), the earthquake affected an extensive area: territories of Khait, Jirgatal, Garm and Kalai-Labiob (Tajikabad). More than 150 villages were destroyed or substantially damaged. More than 20,000 people were killed.

The IX-intensity zone covered the upper and middle reaches of the Surhob river valley and the Yasman river valley. Its length was about 60-65 km and its width 6-9 km. The earthquake triggered numerous landslides, rockslides and debris-flows over a vast territory. They buried Khait, 20 villages in the Yasman river valley, and 12 villages in the Obi-Kabud and Surhob valleys.

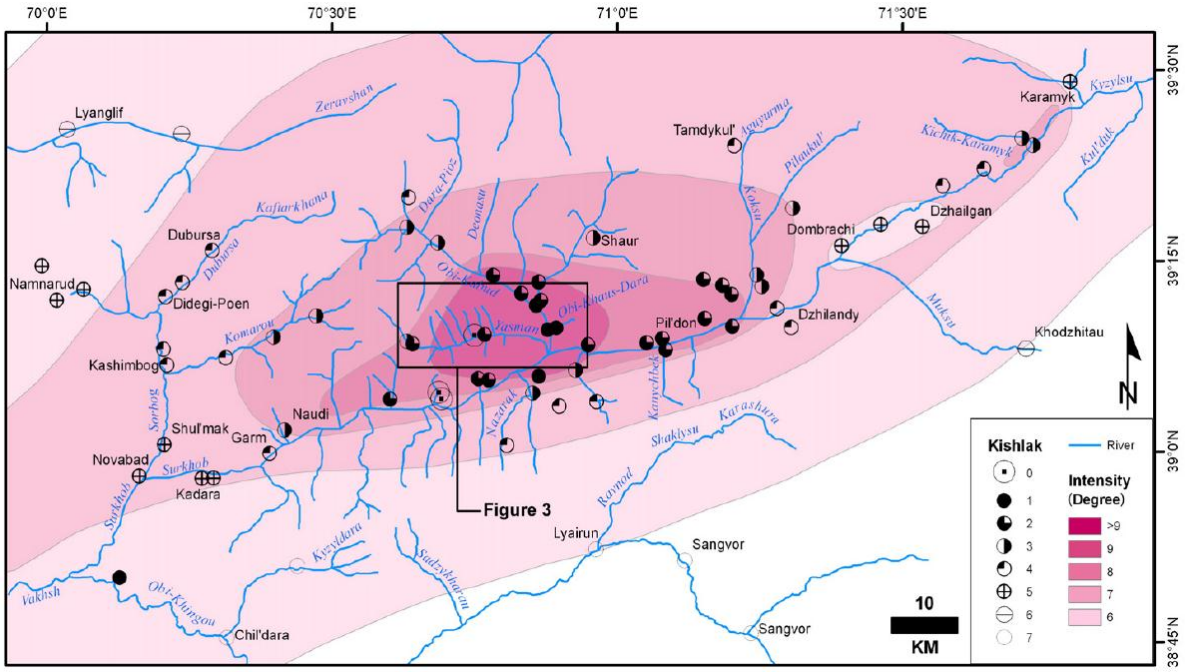

Figure 17 - (from Evans et al., 2009). Isoseismals based on degree of damage to "kishlaks" (rural semi-nomadic settlements) in the Khait area (modified after Figure 5 in Leonov, 1960). Damage scale: 1 = total destruction of kishlak and 7 = no damage to the kishlak. Intensity scale is MSK-64 (see Rautian and Leith, 2002).

6.2.1.3 Macroseismic data for other significant earthquakes

- ***Yasman earthquake July 8 1949 (Table 4)*** *(CASRI catalogue)*

Year	Month	Day	Lat	Long	Depth	Mw
1949	7	8	39.2	70.8	18	5.8

Table 4: the Yasman earthquake July 8 1949 (from CASRI catalogue 1895-2009).

The earthquake occurred 10-15 km north-west of Khait, which suffered damage (Figure 18). In the middle part of Yasaman river valley, a large human settlement was buried by a landslide. The Garm-Khait road was affected by many landslides.

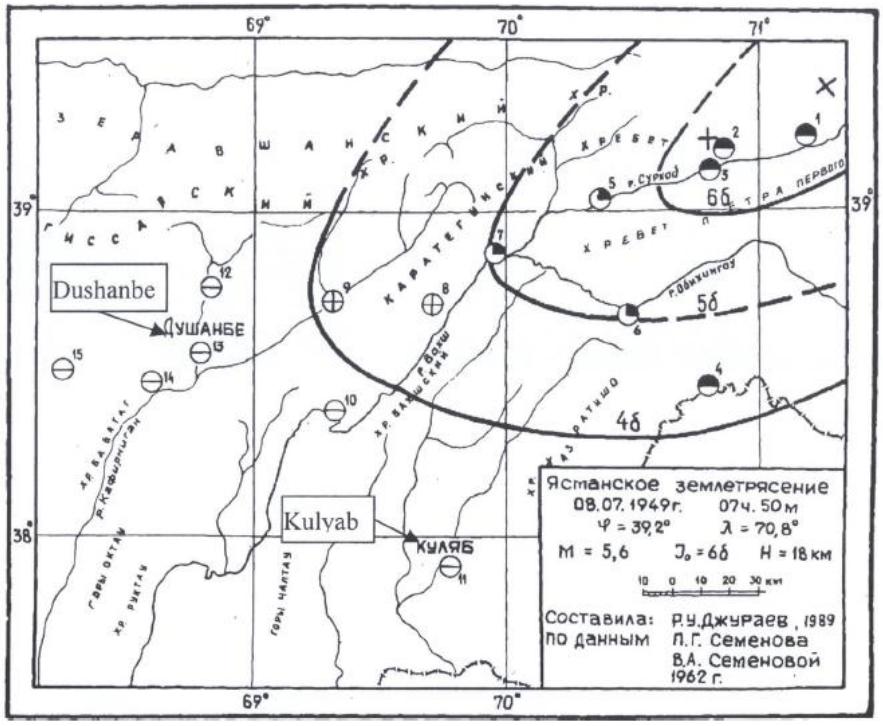

Figure 18 - Isoseismal lines of the Yasman earthquake July 8 1949 (from the Hydrospecproject technical report n°2360-BTK2-001, 2005).

- ***Jirgatal earthquake October 26 1984 (table 5)*** (CASRI catalogue)

Year	Month	Day	Lat	Long	Depth	Mw
1984	10	26	39.25	71.26	15	6.3

Table 5: the Jirgatal earthquake October 26 1984 (from CASRI catalogue 1895-2009).

The unusual characteristic of this earthquake is the north-west trending elongated area of maximum intensity (i.e. transverse to the regional geological structure, see Figure 19). Numerous old pise-walled houses totally or partially collapsed. After the main shock, and during the following year, more than 1000 aftershocks were recorded.

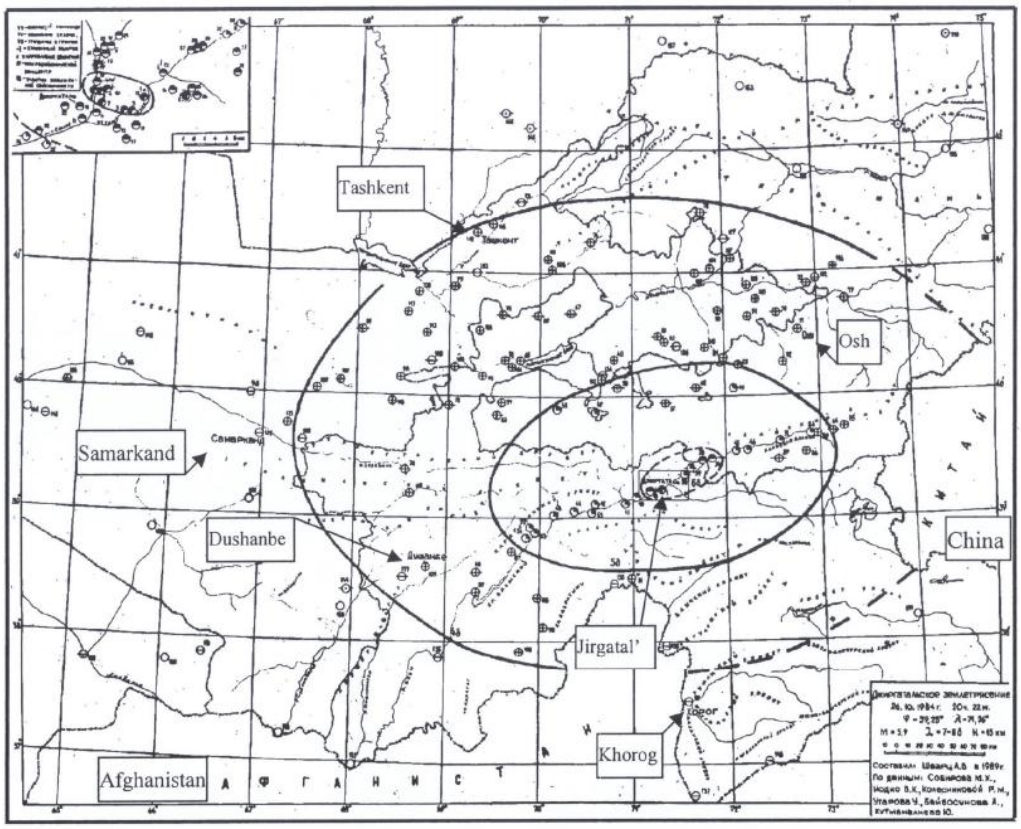

Figure 19 - Isoseismal lines of the Jirgatal earthquake on October 26 1984 (from the Hydrospecproject technical report n°2360-BTK2-001, 2005).

6.2.1.4 Maximum Historical Earthquake (MHE) along the Gissar-Kokshal Fault

From the CASRI earthquake catalogue, it may be concluded that the Maximum Historical Earthquake associated with the Guissar Fault is a shallow magnitude 7.4 (M_w) earthquake. As shown above, the focal depth of significant earthquakes along that structure is roughly 10km.

For the seismic hazard estimation, it has been assumed that the fault runs about 5 km from the dam site and that it dips northward at a mean value of 60-70°.

6.2.2 Significant seismicity associated with the Vakhsh fault

The Vakhsh fault system also shows significant seismicity. Several crustal earthquakes with magnitudes greater than 5.5 are reported along that structure, which are listed below (Table 6) (CASRI catalogue).

Even if for some earthquakes depths are greater than 20km, most of these earthquakes occurred at shallow depths (about 10km). The estimation of the depths may be poor for the period before the beginning of compilation of catalogues reviewed by international agencies (1964 for ISC, 1973 for NEIC).

Year	Month	Day	Lat	Long	Depth	Mw
1924	9	16	38.9	70.5	20	6.4
1943(*)	1	11	38.62	69.3	10	6.1
1939(**)	5	30	38.98	70.45	6	5.9
1926	6	30	38.8	70	10	5.9
1925	1	2	38.8	70	10	5.8
1958	1	7	38.91	70.31	10	5.7
1956	9	22	38.45	69.28	7	5.6
1959	7	31	38.9	70.4	8	5.6
1961	8	23	38.55	68.5	25	5.6
1969	3	22	38.93	70.56	9	5.6
1966	4	14	38.96	70.55	10	5.6
1996	11	23	38.99	70.83	50	5.5

Table 6: Significant seismicity associated with the Vakhsh Fault, from CASRI catalogue (1895-2009) and ISC catalogue (2010-2013). (*) It must be noted the association of the 1943 (January) with the Vakhsh fault remains questionable due to its closeness to the the Guissar fault. (**) The 1939 event is very close to the Vakhsh fault but it could also be attributed to the fold-and-thrust belt (see §6.2.3).

6.2.2.1 Norak earthquake in 1956

The CASRI catalogue indicates the following parameters for this earthquake (table 7):

Year	Month	Day	Lat	Long	Depth	Mw
1956	9	22	38.45	69.28	7	5.6

Table 7: the Norak earthquake in 1956 (from CASRI catalogue 1895-2009).

As can be seen from the isoseimal map on Figure 20, this earthquake occurred 45 km south-east of Dushanbe. It strongly affected the area of Vakhsh-Ilyak interfluve in the range of Faizabad in the north and Norak in the south with numerous wall collapses. Maximum intensity of VII was recorded in several small villages situated a few kilometres north-west of the city of Nurek.. Numerous landslides, rockslides and surface fissures occurred.

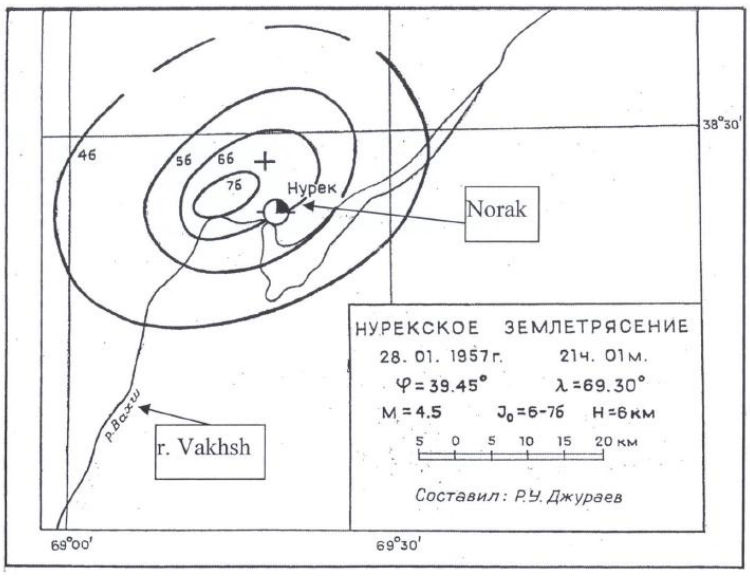

Figure 20 - Isoseismal lines of the Norak earthquake in 1956 (from the Hydrospecproject technical report n°2360-BTK2-001, 2005).

6.2.2.2 Maximum Historical Earthquake (MHE) along the Vakhsh Fault

From the CASRI earthquake catalogue, it may be concluded that the Maximum Historical Earthquake associated with the Vakhsh-Illiak Fault is a shallow magnitude 6.4 (Mw) earthquake. As shown above, the focal depth of significant earthquakes along that structure may reach 10 km and above.

For the DSHA, it has been assumed that the fault runs along the upstream foot of the dam and that it dips south-westward at a mean value of 60-70°.

6.2.3 *Significant seismicity associated with the Tajkikistan fold-and-thrust belt (in particular Ionaksh and Gulizindan faults)*

Significant seismicity may also be associated with the Tajikistan fold-and-thrust belt, which is controlled by a décollement within Jurassic Gaurdak salt (Bekker, 1996; Hamburger et al., 1992). Earthquakes may occur either on the basal décollement or along ramps such as the Ionaksh and the Gulizindan Faults. According to the balanced cross-section proposed by Hamburger et al. (1992), the décollement lies at a depth of 8 km in the dam surroundings. The CASRI earthquake catalogue (1895-2009), provided by the Institute of Earthquake Engineering and Seismology of Dushanbe, shows that this seismicity is widespread, moderate and shallow. Only the following handful of earthquakes reached a magnitude above Mw 5.5 (Table 8) (CASRI for 1895-2009 and ISC for the 2010-2013 period).

It should be noted that an earthquake occurred very recently on May 12 2012 (mb=6.0 according to CSEM, Mw=5.7 according NEIC). The depth is estimated as 10 km by NEIC and is therefore coherent with shallow depths estimated for pre-instrumental earthquakes. The converted Mw magnitude would be for this event Mw=6.1 based on mb=6.0 (see Figure 12 and Figure 15). Nevertheless we prefer to consider here the Mw=5.7 evaluation of NEIC because that Mw is directly evaluated and not converted.

Depths of events associated with the fold-and-thrust belt are very shallow (less than 10 km), except for the 1907 event. Nevertheless the estimated location of this historical event may be poor and it could be considered that events occurred at 3-10 km depths.

Year	Month	Day	Lat	Long	Depth	Mw
1930	9	22	38.53	69.45	5	5.9
1989	1	22	38.49	68.67	3	5.9
1937	11	13	38	69.5	10	5.8
1925	8	30	38	69.5	10	5.7
1943	1	12	38.47	69.26	5	5.7
2012	5	12	38.40	72.85	10	5.7
1950	11	17	38.75	70.5	8	5.6
1907	10	24	38	68.8	18	5.5

Table 8: Significant earthquakes associated with the Tajkikistan fold-and-thrust, from CASRI catalogue (1895-2009) and ISC catalogue (2010-2013).

6.2.4 Tavil Dara earthquake in 1937

The CASRI catalogue indicates the following parameters for this earthquake (Table 9):

Year	Month	Day	Lat	Long	Depth	Mw
1937	11	13	38	69,5	10	5.8

Table 9: theTavil Dara earthquake in 1937 (from CASRI catalogues (1895-2009)).

In the village of Tavil Dara (red square on Figure 21), the hospital and houses were strongly affected. In the mountains, numerous landslides and rockfalls occurred. Several tens of aftershocks were felt within the two months following the main shock.

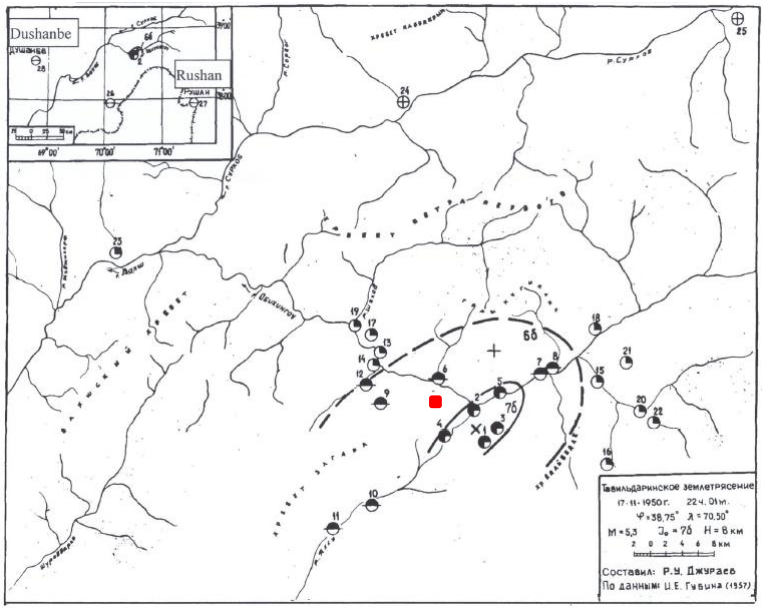

Figure 21 - Isoseismal lines of the Tavil Dara earthquake in 1937 (from the Hydrospecproject technical report n°2360-BTK2-001, 2005). The village of Tavil Dara is indicated with a red square.

6.2.4.1 Guissar earthquake in 1989

This earthquake occurred on January 22 1989 at 23:02 (GMT) in the southern part of the Guissar valley (table 10) (CASRI catalogue). The maximum macroseismic intensity of VII-VIII on the MSK-64 scale was noted 15 km to the south-west of Dushanbe, in the village of Okuli-bolo where 108 houses were destroyed ('A' type according to MSK-64, see Figure 22).

Year	Month	Day	Lat	Long	Depth	Mw
1989	1	22	38.49	68.67	3	5.9

Table 10: The Guissar earthquake in 1989 (from CASRI catalogue, 1895-2009).

According to Babaev et al. (2005), this earthquake was accompanied by residual deformations of two types: liquefaction of loess-like loam and landslide processes caused by this event and opening of fault on the surface. Four landslides occurred as a result. Three of them took place on the northern slope of the upland Okuli. The largest one buried the village of Sharora, where 270 residents lost their lives. The total number of deaths reported was 274.

The largest flow slide (3.25 km long and, on average, 500 m wide) came down the southern slopes of the upland Okuli. It formed on a slope 40-60° steep and moved as a flow for about 2 km destroying the outskirts of the Okuli-bolo village and filling two-thirds of the area of Okuli-poyon with mud.

Similar earthquakes had occurred in the same epicentral area before:

- July 31 1953 with M=4, intensity I_0=V-VI;
- August 4 1953 with M=4, intensity I_0=VI; and

- April 21 1968 with M=4.5, intensity I_0=VII.

No significant damage had been observed for those earthquakes. Starting from 1960s cotton fields were introduced in the area and channels to irrigate them were constructed. Intensive watering of cotton plantations for 20 years from irrigation channels running along the slopes were the main cause of the tragedy.

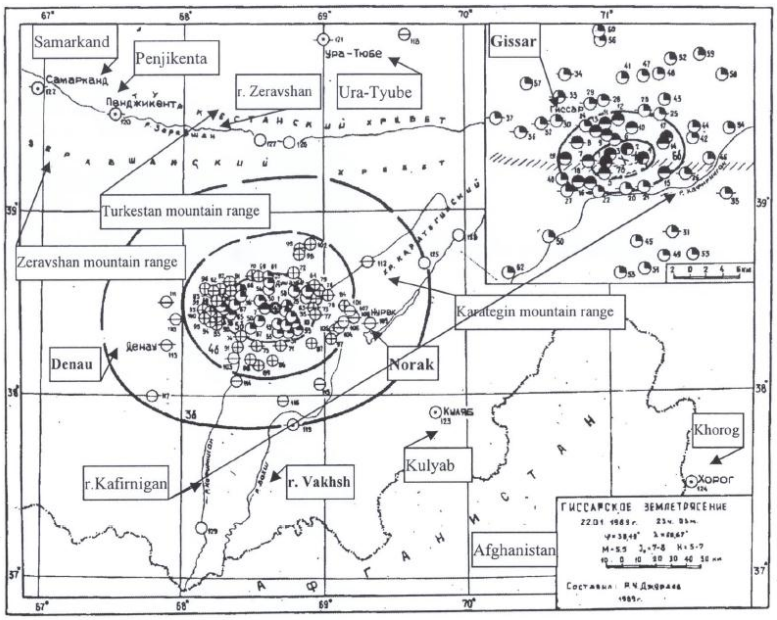

Figure 22 - Isoseismal lines of the Guissar earthquake earthquake in 1989 (from the Hydrospecproject technical report n°2360-BTK2-001, 2005)

6.2.4.2 Maximum Historical Earthquake (MHE) along the Ionaksh and Gulizindan Faults

From the CASRI earthquake catalogue, it may be concluded that the Maximum Historical Earthquake associated to the Ionaksh and Gulizindan Faults is a shallow magnitude 5.9 (M_w) earthquake. For the seismic hazard assessment, it is assumed that this earthquake occurs within the hanging wall of the Vakhsh Range at a depth of 5km (at a distance of 4.6 km from the site).

7 ASSUMPTIONS FOR DSHA

As a result of the seismotectonic diagnosis, the following assumptions on the Maximum Historical Earthquake have to be taken into account to assess the seismic hazard for the feasibility study of the various design options of the Rogun dam (Table 11).

Fault	MHE (M_w)	Depth	Epicentral distance	Reference earthquake
Guissar	7.4	10 km	7-8 km	October 21, 1907 July 10, 1949
Vakhsh	6.4	10 km	4-5 km	September 16, 1924
Ionaksh and Gulizindan ramps	5.9	5 km	4-5 km	September 22, 1930 January 22, 1989

Table 11: Assumptions on the Maximal Historical Earthquakes (MHEs) to assess the seismic hazard

As has been discussed in Section 6.2.1 the historical events on the Guissar fault occurred at depths from 8-10km to 50km. To be conservative we consider a depth of 10km for this MHE in Table 11.

On the Vakhsh fault, as has been discussed in Section 6.2.2, most of earthquakes associated to this fault occurred at depths of about 10km. Hence, a depth of 10 km has been considered for the MHE in Table 11.

As has been discussed in Section 6.2.3 the Tajikistan fold-and-thrust belt seismicity is controlled by a décollement within Jurassic Gaurdak salt. The minimal depth of this décollement is about 5 km. To be conservative, we also consider a 5km-depth for the Ionaksh fault in Table 11. It is coherent with depths estimated for events associated to these faults (depths between 3 and 10km, see Section 6.2.3).

Considering the epicentral distance of the reference earthquake relative to the dam site: these have been derived taking into account: (i) the Hamburger cross-section representative of the mechanisms of deformation, (ii) the actual location of the fault traces close to the dam site and (iii) conservative assumptions on the mean dip of the fault (70°)

The following figure (Figure 23) illustrates the principles of these assumptions:

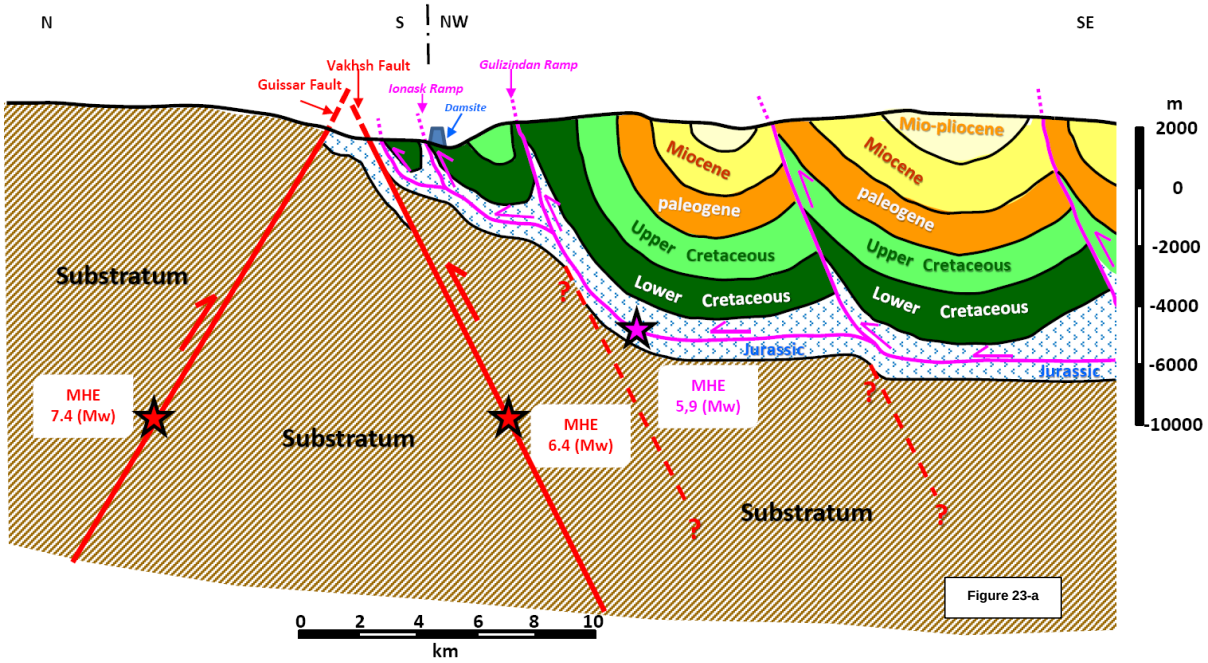

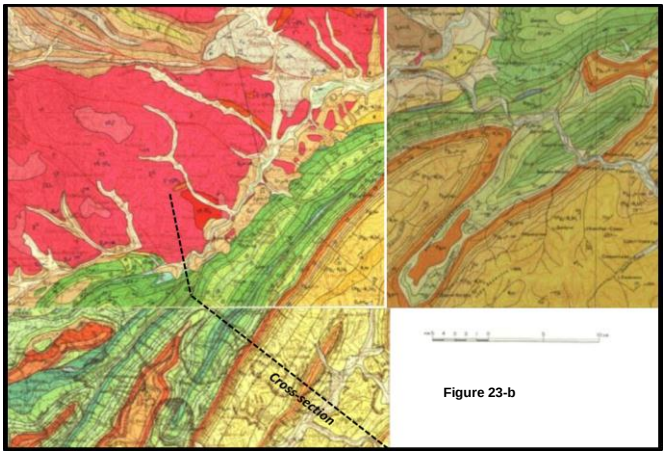

Figure 23 – a) Synthetic assumption for Maximum Historical Earthquake. Guissar and Vakhsh faults are reported in red. The Jurassic Gaurdak décollement and associated ramps (such as the Ionaksh fault) are in purple. Blue trapezium represents the relative location of the Rogun dam.
b) Location of the section presented in Figure 23-a (Extracts of 1:200 000 scale geological maps (J42-X, J42-XI and J42-XVI)).

.

8 SEISMIC HAZARD ASSESSMENT

8.1 Introduction

In previous studies, seismic hazard assessment for the Rogun HPP was conducted through statistical and probabilistic approaches that are very sensitive to: (i) the seismotectonic model selected, (ii) the completeness (homogeneous and exhaustiveness) of the earthquake catalogue, (iii) the method used to characterize the seismic activity of the seismogenic sources, and (iv) the choice of a probabilistic distribution model for future earthquakes. From a general point of view, available project reports do not provide sufficient details on these aspects. Consequently, it is quite difficult to estimate the impact of the significant uncertainties that seem to prevail in the regional and local seismotectonics framework (see chapter 2 to 6 above) on the derived seismic hazard. This impact can be properly addressed only by conducting a state-of-the-art PSHA, as recommended hereafter.

For the purpose of this study, which as described in the introduction is to derive representative parameters against which the safety of each dam alternative shall be ensured, and preliminarily to a PSHA that is necessary for design aspects of the future dam, our strategy was to carry out an independent preliminary assessment to estimate the ground motion expected at the dam site.

This seismic hazard assessment was carried out in several steps:

- Determination of the magnitudes and distances of the Maximum Credible Earthquakes likely to occur on each identified active faults or/and seismogenic sources that may affect the dam;
- Estimates of the Peak Ground Accelerations (PGAs) at the site induced by each reference earthquake on each identified active fault; and
- Estimates of the expected ground motions at the site.

8.2 Estimate of the Maximum Credible Earthquake (MCE)

The Maximum Credible Earthquake (MCE) is the event that produces the largest ground motion expected at the dam site on the basis of the observed historical seismicity and the seismotectonics of the region. It is estimated based on deterministic earthquake scenarios.

When estimated from historical seismicity, the MCE is derived from the Maximum Historical Earthquake (MHE) assigned to each identified critical seismogenic source, e.g. faults capable of representing a threat to the site of interest. This MHE is placed in the most unfavourable position for the studied site.

We calculate the ground motion associated to the MCE in two ways :

1. MCE=MHE increased by 0.5 magnitude units and ground motion parameters taken as the median plus half a standard deviation; or

2. MCE=MHE and ground motion parameters taken as the median plus one standard deviation.

In the second approach the ground-motion parameters correspond to the 84^{th} percentiles (mean plus one standard deviation) as recommended by ICOLD (2010). In the first approach conservatism is assured by a mixture of an increase in magnitude and the use of a higher percentile (69^{th}) of the ground-motion distribution. We decided to calculate PGA with the two methods and choose the most penalizing results as the ground motion expected at the dam.

Distances, depth and magnitudes proposed for the largest expected earthquakes on each critical seismogenic source are presented in the following table. Joyner-Boore and rupture distances are calculated taking into account the dip of the faults and the surface ruptures (down-dip rupture width) estimated from the

equations of Wells & Coppersmith (1994) with the magnitudes Mw for the MHE and MHE+0.5, as given in Table 12.

Seismogenic source	**MHE** **Depth, width, distances to the site, Mw**	**MHE + 0.5** **Depth, width, distances to the site, Mw**
Guissar Fault	Mw=7.4 Focal depth = 10 km Down-dip rupture width=26 km Joyner-Boore distance = 5 km Rupture distance = 5 km	Mw=7.9 Focal depth = 10 km Down-dip rupture width=42 km Joyner-Boore distance = 5 km Rupture distance = 5 km
Vakhsh Fault	Mw=6.4 Focal depth=10 km Down-dip rupture width=10 km Joyner-Boore distance = 2.3 km Rupture distance = 6.2 km	Mw=6.9 Focal depth=10 km Down-dip rupture width=16 km Joyner-Boore distance = 1 km Rupture distance = 3.4 km
Ionaksh and Gulizindan ramps	Mw=5.9 Focal depth=5 km Down-dip rupture width=6 km Joyner-Boore distance = 0 km Rupture distance = 2.4 km	Mw=6.4 Focal depth=5 km Down-dip rupture width=9 km Joyner-Boore distance = 0 km Rupture distance = 1.1 km

Table 12: Distances, depth and magnitudes proposed for the largest expected earthquakes on each critical seismogenic source

The selection of appropriate GMPEs for the Rogun site was based on applying the ten criteria proposed by Bommer et al. (2010) 'in order to produce predictive equations that will be routinely applicable to state-of-the-art seismic hazard analyses' to the set of published GMPEs for PGA and response spectral ordinates compiled by Douglas (2011). Bommer et al. (2010) list the eight GMPEs that pass all these criteria. Two of these are for stable continental regions and hence they are excluded from consideration since Rogun is situated in a region of active tectonics. Of the remaining six models, two (out of four) models derived during the NGA West project (Boore and Atkinson, 2008; Campbell and Bozorgnia, 2008) and the only surviving one derived for Europe and the Middle East (Akkar and Bommer, 2010) were selected. For the earthquake scenarios considered in this report the three other potential GMPEs proposed by Bommer et al. (2010) for active regions would predict similar ground motions.

In the absence of any available measurements of the near-surface velocities at the Rogun dam site, we have assumed a Vs30 value of 1000m/s to evaluate the GMPEs of Boore and Atkinson (2008) and Campbell and Bozorgnia (2008) (table 13). Histograms shown in Figure 3.2 of Ancheta et al. (2013) summarize the measured Vs30 values collected for the recently completed Next Generation Attenuation (NGA) West 2 strong-motion database, probably the most complete strong-motion database currently available. From these histograms in can be seen that there are few (186 values) available measurements of Vs30 from rock sites [defined by Akkar and Bommer (2010) to be sites with Vs30>750m/s]. The highest measured Vs30 is about 1500m/s. Table 3.2 of Ancheta et al. (2013) provides average (mean and median Vs30) for sites defined by their Geomatrix third letter. The median Vs30 for the class A [Rock: Instrument on rock (Vs > 600 mps) or <5m of soil over rock] is 660m/s while the mean Vs30 is 720m/s. Therefore, in the absence of information on the rock type at Rogun a slightly lower Vs30 could have been assumed. Changing the value assumed for Vs30 from 750m/s (the minimum Vs30 assumed by Akkar and Bommer, 2010 for their rock sites) to 1500m/s would lead to small changes (roughly 5% increase when using 750m/s and roughly 5% decrease when using 1500m/s) in the predicted PGAs for Boore and Atkinson (2008) and Campbell and Bozorgnia (2008) and would have no effect on the prediction from the GMPEs of Akkar and Bommer (2010). We do not believe that the Vs30 at the Rogun site is likely to be higher than 1500m/s since such high near-surface velocities are generally associated with sites in stable continental regions (e.g. eastern North America) where glacial weathering has removed weathered layers from hard granite.

Id	Name	Distance metric	V_{s30} (m/s)
ab10	Akkar & Bommer (2010)	Joyner- Boore distance	>750
ba08	Boore & Atkinson (2008)	Joyner- Boore distance	1000
cb08	Campbell & Bozorgnia (2008)	Rupture distance	1000

Table 13: Assumed Vs30 for the various GMPEs *and their distance metrics*

For each seismogenic sources, the horizontal geometric-mean PGAs assuming a reverse focal mechanism were calculated (see appendix 2 for an example of the input file used to evaluate the GMPEs using our in-house computer code, whose predictions have been checked against independent implementations). The site is on the hanging wall for the Vakhsh and Ionaksh Faults. Results are given for the two methods of calculation described above and for each GMPE. An average of the results obtained for the three GMPEs is given in the last line of the following tables.

MCE=MHE+0.5 / median PGA + 0.5 standard deviation			
GMPE	PGA for Guissar Fault (g)	PGA for Vakhsh Fault (g)	PGA for Ionaksh and Gulizindan ramps (g)
ab10	0.53	0.64	0.59
ba08	0.46	0.59	0.57
cb08	0.47	0.91	0.99
Average of the three GMPES	**0.49**	**0.71**	**0.71**

Table 14: Horizontal geometric-mean PGAs calculated assuming MCE=MHE+0.5 / median PGA + 0.5 standard deviation

MCE=MHE / median PGA + 1 standard deviation			
GMPE	PGA for Guissar fault (g)	PGA for Vakhsh Fault (g)	PGA for Ionaksh and Gulizindan ramps (g)
ab10	0.78	0.78	0.67
ba08	0.55	0.55	0.60
cb08	0.59	0.78	0.78
Average of the 3 GMPES	**0.64**	**0.70**	**0.68**

Table 15: Horizontal geometric-mean PGAs calculated assuming MCE=MHE / median PGA + 1 standard deviation

The Vakhsh and the ramps scenarios give PGAs that are quite similar. The Guissar scenario gives lower PGAs for the two studied cases (MHE+0.5 and MHE). The MHE+0.5 scenario seems to be slightly more penalizing than the MHE scenario for both the Vakhsh and ramps scenarios. When the whole spectrum is studied, and not only PGA, we note that the spectrum for the Vakhsh scenario is higher than that from the ramps scenario for low and medium frequencies. Therefore, this scenario is considered as the most penalizing for the dam, it means that the proposed MCE is a MHE+0.5 earthquake on Vakhsh Fault.

- **Maximum Historical Earthquake on the Vakhsh Fault with a magnitude M_w 6.9 and a focal depth of 10 km placed at the shortest distance to the dam site (rupture distance ~3.5 km)**

- **PGA = 0.71g[2] (calculated based on the median plus a half of standard deviation : 0.585g +0.125g)**

8.3 Response spectrum at the dam site

The average response spectrum (rock conditions) obtained for the MCE on the Vakhsh Fault is reported in the following figure (Figure 24).

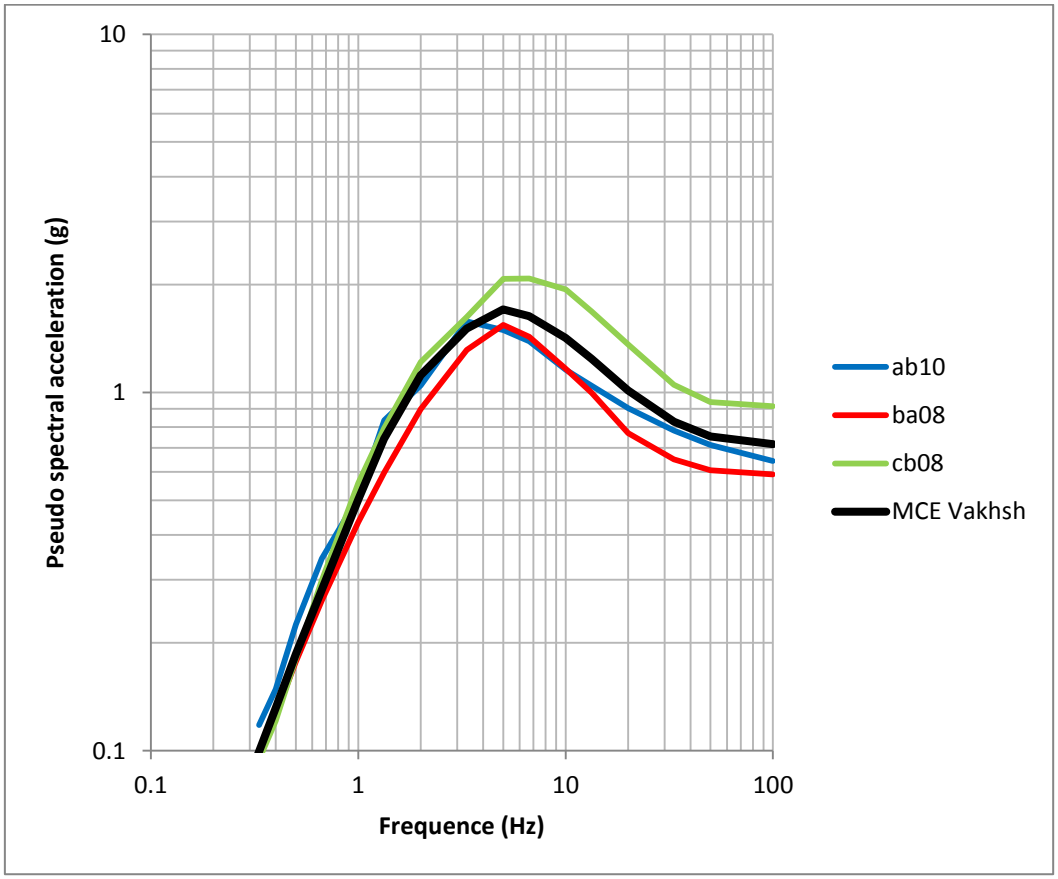

Figure 24 - *Response spectrum relative to the Vakhsh fault MCE obtained using the GMPEs of Akkar and Bommer (2010, ab10), Boore and Atkinson (2008, ba08) and Campbell and Bozorgnia (2008, cb08) and the proposed response spectrum for 5% damping (black)*

The 'mean' spectrum (black curve) is based on an eye-ball average of the spectra from the three GMPEs in order to obtain a smooth design spectrum. Consequently the lack of predictions from the GMPE of Akkar and Bommer (2010) does not affect the black curve for periods longer than 3s since the 'average' is based on the other two GMPEs for these periods. At short periods, Akkar and Bommer (2010) provide coefficients for the prediction of PGA, which we assume to equal the pseudo-spectral acceleration at 0.01s (100Hz), and pseudo-spectral acceleration at 0.05s (20Hz) but no coefficients for periods between these two. Therefore, we linearly interpolate these coefficients in the logarithmic frequency domain between 100Hz and 20Hz to

[2] *In accordance with the instrumental seismic scale of the US Geological Survey EEIS, PGA values obtained are within the range of 6,5 m/s² (0.64g) to 12,4 m/s² (1.24g) which would correspond to intensity of 9 points on 12 points scale. Such relation may be used for communication purposes. However the dam design must be based on acceleration values and cannot be based on intensity.*

obtain predictions for intermediate frequencies. Alternatively, the short-period extension proposed by Bommer et al. (2012) could have been used to extend the predictions of Akkar and Bommer (2010) for periods between 0.01 and 0.05s. After the calculations of the spectra for the earthquake scenarios considered here, updates of the three GMPEs used here have been published online (Akkar et al., 2013; Boore et al., 2013; Campbell and Bozorgnia, 2013), whose use would lead to slightly different estimated spectra for the earthquake scenarios considered here. However, we believe that the differences in predicted motions are unlikely to be large. For future hazard assessments for this site we recommend that the selection of the GMPEs is repeated based on an updated list of published GMPEs.

In order to compare its frequency content with the spectrum from the Vakhsh Fault, the response spectrum associated with the Guissar Fault has been estimated in the same way (Figure 25).

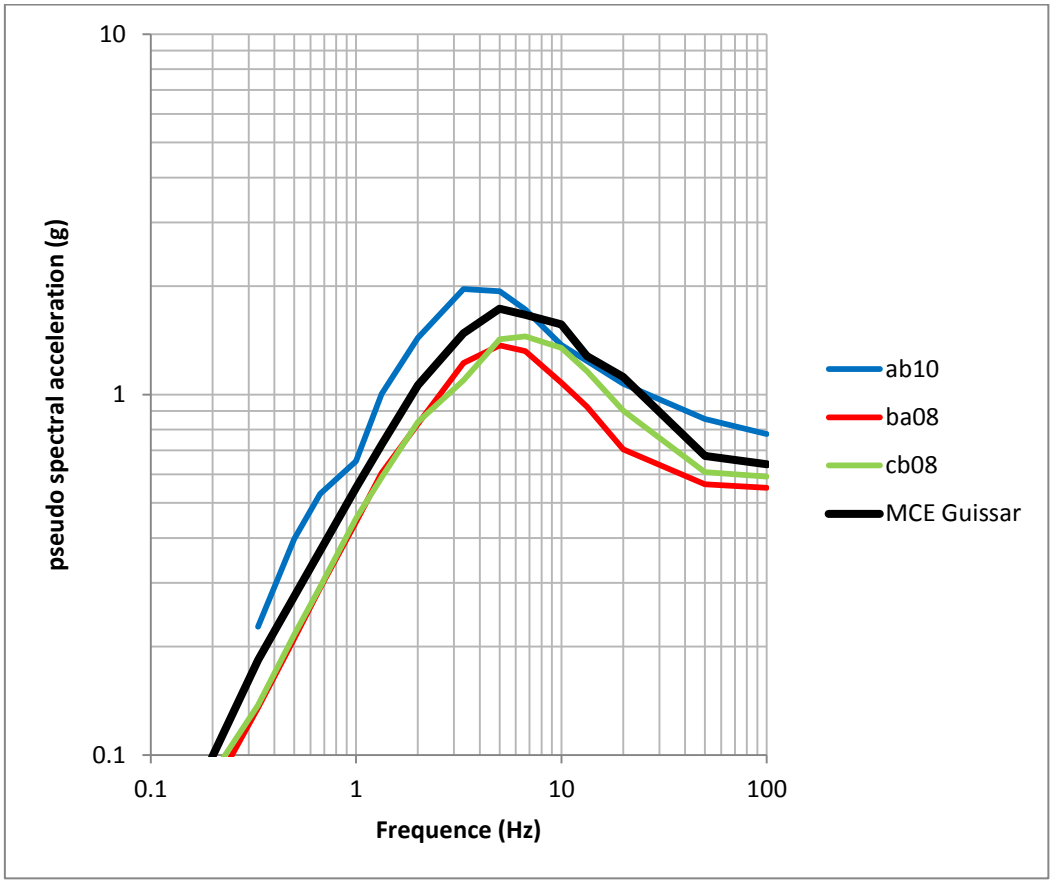

Figure 25 - *Response spectrum relative to the Guissar Fault MCE obtained using the GMPEs of Akkar and Bommer (2010, ab10), Boore and Atkinson (2008, ba08) and Campbell and Bozorgnia (2008, cb08) and the proposed response spectrum for 5% damping (black)*

As shown on Figure 26, the Guissar Fault appear to provide similar level of pseudo-spectral acceleration taking into account the precision associated to the method employed. Special care has to be taken for the range of periods from 0.3 to 2 seconds corresponding to the periods of the dominating Egen modes of the dam.

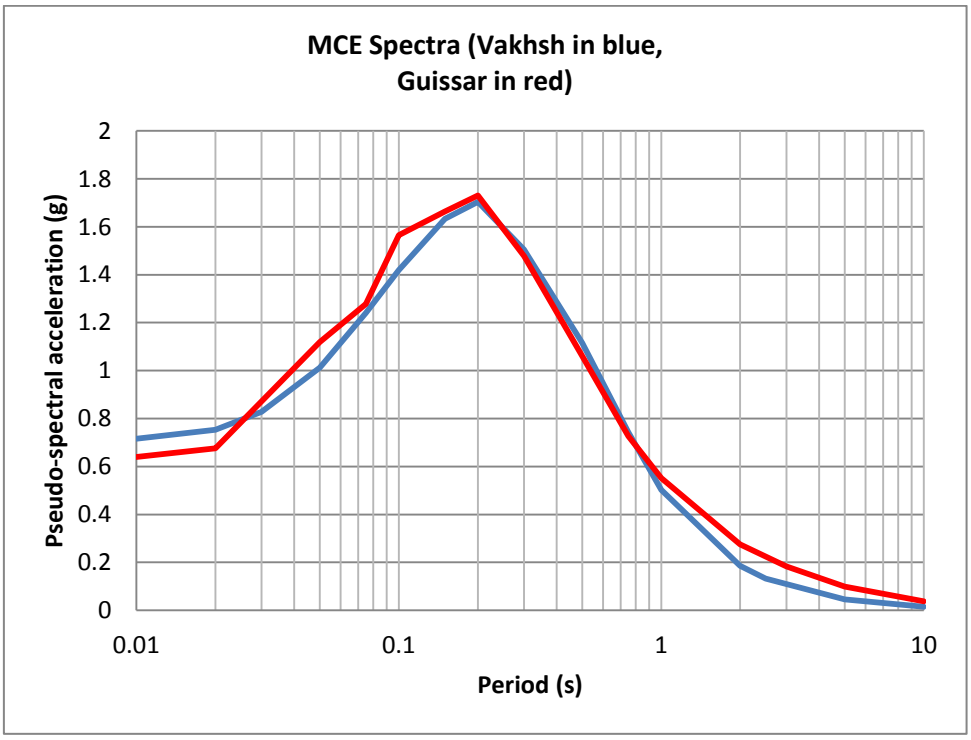

Figure 26 – *Comparison between the proposed response spectra for 5% damping associated to both the Guissar and Vakhsh faults.*

8.4 Co-seismic displacements potentially affecting the dam foundation

To evaluate co-seismic displacement on critical faults, we used the internationally-recognized Wells and Coppersmith (1994) relationships. These relationships have been derived from an international and large data set and are considered more representative than those proposed by Nikonov (1975) for the mountain regions of Middle Asia.

8.4.1 For the Guissar fault system:

Taking into account its location and attitude (north-western dip), this fault cannot generate co-seismic rupture directly in the dam foundation.

8.4.2 For the Vakhsh thrust system:

Taking into account its location and attitude (south-eastern dip), this fault cannot generate co-seismic rupture directly in the dam foundation.

8.4.3 For the Ionakhsh ramps:

Taking into account the location of the Ionaksh ramps in the upstream part of the dam foundation, a first appraisal of potential co-seismic displacement along the Ionaksh ramp associated with the MCE (Mw 5.9) has been carry out. In this study, we estimate both the average and the maximum displacements (mean and mean ±1σ) derived for reverse faulting (Wells and Coppersmith, 1994). At this stage we assumed that all significant co-seismic displacement occurs on the main fault plane. Estimates are reported in Table 16.

Ionakhsh ramp (5.9 Mw)	Mean value - 1 standard deviation	Mean value	Mean value + 1 standard deviation
Maximum displacement	0.28 m	0.74 m	1.95 m
Average displacement	0.22 m	0.54 m	1.30 m

Table 16: Estimates of co-seismic displacements associated with the MCE on the Ionaksh ramp.

It must be noted that these estimates show large uncertainties. A conservative scenario would be to adopt the value obtained throughout the maximum displacement value at the mean-plus-one-standard-deviation. Based on present knowledge, one cannot disregard that part of the displacement occurs by creeping and/or by secondary faulting. This point should be carefully considered during the next stage of the design.

8.4.4 For the Gulizindan ramp:

Taking into account its location and attitude (south-eastern dip), this fault cannot generate co-seismic rupture directly in the dam foundation.

8.4.5 Dam foundation between Ionakhsh and Gulizindan ramps

Potential internal deformation of the block between the Ionaksh and Gulizindan Faults also has to be considered since it forms the foundations of the dam and its appurtenant structures.

Intense shortening of the Mesozoic cover can be assumed to have caused the formation of antithetic faults (back thrust) such as F#35, allowing for the upwards extrusion of blocks.

Based on such assumptions, shearing along these secondary faults are very likely disconnected from deep seismic rupture along the Ionaksh and Gulizindan ramps (faults) and may be interpreted as stress relaxation within the hanging wall post-dating the earthquake event. Taking into account the limited extension of those faults (a few hundreds of meters), we consider that maximum incremental displacement (the nature of which is still to be identified) should be around a tenth of the deformation on the bounding fault and thus remains of the order of 10-20 cm.

8.5 Design Earthquake for the Construction phase

The PSHA will furnish response spectra for various periods of return that will allow assessing, during the detailed design phase, the stability and safety conditions of the dam and other structures during the construction and operation of Rogun.

9 RESERVOIR TRIGGERED SEISMICITY

9.1 Potential induced seismicity linked to the dam

It has long been known that the creation of reservoirs (e.g. through the construction of a dam) can lead to increased seismicity [the state of knowledge on the subject can be found in Bulletin ICOLD 137 (2011) “Reservoirs and seismicity, State of knowledge”]. This seismicity is caused by over-loading of nearby faults and/or to lubrication of wetted faults in the surrounding rock. The chance of such seismicity is linked to the height of the water column and its variation and seismicity may occur immediately after the filling or some years later (e.g. Simpson et al., 1988). These induced/triggered earthquakes can be large and destructive. For example, reservoir impoundment at Koyna Dam (Maharashtra, India) led to a significant increase in seismicity, with a damaging earthquake of Ms 6.3 occurring on 10th December 1967 (Gupta, 2002).

The assessment of the chance of triggered/induced seismicity and its characteristics is highly uncertain and would require detailed information on, for example, the state of stress in the region, status of nearby faults and information on the planned filling programme of the reservoir. Wieland (2013) states that any large dam of height greater than 100m (the case for the Rogun dam) has the potential of triggering/inducing seismicity. Wieland (2013) states that the required information to make an assessment includes: tectonic conditions and data on structural geology, supported by the study of aerial photographs; macroseismic data; information on all active faults and details on recent fault activity in region; assessment of seismic capability of all faults in region; and the information on the underground water. Even if such information was available it would require considerable time and resources to make a site-specific estimate and it would still be prone to large uncertainties.

Therefore, in this chapter a simple approach based on analogues to previous cases of induced seismicity for similar reservoirs in tectonically-comparable regions will be followed. This work is based on recent reviews of triggered/induced seismicity by, for example, Gupta (2002), the National Research Council (2012) and Klose (2013). It will lead to rough estimates of the characteristics (e.g. magnitude) of the induced earthquakes that could be expected. However, as stated above there is considerable uncertainty in the assessment of triggered/induced seismicity and, therefore, other earthquakes could be possible.

The following section lists previous examples of reservoir-triggered/induced seismicity in tectonically-comparable areas to Tajikistan for similar-sized dams and volumes of water. Based on these examples, the subsequent section presents the scenarios of induced seismicity considered within the seismic hazard assessment.

Reservoir-induced seismicity refers to earthquakes that are directly caused by the reservoir and would not have occurred without its presence whereas reservoir-triggered seismicity refers to earthquakes that would probably have occurred in the future without the reservoir but their occurrence time is brought forward by its presence. Often these two terms have been used interchangeable and lists of reservoir-related earthquakes general include both.

9.2 Previous examples of reservoir-triggered/induced seismicity

The following examples of reservoir-triggered/induced seismicity that could be considered analogues of the Rogun Dam are taken from Appendix C of the report of the National Research Council (2012), which appears to be strongly based on the review by Gupta (2002), and Table 1 of Klose (2013). One key characteristic of the reservoir that helps assess the characteristics of the induced seismicity is the reservoir’s gross capacity (full supply level, FSL). Another key indicator for assessing the chance of triggering or inducing large earthquakes is the tectonic regime, which for Tajikistan is compressional leading to reverse-faulting events.

Searching the list of triggered/induced earthquakes by Klose (2013) for reverse-faulting events with magnitudes (provided by Klose, 2013) over 5 associated with such large reservoirs highlights these examples:

- Mw 7.9: 2008 Sichuan/Wenchuan (China) earthquake associated to the Zipingpu Dam (reservoir volume 1.1 billion m^3) – this is the largest triggered/induced earthquake listed by Klose (2013) in any tectonic regime or by any type of human cause (e.g. injection, mining or extraction);
- Mw 6.1: 1993 Killari (India) earthquake associated to the nearby reservoir (reservoir volume 125 million m^3);
- ML 5.9: 1983 Srinagarind (Thailand) earthquake associated to the nearby dam (reservoir volume 11.8 billion m^3);
- ML 5.0: 1996 Thomson (Australia) earthquake associated to the nearby dam (reservoir volume 1.1 billion m^3).

For other faulting mechanisms (normal and strike-slip) Klose (2013) lists these large earthquakes (again the magnitudes are provided by Klose, 2013):

- Ms 7.1: 1959 Lake Hebgen (USA) normal earthquake associated to the nearby dam (reservoir volume 994 million m^3);
- Ms 6.3: 1967 Koyna (India) normal earthquake associated to nearby dam (reservoir volume 2.78 billion m^3);
- Ms 6.1: 1962 Xinfengjiang (China) strike-slip earthquake associated to nearby dam (reservoir volume 11.5 billion m^3);
- mb 5.8: 1962 Kariba (Zambia) normal earthquake associated to nearby dam (reservoir volume 175 billion m^3);
- ML 5.8: 1975 Oroville (USA) normal earthquake associated to nearby dam (reservoir volume 4.4 billion m^3);
- Mw 5.7: 1981 Aswan (Egypt) normal earthquake associated to nearby dam (reservoir volume 164 billion m^3);
- Ms 5.6: 1966 Kremasta (Greece) normal earthquake associated to nearby dam (reservoir volume 4.75 billion m^3);
- ML 5.3: 1962 Monteynard (France) normal earthquake associated to nearby dam (reservoir volume 275 million m^3);
- ML 5.3: 1977 Charvak (Uzbekistan) normal earthquake associated to nearby dam (reservoir volume 3 billion m^3);
- ML 5.2: 1974 Shenwo (China) strike-slip earthquake associated to nearby dam (reservoir volume 540 million m^3);
- ML 5.0: 1966 Benmore (New Zealand) normal earthquake associated to nearby dam (reservoir volume 2.04 billion m^3);
- ML 5.0: 1939 Hoover (USA) normal earthquake associated to nearby dam (reservoir volume 36 billion m^3).

The list by the National Research Council (2012) includes these additional examples (magnitude scales not given):

- M 5.7: 1938 Marathon (Greece)
- M 5.4: 1973 Varragamba (Australia)
- M 5.3: 1964 Akosombo (Ghana)
- M 5.3: 1969 Kinnersani (India)
- M 5.2: 1962 Coyote Valley (USA)
- M 5.1: 1974 Porto Colombia (Brazil)
- M 5.0: 1959 Eucumbene (Australia)

Klose (2013) suggests a positive correlation between the mass change (in the case of reservoirs due to the water volume) and the size of the maximum triggered/induced earthquake but this correlation is quite weak (e.g. his Figure 3).

Based on this list of previous earthquakes it could be suggested that the magnitude of the scenario for the triggered/induced earthquake for the Rogun Dam should be at least Mw 7.9 based on the Sichuan/Wenchuan earthquake or Ms 7.1 based on the Lake Hebgen earthquake (although this occurred in an extensional tectonic regime so it may not be relevant for Tajikistan). However, whether these earthquakes were actually triggered/induced by the presence of the nearby dams is not clear.

The 1959 Lake Hebgen (Montana) earthquake occurred, in a seismically-active region, 44 years after the reservoir began to be filled by the creation of Hebgen Dam. The Bulletin of the Seismological Society of America volume 52 (number 2, 1962) includes five articles on this earthquake that remain the most comprehensive studies on this event, which occurred in a sparsely-populated and poorly-instrumented area before the advent of a worldwide (digital) seismographic network. Although the epicentral area of this earthquake coincided with the dam and reservoir there seems to be little evidence in the literature (e.g. none of the 1962 series of articles mention this possibility) that this event was triggered by the presence of the dam. Lists of reservoir-related earthquakes other than that by Klose (2013) do not include this event (e.g. Gupta, 2002).

In contrast to this 1959 earthquake the 2008 Sichuan/Wenchuan shock has been extremely well studied in hundreds of published articles. The question of whether it was triggered by the loading of the reservoir impounded by the Zipingpu Dam, which began filling in 2006 (i.e. roughly two and half years before) has been studied by various authors. Ge et al. (2009) model the static surface loading from the reservoir on the nearby Beichuan thrust fault system, which ruptured during the 2008 earthquake and which was within a few hundred metres of the reservoir. They conclude that this loading 'advanced the clock' on the occurrence of the mainshock by tens to hundreds of years. Klose (2011) undertakes a similar analysis and reaches similar conclusions. On the other hand Deng et al. (2010) undertake comparable analysis and conclude that there is a very low probability that the mainshock, which propagated from a depth of around 20km, was induced by the reservoir (although the shallower, at depths of less than 5km, seismicity may have been induced). Similar conclusions were reached by Gahalaut and Gahalaut (2010). In addition, many other articles on both sides of the argument have been published to date.

If these two earthquakes are excluded from consideration then the largest triggered/induced earthquake yet recorded is the Koyna 1967 earthquake (Ms 6.3). Wieland (2013) states that the size of the largest reservoir-trigger earthquake has, up until now, always been lower than the Safety Evaluation Earthquake.

Another way of seeking to assess the chance of induced seismicity from the Rogun Dam is to look at the seismicity connected with existing dams in the same region. In Tajikistan, the Nurek dam is one of first large dams with seismic records before and after impounding (Simpson & Negmatullaev, 1981; Keith et al 1982). The seismotectonic setting for Nurek is similar to the one at Rogun. In the case of the Nurek dam, recorded seismicity is in the magnitude range 1.4 to 4.6. The most intense bursts of increased seismicity were related to rapid increases in water level during the first stages of filling. The largest earthquakes all followed decreases in the filling rate of approximately 0.5 m/day (Simpson & Negmatullaev, 1981). An increase of seismicity is not observed on the major faults near the dam (Keith et al., 1982).

Earthquakes of non-tectonic nature have shallow focus, have relatively small magnitudes and often occur shortly after reservoir impounding or following sudden reservoir water level fluctuations. Generally, on the basis of existing case histories, these earthquakes have magnitudes of less than 5 (from waterpowermagazine.com: the relationship between large reservoirs and seismicity, 2010).

In the case of the Rogun dam, if induced seismicity is of non-tectonic nature, we can expect a maximum magnitude less than 5. Higher earthquakes could be observed if the changes in the stress field affect the closest active faults, but this will not increase the maximum magnitude on the faults. Maximum observed magnitude clearly related with a dam is 6.3. "In all the cases, it is unlikely to trigger the Safety Evaluation Earthquake (SEE) by a reservoir –this has not yet happened (sic)" (Wieland, 2013).

Wieland (2013) states moreover that, rather than reservoir-related seismicity, the most dangerous hazards for large dams are mass movements (e.g. rock falls and landslides) into the reservoir, causing overtopping of the dam or large forces onto the structure, or directly onto the dam itself. Such mass movements could be triggered by earthquakes as well as other causes, e.g. heavy rain fall. These hazards are outside the scope of this analysis and are not discussed further here.

10 PROPOSED SEISMIC MONITORING

In the context of Rogun, two kinds of seismic instrumentation are required:

- **a strong-motion network** (accelerometers) to survey the seismic behavior of the dam under strong earthquakes. For this purpose, accelerometers need to be located in the free field away from the dam, in the dam abutments and in the dam body.

- **a microseismic network** around the dam and in the reservoir region, which could record the background seismicity prior to the start of dam construction (at least two years before is generally the time period recommended) and the seismicity during construction, the first filling of the reservoir and the subsequent years of reservoir operation. Instruments should be digital seismic stations with velocity sensors. The number of instruments and geographic distribution depend on the desired threshold magnitude, the size of the reservoir and the regional seismic network already in place. Six to eight stations seems to be a minimum. A distribution of one station every 5 km is required if the network is to detect events as low as M~1.0.

It is recommended to implement this seismic monitoring as soon as possible in order to estimate the background (base-line) seismicity prior to the dam construction.

11 RECOMMENDATIONS FOR PSHA

For the seismic design of the different structures and elements of a large dam project ICOLD (2010) recommends defining the following design earthquakes:

Maximum Design Earthquake (MDE): For large dams the return period of the MDE is taken as **10,000 years**. The MDE ground motion parameters are to be **estimated based on a PSHA**. According to ICOLD (2010) the mean values of the ground motion parameters of the MDE shall be taken. In the case where a single seismic source (fault) mainly contributes to the seismic hazard, uniform hazard spectra can be used for the seismic design. Otherwise, **based on the disaggregation of the seismic hazard** (magnitude versus source-to-site distance) different scenario earthquakes may be defined. This seems to be the case for Rogun.

Safety Evaluation Earthquake (SEE): The SEE is the earthquake ground motion a dam must be able to resist without uncontrolled release of the reservoir. For major dams the **SEE can be taken as the MDE ground motions** discussed above. The SEE is the governing earthquake ground motion for the safety assessment and seismic design of the dam and safety-relevant components, which have to be functioning after the SEE. **MCE is considered as an upper limit for the SSE.**

Design Basis Earthquake (DBE): The DBE with a return period of 475 years is the reference design earthquake for the appurtenant structures in Europe. The DBE ground-motion parameters are **estimated based on a PSHA**. The mean values of the ground motion parameters of the DBE can be taken.

Operating Basis Earthquake (OBE): The OBE may be expected to occur during the lifetime of the dam. No damage or loss of service must occur. It has a probability of occurrence of about 50% during the service life of 100 years. The return period is taken as 145 years (ICOLD 2010). The OBE ground motion parameters **are estimated based on a PSHA**. The mean values of the ground motion parameters of the OBE can be taken.

The design criteria are associated to return periods of earthquake ground motion. Only PSHA can define these ground motion levels, taking into account epistemic uncertainties associated with the assumptions and the choice of parameters and procedures. We highly recommend performing such a state-of-the-art PSHA to derive the seismic criteria to be used in the future detailed dam design phase.

Guidelines for such a PSHA are given in appendix 3.

12 REFERENCES

12.1 Reports

Babaev et al. (2005) “Seismic Conditions on the Territory of Tajikistan”

Bankable Feasibility Study for Stage 1 Construction - Volume 3C - "Geology, Geotechnics and Seismic Characteristics" - Part 3 of 3 - Lahmeyer - April 2006.

Rogunskaya hydropower station on the Vaksh River, Technical project. Gidroproyekt Tashkent 1978.

Rogun Hydroelectric Plant in the Republic of Tajikistan, Bankable Feasibility for Stage 1 Construction Completion. Geology, Geotechnics and Seismic Characteristics. LI, 2006Specification of prestack seismicity of the area of Rogunskaya HPS and definition of design EQ effect parameters - Information Report - Geodynamics Research Center LCC – 2005.

Specification of initial seismicity of Rogun HPP area and characterization of the designed seismic loads (second stage) - Hydrospecproject - report n°2360-BTK2-001 – 2005.

Specifying the initial seismicity of Rogun HPS region and determining the parameters of predicted seismic effect (first phase) - Hydrospecproject- report n°2360-VTK2-001 – 2005.

Verification of reference seismicity of Rogun HEP Site and Estimation of design seismic impact parameters - Estimation of design seismic impact parameters of Rogun HEP - Geodynamics Research Center LCC – 2005.

12.1 Articles

Akkar, S., and Bommer, J. J., 2010, Empirical equations for the prediction of PGA, PGV and spectral accelerations in Europe, the Mediterranean region and the Middle East, Seismological Research Letters, 81(2), 195–206.

Akkar, S., Sandıkkaya, M. A. and Bommer, J. J., 2013, Empirical ground-motion models for point- and extended-source crustal earthquake scenarios in Europe and the Middle East. Bulletin of Earthquake Engineering, in press.

Ancheta, T. D., Darragh, R. B., Stewart, J. P., Seyhan, E., Silva, W. J, Chiou, B. S. J., Wooddell, K. E., Graves, R. W., Kottke, A. R., Boore, D. M., Kishida, T., Donahue, J. L., 2013, PEER NGA-West2 Database, PEER Report 2013/03, Pacific Earthquake Engineering Research Center, University of California, Berkeley.

Bazhenov, M. L., and Burtman, V. S., 1982, Kinematics of the Pamir arc, Geotectonics, 3, 100-120

Bekker, A., 1996, Tectonics of the Afghan-Tajik depression (in Russian), Geotektonika, 1, 76-82,

Billington, S., Isacks, B. L. and Barazangi, M., 1977, Spatial distribution and focal mechanisms of mantle earthquakes in the Hindu Kush-Pamir region: A contorted Benioff zone, Geology, 5, 699-704.

Bommer, J. J., Douglas, J., Scherbaum, F., Cotton, F., Bungum, H. and Fäh, D., 2010, On the selection of ground-motion prediction equations for seismic hazard analysis, Seismological Research Letters, 81(5), 783-793. DOI: 10.1785/gssrl.81.5.783.

Bommer, J. J., Akkar, S. and Drouet, S., 2012, Extending ground-motion prediction equations for spectral ordinates to higher response frequencies, Bulletin of Earthquake Engineering 10(2), 379-399.

Boore, D. M., and Atkinson, G. M., 2008, Ground-motion prediction equations for the average horizontal component of PGA, PGV, and 5%-damped PSA at spectral periods between 0.01 s and 10.0 s, Earthquake Spectra, 24(1), 99–138.

Boore D. M., Stewart, J. P., Seyhan, E., Atkinson, G. M., 2013, NGA-West2 Equations for Predicting Response Spectral Accelerations for Shallow Crustal Earthquakes, PEER Report 2013/05, Pacific Earthquake Engineering Research Center, University of California, Berkeley.

Bulletin ICOLD 137, 2011, Reservoirs and seismicity, State of knowledge".

Burtman, V. S., Molnar, P., 1993, Geological and geophysical evidence for deep subduction of continental crust beneath the Pamir. Special Paper of the Geological Society of America, 281.

Burtman, V. S., 2000, Cenozoic crustal shortening between the Pamir and Tien Shan and a reconstruction of the Pamir–Tien Shan transition zone for the Cretaceous and Palaeogene, Tectonophysics, 319, 69–92.

Campbell, K. W., and Bozorgnia, Y., 2008, NGA ground motion model for the geometric mean horizontal component of PGA, PGV, PGD and 5% damped linear elastic response spectra for periods ranging from 0.01 to 10 s, Earthquake Spectra, 24(1), 139–171.

Campbell, K. W., and Bozorgnia, Y., 2013. NGA-West2 Campbell-Bozorgnia Ground Motion Model for the Horizontal Components of PGA, PGV, and 5%-Damped Elastic Pseudo-Acceleration Response Spectra for Periods Ranging from 0.01 to 10 sec, PEER Report 2013/06,Pacific Earthquake Engineering Research Center, University of California, Berkeley

Chatelain, J. L., Roecker, S. W. Hatzfeld, D., and Molnar, P., 1980, Microearthquake seismicity and fault plane solutions in the Hindu Kush region and their tectonic implications, Journal of Geophysical Research, 85, 1365-1387.

Deng, K., Zhou, S., Wang, R., Robinson, R., Zhao, C. and Cheng, W., 2010. Evidence that the 2008 Mw 7.9 Wenchuan earthquake could not have been induced by the Zipingpu Reservoir, Bulletin of the Seismological Society of America, 100(5B), 2805-2814, DOI: 10.1785/0120090222.

Douglas, J., 2011. Ground-motion prediction equations 1964-2010, Final report, BRGM/RP-59356-FR, 444 pages, 9 illustrations.

Evans, S. G., Roberts, N. J., Ischuk, A., Delaney, K. B., Morozova, G. S. and Tutubalina, O., 2009. Landslides triggered by the 1949 Khait earthquake, Tajikistan, and associated loss of life, Engineering Geology, 109, 195–212.

Fan, G., Ni, J. F. and Wallace, T. C., 1994, Active tectonics of the Pamirs and Karakorum, Journal of Geophysical Research, 99, 7131–7160.

Gahalaut, K. and Gahalaut, V. K., 2010, Effect of the Zipingpu reservoir impoundment on the occurrence of the 2008 Wenchuan earthquake and local seismicity, Geophysical Journal International, 183(1), 277-285, DOI: 10.1111/j.1365-246X.2010.04715.x.

Ge, S., Liu, M., Lu, N., Godt, J. W. and Luo, G.,2009. Did the Zipingpu Reservoir trigger the 2008 Wenchuan earthquake? Geophysical Research Letters, 36(20), DOI: 10.1029/2009GL040349.

Gubin, I., 1960, Patterns of seismic events in the territory of Tadzhikistan [in Russian]: Moscow, Akademii Nauk SSSR, 464 p.

Gupta, H. K., 2002, A review of recent studies of triggered earthquakes by artificial water reservoirs with special emphasis on earthquakes in Koyna, India, Earth-Science Reviews, 58(3–4), 279–310

Guseva, T. V., Lukk, A. A., Pevnev, A. K., Skovorodkin, Y. P., and Shevchenko, V. I., 1983, Geodynamics of the Garm polygon region in Tadzhikistan, Izvestiya, Physics of the Solid Earth, 19, 506-518.

Hamburger, M. W., Sarewitz, D. R., Pavlis, T. L. and Popandopulo, G. A., 1992, Structural and seismic evidence for intracontinental subduction in the Peter the First Range, Central Asia. Bulletin of the Geological Society of America, 104, 397–408.

ICOLD ,2010, Selecting seismic parameters for large dams: guidelines, Bulletin 148 (Bulletin 72, 2010 revision), International Commission on Large Dams.

Keith, C., Simpson, D. W. and Soboleva, O. V., 1982, Induced seismicity and style of deformation at Nurek Reservoir, Tadjik SSR, Journal of Geophysical Research, 87, 4609-4624.

Klose, C. D., 2011, Evidence for anthropogenic surface loading as trigger mechanism of the 2008 Wenchuan earthquake, Environmental Earth Science, 66, 1439-1447. DOI 10.1007/s12665-011-1355-7.

Klose, C. D., 2013, Mechanical and statistical evidence of the causality of human-made mass shifts on the Earth's upper crust and the occurrence of earthquakes, Journal of Seismology, 17(1), 109-135.

Kravchenko, K. N., 1979, Tectonic evolution of the Tien Shan, Pamir, and Karakorum, in Farah, A., and DeJong, K. A., eds., Geodynamics of Pakistan: Islamabad, Pakistan, Geological Survey of Pakistan, 303-317.

Kristy, M. J., and Simpson, D. W., 1980, Seismicity changes preceding two recent Central Asian earthquakes: Journal of Geophysical Research, 85, 4829-4837.

Leith, W., 1982, Rock assemblages in Central Asia and the evolution of the southern Asian margin, Tectonics, 1, 303-318.

Leith, W., 1985, A mid-Mesozoic extension across Central Asia?: Nature, 313, 567-570.

Leith, W., and Alvarez, W., 1985, Structure of the Vakhsh fold and thrust belt, Tadjik SSR: An application of Landsat imagery to continuous-structure mapping, Bulletin of the Geological Society of America, 96, 875-885.

Leith, W., and Simpson, D. W., 1986, Seismic domains within the Gissar-Kokshal seismic zone, Soviet Central Asia, Journal of Geophysical Research, 91, 689-697.

Leonov, N.N., 1960, The Khait, 1949 earthquake and geological conditions of its occurrence, Izvestia of the Academy of Sciences of the USSR, Geophysical Series, 3, 409–424 (In Russian).

Leonov, Y. G., and Nikonov, A. A., 1988, Problems of the neotectonic development of the Pamir-Tien Shan mountain complex, Geotectonics, 22(2), 178-187.

Loziyev, V. P., 1968, Geologic structure, in Nebzevetsky, P., ed., Atlas of Tadjikistan: Dushanbe, Akademii Nauk Tadzhik SSR, 16.

Lukk, A. A., Nersesov, I. L., Pevnev, A. K., and Yunga, S. L., 1980, Present day movements of the western part of the Peter I Range from geodetic and seismological data: Izvestiya, Physics of the Solid Earth, 16(5), 32-41.

Lukk, A. A., and Shevchenko, V. I., 1986, Character of the deformation of the earth's crust in the Garm region, Tadjikistan, from geological and seismic data: Izvestiya, Physics of the Solid Earth, 22(7), 527-539.

Lukk, A. A., and Yunga, S. L., 1988, Stress-strain state of the earth's crust in the Garm region. II. Reconstruction results: Izvestiya, Physics of the Solid Earth, 24, 513-523.

Lukk, A. A., Yunga, S. L., Shevchenko, V. I. and Hamburger, M. W., 1995, Earthquake focal mechanisms, deformation state, and seismotectonics of the Pamir–Tien Shan region, Central Asia, Journal of Geophysical Research, 100 (B10), 20321–20343.

Makhamov, R., Mavlyanov, S. R., Niyazov, B. N. and Dzhumankulov, M. Kh., 1985, Non-anticlinal traps—a source for increasing oil and gas reserves in the Soviet part of the Afghan–Tajik depression, Petroleum Geology, 19, 486–488.

Molnar, P., Fitch, T., and Wu, F., 1973, Fault plane solutions and contemporary tectonics in Asia, Earth and Planetary Science Letters, 9, 101-112.

Molnar, P., and Tapponnier, P., 1975, Cenozoic tectonics of Asia: Effects of a continental collision, Science, 189, 419-426.

National Research Council, 2012, Induced seismicity potential in energy technologies, The National Academies Press, Washington D.C., USA

Negredo, A. M., Replumaz, A., Villaseñor, A. and Guillot, S., 2007, Modeling the evolution of continental subduction processes in the Pamir–Hindu Kush region, Earth and Planetary Science Letters, 259, 212–225.

Nelson, M. R., McCaffrey, R., and Molnar, P., 1987, Source parameters for 11 earthquakes in the Tien Shan Central Asia, determined by P and SH waveform inversion, Journal of Geophysical Research, 92, 12629-12648.

Ni, J., 1978, Contemporary tectonics in the Tien Shan region, Earth and Planetary Science Letters, 41, 347-354.

Nikonov A. A., 1975, Recent seismotectonic fault movement in the mountain regions of middle Asia and their relation with earthquake magnitude, Tectonophysics, 29, 439-446

Pavlis, T. L. and Hamburger, M. W., 1990, The Jura-Cretaceous Tadjik depression, Soviet central Asia: Rifted margin of Asia vs foreland basin, Geological Society of America Abstracts with Programs, 7, A144.

Pavlis, T. L., Hamburger, M. W. and Pavlis, G. L., 1997, Erosional processes as a control on the structural evolution of an actively deforming fold and thrust belt: an example from the Pamir–Tien Shan region, central Asia, Tectonics, 16, 810–822.

Pavlis, G. L., Das, S., 2000, The Pamir–Hindu Kush seismic zone as a strain marker for flow in the upper mantle, Tectonics, 19, 103–115.

Pegler, G., Das, S., 1998, An enhanced image of the Pamir–Hindu Kush seismic zone from relocated earthquake hypocentres, Geophysical Journal International, 134, 573–595.

Pevnev, A. K., Guseva, T. V., Odinev, N. N., and Saprykin, G. V., 1975, Regularities of the deformations of the Earth's crust at the joint of the Pamirs and the Tien Shan, Tectonophysics, 29, 429-438.

Rautian, T. and Leith, W., 2002, Composite regional catalogs of earthquakes from the Former Soviet Union, United States Geological Survey Open File Report 02-500.

Schneider F. M., Yuan, X., Schurr, B., Mechie, J., Sippl, C., Haberland, C., Minaev, V., Oimahmadov, I., Gadoev, M., Radjabov, N., Abdybachaev, U., Orunbaev, S. and Negmatullaev, S., 2013. Seismic imaging of subducting continental lower crust beneath the Pamir, Earth and Planetary Science Letters, 375, 101–112.

Scordilis E. M., 2006. Empirical global relations converting MS and mb to moment magnitude. Journal of Seismology 10: 225–236.

Shebalin, N. V., 1959, Determination of earthquake depth on its magnitude and microseismicity data (on the example of Caucasus earthquakes), Th Of Institute of Geophysics of AS of Georg. SSR, 20, 1959.

Shirokova, Y. I., 1974, A detailed study of the stresses and fault planes at earthquake foci of Central Asia, Izvestiya, Physics of the Solid Earth, II, 707-717.

Shirokova, Y. I., 1979, Features of the mechanism of the earthquake foci of Central Asia, Izvestiya, Physics of the Solid Earth, 15, 714-722.

Simpson, D. W. and Negmatullaev, S. K., 1981, Induced seismicity at Nurek Reservoir, Bulletin of the Seismological Society of America, 71, 1561-1586.

Simpson, D. W., Leith, W. S. and Scholz, C. H., 1988, Two types of reservoir-induced seismicity, Bulletin of the Seismological Society of America, 78, 2025–2040.

Skobolev, S. F., and Florensky, P. V., 1974, Holocene tectonic deformation and landslides in the Vakhsh thrust zone, Geotectonics, 8, 104-107.

Skobolev, S. F., 1977, Horizontal compression and folding in the Peter I Range, Geotectonics, 11, 144-152.

Tapponnier, P., Mattauer, M., Proust, F., and Cassaigneau, C., 1981, Mesozoic ophiolites, sutures, and large-scale tectonic movements in Afghanistan, Earth and Planetary Science Letters, 52, 355-371.

Tapponnier, P., Peltzer, G., Le Dain, A. Y., Armijo, R. and Cobbold, P., 1982, Propagating extrusion tectonics in Asia: new insights from simple experiments with Plasticine, Geology, 10, 611-616.

Trifonov, V. G., 1978, Late Quaternary tectonic movements of western and central Asia, Bulletin of the Geological Society of America, 89, 1059-1072.

Villaseñor, A., Spakman, W., Engdahl, E. R., 2003. Influence of regional travel times in global tomographic models. EGS–AGU– EUG Joint Assembly, Nice

Wells, D. L and Coppersmith, K. J., 1994, New empirical relationships among Magnitude, Rupture Length, Rupture Width, Rupture Area, and Surface Displacement, Bulletin of the Seismological Society of America, 84(4), 974-1002.

Wieland, M., 2013, Dam Safety Aspects of Reservoir-Triggered Seismicity, Presentation at the workshop on ‘Seismic impacts to dams and reservoirs’, Hanoi, March 17th – 19th.

Zakharov, S. A., Kukhtikov, M. M., Leven, Y. Y. and Vinm'chenko, G. T., 1968, Tectonics, in Nebzevetsky, P., ed., Atlas of Tadjikistan: Dushanbe, Akademii Nauk Tadzhik SSR, 17-20.

Zonenshain, L. P., Kuzmin, M. I., and Natapov, L. M., 1990, Geology of the USSR: A plate-tectonics synthesis, Washington, D.C., American Geophysical Union Geodynamics Series, 21, 242 p.

APPENDIX 1

SEISMICITY CATALOGUE

CASRI (1895-2009) + ISC (2010-2013)

APPENDIX 1

Seismicity catalogue

CASRI (1895-2009) + ISC (2010-2013)

Year	Month	Day	Hour	Min	Sec	Lat	Lon	Depth	Mw_conv	Name
1896	9	23	23	20		37	71	160	7,5	
1907	10	21	4	23	20	38,5	67,9	35	7,4	Karatagskoye 1
1949	7	10	3	53	38	39,2	70,8	16	7,4	Khaitskoye
1962	7	6	23	5	33	36,8	70,1	210	7,4	
1907	10	21	4	44		38,7	68,1	24	7,3	Karatagskoye 2
1917	4	21	0	49	49	37	70,5	220	7,3	
1908	10	24	21	16	36	37	70	220	7,1	
1943	2	28	12	54	35	36,8	70,8	280	7,1	
1903	4	19	13	25		37	71	160	7,0	
1902	8	30	21	50		37	71	33	6,8	
1922	12	6	13	55	36	37,4	71,3	230	6,8	Sheevskoye
1927	4	18	15	2	0	37	71	200	6,8	
1897	9	17	17	19		39,9	68	45	6,7	Uratubynskoye 2
1948	9	7	8	15	22	36,9	70,6	220	6,7	
1897	9	17	15	10		39,8	68,4	25	6,6	Uratubynskoye 1
1934	8	31	14	57	47	38,9	70,9	8	6,5	Argankulskoye 1
1937	10	29	7	26	37	36,6	70,1	200	6,5	
1998	5	30	6	22	28	37,15	70,12	30	6,5	
1923	12	28	22	24	48	39,6	69,2	18	6,4	Gardanskoye
1924	9	16	2	36	2	38,9	70,5	20	6,4	
1941	4	20	17	38	27	39,2	70,5	8	6,4	Garmskoye 1
1960	1	9	7	24	5	36,7	70,1	210	6,4	
1888	11	28	6	40		40	69,8	20	6,3	Kostakozskoye
1955	6	3	14	1	53	36,9	70,8	80	6,3	
1955	7	3	14	1	53	36,9	70,8	80	6,3	
1958	3	28	12	6	25	36,9	71	190	6,3	
1984	10	26	20	22	20	39,25	71,26	15	6,3	Dzhygartalskoye
1822	9					40,3	71,5	12	6,2	
1823	1	1				40,3	71,5	12	6,2	
1907	10	27	5	17		38,8	68,4	24	6,2	Chuyanchynskoye
1924	9	17	10	20	51	36,8	70,7	100	6,2	
1930	9	11	17	20	12	36,7	70,1	220	6,2	
1935	7	5	17	53	0	38,3	67,4	18	6,2	Baysunskoye 1
1949	7	10	15	49	17	39,2	71,1	19	6,2	
1949	7	10	16	24	0	39,1	71	14	6,2	
1952	11	27	7	20	32	36,6	70	150	6,2	
Year	**Mont**	**Day**	**Hour**	**Min**	**Sec**	**Lat**	**Lon**	**Depth**	**Mw_con**	**Name**

	h								v	
1990	2	5	5	16	44	37,09	71,29	89	6,2	
1935	10	8	9	19	6	38,8	70,8	8	6,2	Argankulskoye 2
1951	6	12	22	40	41	36,7	70,4	240	6,2	
1952	5	28	7	47	44	37	70,8	230	6,2	
1960	7	6	5	16	48	36,8	70,5	210	6,2	
1969	11	24	17	23	21	37,3	71,4	113	6,2	
1902	8	12	17	16		39,5	68,5	35	6,1	
1925	5	14	7	10	56	37	69,5	150	6,1	
1929	3	3	3	11	3	36,8	70,7	200	6,1	
1935	5	12	5	20	24	37,5	71,2	100	6,1	
1943	1	11	19	50	18	38,62	69,3	10	6,1	Fayzabadskoye 2
1957	4	26	2	11	54	36,8	70,6	180	6,1	
1957	8	20	15	21	11	36,9	71	210	6,1	
1959	3	2	15	51	43	37	70,5	220	6,1	
1961	9	28	5	0	45	36,8	70,5	200	6,1	
1893	11	5	3	30		39,5	69,4	40	6,0	
1923	8	31	2	15	54	38,5	72	10	6,0	
1932	10	29	11	8	50	39,2	72,2	20	6,0	
1951	4	14	4	10	6	39,1	71,6	25	6,0	
1968	1	29	5	0	11	36,7	70,2	230	6,0	
1970	9	4	13	12	1	36,7	70,1	280	6,0	
1977	1	31	14	26	15	40,08	70,86	20	6,0	Isfara-Batkenskoye
2007	1	8	17	21	48	39,7	70,35	0	6,0	
1902	4	17	21	10	0	40	71	30	6,0	
1933	5	27	22	41	58	37	70,5	230	6,0	
1939	5	30	10	7	6	38,98	70,45	6	6,0	Karategynskoye 2
1940	10	5	14	44	33	37,2	69	15	6,0	
1949	7	10	15	19	0	39,1	71	10	6,0	
1949	7	19	17	42	12	39,1	71,1	10	6,0	
1955	1	10	4	25	50	37,2	70,8	100	6,0	
1957	1	20	18	12	50	36,9	71	80	6,0	
1958	1	6	1	54	37	37	71	70	6,0	
1958	8	8	12	52	9	36,8	70,8	210	6,0	
1964	7	6	10	13	45	37,1	71,3	100	6,0	
1998	2	4	14	33	21	37,08	70,08	33	5,9	
1915	2	24	15	41	0	39,2	67,8	30	5,9	
1926	6	30	22	51	46	38,8	70	10	5,9	
1930	9	22	16	26	40	38,53	69,45	5	5,9	Fayzabadskoye 1
1947	12	7	1	44	18	36,7	70,5	200	5,9	
1974	6	3	11	45	36	36,9	71,2	100	5,9	
1977	5	4	2	37	43	37,05	71,31	110	5,9	
1989	1	22	23	2	3	38,49	68,67	3	5,9	
1923	7	16	13	23	42	37,5	70,5	15	5,8	
1923	12	20	15	13	24	39,5	72	15	5,8	
Year	**Month**	**Day**	**Hour**	**Min**	**Sec**	**Lat**	**Lon**	**Depth**	**Mw_conv**	**Name**

1925	1	2	23	15	50	38,8	70	10	5,8	
1937	11	13	11	50	37	38	69,5	10	5,8	
1940	7	17	11	44	44	36,8	70,7	15	5,8	
1941	5	6	16	55	29	39,3	70,6	10	5,8	Nazaraylokskoye
1942	5	28	15	20	3	38,8	70,9	10	5,8	
1943	6	2	2	55	24	39,2	71,8	10	5,8	
1946	6	26	15	21	35	36,7	70,5	200	5,8	
1949	7	8	8	2	16	39,2	70,8	18	5,8	iasmanskoye 2
1950	5	20	18	53	50	37,1	70,9	160	5,8	
1954	5	16	22	10	40	36,8	70,8	180	5,8	
1959	9	12	21	20	3	36,9	71	200	5,8	
1962	4	24	14	20	13	36,9	70,2	220	5,8	
1975	6	28	4	26	35	36,6	70	200	5,8	
1979	12	5	8	42	26	37,6	71,9	130	5,8	
1985	10	13	15	59	52	40,3	69,8	10	5,8	Kayrakkumskoye
2004	11	17	20	58	22	39,19	71,80	25	5,8	Karamykskoye
2006	7	6	3	57	54	39,09	71,80	25	5,8	
1869	3	25	0	30		39,8	69,5	30	5,8	
1903	1	20	8	24		37	71	30	5,8	
1933	9	9	19	34	21	40,1	70,7	26	5,8	
1935	5	16	17	24	16	37,5	69,2	52	5,8	
1941	4	26	23	10	58	39,3	70,6	10	5,8	
1942	2	28	4	54	55	39,2	70,9	10	5,8	
1943	1	12	9	5	9	38,47	69,26	5	5,8	Kafdonskoye 1
1955	12	11	5	42	39	37,3	71,3	100	5,8	
1958	1	7	6	5	10	38,91	70,31	10	5,8	Kamchyrakskoye
1958	9	25	6	54	4	36,6	69,9	230	5,8	
1982	5	6	15	42	22	40,22	71,5	20	5,7	Chymynskoye
1905	2	25	10	35	0	37	70,5	30	5,7	
1925	8	30	13	16	13	38	69,5	10	5,7	
1926	4	11	6	26	24	40,6	69,5	18	5,7	
1930	3	6	15	44	20	39	72	10	5,7	
1930	9	23	10	15	20	37,6	71,6	120	5,7	
1933	12	9	7	52	7	36,7	69,4	15	5,7	
1934	9	8	6	44	55	38,4	71,2	11	5,7	
1938	1	12	1	8	21	38,8	71	10	5,7	
1948	11	22	16	6	4	39,2	68,1	30	5,7	
1949	7	10	14	13	24	39,2	71,1	10	5,7	
1951	5	12	22	7	52	39,62	71,2	25	5,7	
1959	2	1	3	13	36	37,1	70,9	220	5,7	
1962	10	9	15	59	21	36,8	70,9	230	5,7	
1962	11	26	1	41	8	36,6	70	160	5,7	
1965	2	16	20	46	42	36,8	70,8	180	5,7	
1966	12	13	12	21	1	37,4	71,8	119	5,7	
Year	**Month**	**Day**	**Hour**	**Min**	**Sec**	**Lat**	**Lon**	**Depth**	**Mw_conv**	**Name**
1975	10	17	1	9	5	37,35	71,27	80	5,7	

1979	12	12	10	3	42	37,1	71,2	80	5,7	
1926	5	2	10	0	50	39,5	72	10	5,6	
1930	1	7	17	27	36	39,2	72,1	10	5,6	
1935	4	22	13	15	27	39,8	67,5	25	5,6	
1936	8	29	12	41	50	38,2	72	30	5,6	
1939	6	19	0	42	40	37,3	71,4	15	5,6	
1941	4	26	7	8	3	36,8	70,2	180	5,6	
1949	8	23	22	3	54	39,2	71,1	25	5,6	
1950	11	17	22	1	4	38,75	70,5	8	5,6	Tavyldarynskoye
1956	9	22	15	54	23	38,45	69,28	7	5,6	Nurekskoye 1
1959	5	26	6	35	58	37	69,9	30	5,6	
1959	7	31	19	53	2	38,9	70,4	8	5,6	
1960	7	17	5	14	35	36,7	70	25	5,6	
1961	8	23	4	12	39	38,55	68,5	25	5,6	Dushanbynskoye
1963	10	14	21	12	38	37,5	71,9	110	5,6	
1969	3	22	4	52	32	38,93	70,56	9	5,6	Garmskoye 3
1975	9	17	3	48	32	37,4	71,6	135	5,6	
1976	6	16	15	29	19	36,6	69,6	160	5,6	
1985	7	8	1	31	53	36,6	70	210	5,6	
1990	12	20	7	2	59	37,6	70,3	5	5,6	
2006	7	29	0	11	53	37,37	68,67	37	5,6	
1907	10	24	5	10	0	38	68,8	18	5,6	
1934	9	23	1	24	31	39,3	71,1	10	5,6	
1935	1	4	10	22	16	38,9	70,9	10	5,6	
1949	5	10	9	13	25	36,9	69,9	180	5,6	
1950	11	21	20	53	57	38,6	70,5	9	5,6	
1955	7	19	8	47	38	39,7	68	14	5,6	Bahmalskoye
1957	10	5	22	40	46	37,6	69,4	50	5,6	
1958	1	13	20	28	43	39,5	71,8	20	5,6	
1958	5	30	1	10	17	36,8	70,6	200	5,6	
1966	4	14	21	6	14	38,96	70,55	10	5,6	Garmskoye 2
1973	1	3	14	31	1	39,16	71,84	10	5,6	
1993	8	8	22	41	43	38,67	70,46	16	5,5	
1996	11	23	1	56	58	38,99	70,83	50	5,5	
2006	7	6	4	17	42	38,92	71,61	10	5,5	
2003	10	21	2	21	33	37,16	71,41	218	5,5	
1986	9	17	12	8	9	37,43	71,68	110	5,5	
1991	4	18	9	18	30	37,46	68,27	33	5,5	Kabadyenskoye
2001	9	2	16	58	33	38,75	72,19	33	5,5	

Date	Hour	Latitude (°N)	Longitude (°E)	Depth (km)	Network	mb (ISC)	Mw converted
19/07/2011	19:35:43.48	40.0810	71.4100	20.0	NEIC	6,1	6,2
24/01/2011	02:45:30.50	38.4018	72.8467	101.9	ISC	6	6,1

12/05/2012	23:28:42.70	38.6500	70.4200		CSEM	6	6,1
17/08/2011	18:21:41.72	38.4798	73.7713		KRNET	5,7	5,9
10/06/2010	06:38:05.70	39.8550	74.8351	30.4	ISC	5,5	5,7
07/09/2010	15:41:41.60	39.5004	73.7684	32.0	ISC	5,5	5,7
19/07/2012	07:36:35.47	37.2480	71.3750	98.4	NEIC	5,5	5,7
03/08/2010	16:26:26.16	38.4227	69.5571	31.7	ISC	5,4	5,6
01/06/2012	12:32:22.54	39.7620	75.1940	9.9	NEIC	5,4	5,6
30/08/2012	13:50:06.93	37.6682	71.6455	0.0	NNC	5,4	5,6
02/01/2010	02:15:10.08	38.2935	71.4519	29.9	ISC	5,3	5,5
11/03/2011	21:26:53.37	40.0277	71.7258	1.0	KRNET	5,3	5,5
26/07/2012	01:06:30.42	38.2680	73.9880	116.3	NEIC	5,3	5,5

APPENDIX 2

INPUT FILE FOR GROUND-MOTION PREDICTION EQUATIONS

APPENDIX 2

Input file for Ground-Motion Prediction Equations

Example of input file for Vakhsh fault and scenario MHE +0.5 (cf. Table 12)

```
D:\Documents\Rogun_
../coefficients/
3
ab10
ba08
cb08
0.50          % number of sigmas (epsilon)
017           % number of periods to compute ground motions for
0.000
0.020
0.030
0.050
0.075
0.100
0.150
0.200
0.300
0.500
0.750
1.000
1.500
2.000
2.500
5.000
10.00
                        E
6.90          % magnitu     E
                        E
R             % mechanism (S=strike-slip, R=reverse, N=normal, T=thrust, B=intraslab, F=interface)
005.0         % de (km)
001.0         % df (km)
003.4         % dr (km)
005.0         % ds (km)
010.0         % dh (km)
007.0         % rx (km) (horizontal distance from top edge of rupture on HW side - only for AS07)
010.0         % focal depth (km) (only used for subduction equations)
gm            % component : gm=geometric mean
y             % on hanging wall?
060.0         % dip of fault (degrees)
-99.9         % depth to top of rupture (km)
-99.9         % rupture width (km)
-99.9         % depth to the 2.5km/s shear-wave velocity horizon in km
-99.9         % depth to the 1.0km/s shear-wave velocity horizon in m
0             % 0=>horizontal, 1=>vertical
1000.0        % Vs30 (m/s)
0             % Aftershock flag (only for Chiou & Youngs, 2008) 0=>not an aftershock, 1=>aftershock
```

Codes for distance metrics

c de = epicentral distance
c df = distance to surface projection of fault (Joyner-Boore distance)
c dh = hypocentral distance
c dr = rupture distance
c ds = seismogenic distance

APPENDIX 3

GUIDELINES FOR PROBABILISTIC SEISMIC HAZARD ASSESSMENT FOR THE ROGUN HYDROPOWER PROJECT, REPUBLIC OF TAJIKISTAN

APPENDIX 3

Guidelines Probabilistic seismic hazard assessment for the Rogun Hydropower Project, Republic of Tajikistan

Overall objective of the study

The next step of design for the proposed Rogun HPP requires a Probabilistic Seismic Hazard Assessment (PSHA) to propose appropriate earthquake loading conditions in terms of elastic response spectral accelerations and associated acceleration time-histories for design purposes at this site.

The hazard assessment in this project will follow three main stages, namely:

1. **Evaluation of the seismicity of the studied area,** by collecting information about historical and instrumental earthquakes from valid sources of data.
2. **Evaluation of the tectonic setting of the studied area**, **seismotectonic analysis and seismic activity parameters.** Seismic sources are defined as seismotectonic units consisting of main and secondary active faults and seismotectonic provinces. Seismic activity is described for each unit.
3. **Probabilistic Seismic Hazard Assessment (PSHA)**

   Preparation, by selecting ground motion prediction equations (GMPEs, also known as attenuation relationships) considering their applicability in the seismotectonic setting and accounting for epistemic uncertainty.

   Determining ground motions on horizontal outcropping rock by PSHA, including calculation of expected peak ground acceleration (PGA), hazard curves, and uniform spectra for several return periods as well as disaggregation and a sensitivity study. This process should take into account the entire available databases on seismicity, tectonics, geology and ground-motion characteristics in the area of interest.

4. **Review of the PSHA.**

Table 1 summarizes the steps to be followed for the regional seismic hazard analysis in this project and the results to be obtained at each stage.

Table 2 - Steps to be performed in the regional seismic hazard analysis

	Description	Main results to be delivered for following stages
1	**Seismicity of the studied area:** • historical • instrumental	• Homogeneous catalogue of seismicity • Different maps showing the seismicity of the studied area
2	**Tectonic setting** of the studied area	• Faults and tectonic maps • Description of main active faults and faults systems
	Seismotectonic analysis and seismic activity parameters	• Seismotectonic schemes • Definition of seismotectonic units and maps: ○ Main and secondary faults ○ Seismotectonic provinces • Description of seismic activity for each unit
3	**PSHA** Preparation	• Input parameter for the PSHA computing and analysis (disaggregation) tools • Appropriate GMPEs for the seismotectonic context • Logic tree to represent epistemic uncertainties • Distribution functions to represent aleatory variabilities
	Ground motion on horizontal outcropping rock	• PGA and Spectral acceleration at different return periods • Hazard curves • Uniform spectra • Disaggregation
4	**Review of the PSHA**	• Discussions and final review of the study

Detailed description of the proposed procedure

Stage 1: Seismicity of the studied area

Studied area in Tajikistan

The location of study area in Tajikistan is plotted in Figure 1

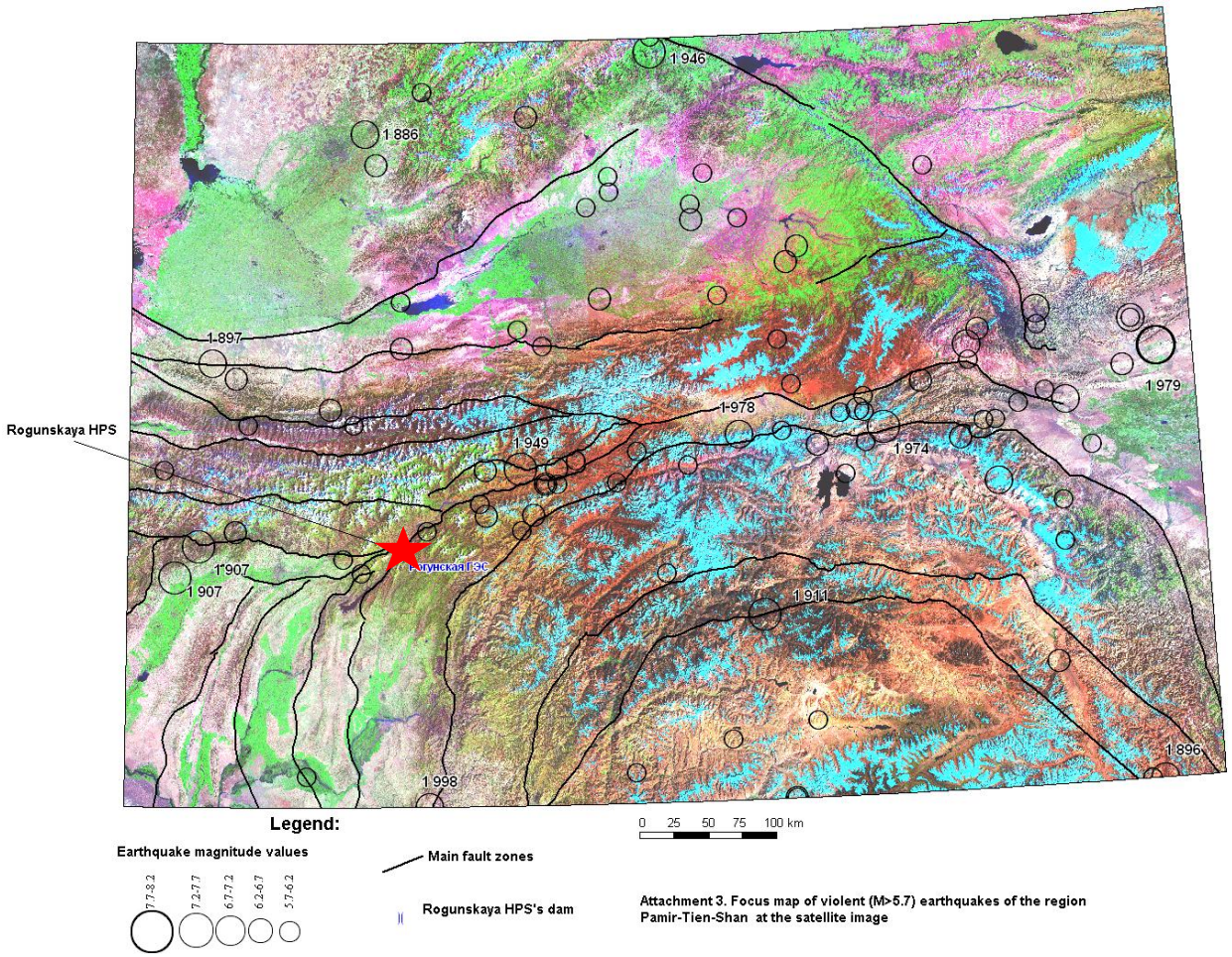

Figure 1 - Study area location in Tajikistan (Rogun HPP is indicated with red star)

Sources of earthquakes information

In order to clearly establish the manner in which current movements are taking place, historical and instrumental earthquake catalogues from worldwide and local networks will be collected and analysed. This synthesis will be based on the data provided to the Seismic Expert by the Institute of Earthquake Engineering and Seismology of Dushanbe. Seismic Expert will first check these data and may if necessary carry out additional processing (insertion into a GIS, etc.)

Earthquake catalogues include macroseismic information on historical earthquakes as well as more precise data from the instrumental period.

- Historical seismicity: Consultation of historical databases is a first source of information on the seismic activity of a region. These can be used to know if, within recent history (i.e. the past few centuries), the region has been subject to one or several major earthquakes. In some cases, when the damage caused by an earthquake is severe and there are numerous historical references to this event, it is possible to correlate the earthquake to a particular tectonic structure. In this case, the return period of strong earthquakes connected to this structure can be estimated.

    - In the framework of this project, historical earthquake catalogues shall be consulted to locate main historical events that have affected the region.

- Instrumental seismicity: The minimal information given by databases of instrumental seismicity, for an individual earthquake, is: its date and time, epicentral location and focal depth, magnitude and the reliability of the information. Study of this information permits the estimation of the return period of earthquakes in the region and their separation with respect to different seismogenic sources. Secondly, a more thorough treatment of these data permits, in certain cases, to characterise the seismic source, notably with respect to its focal mechanism. This information is important for the characterisation of the type of fault movement that occurred during the earthquake.

We will consult earthquake catalogues and draw a map with historical and instrumental seismicity. This analysis will be carried out at least within a 300 km radius, to show how tectonic movements are distributed through time and space.

The data to be analyzed will include, if available, regional earthquake catalogues for Tajikistan and bordering countries (e.g. Uzbekistan, Kyrgyzstan, Afghanistan and China), and worldwide catalogues (for instance, ISC and USGS/NEIC catalogues). These data can also include critical historical seismicity (e.g. macro-seismic data concerning, e.g., slope failures, surface ruptures and damaged buildings).

Processing the seismicity catalogue

Magnitude homogenization

The usually applied magnitude scale for assessments is moment magnitude (M_w) as defined by Hanks and Kanamori (1979; see also Kanamori, 1977). But seismological databases like NEIC, NNC or CASRI contain body wave, surface wave or local magnitudes. Only for some recent events are M_w available in these catalogues. The magnitudes of all catalogues will be converted into a unified magnitude, preferably M_w because the most recent and reliable GMPEs are developed for moment magnitude. For this purpose, results from Heaton (1986) could be applied. Based on this study, it is possible to consider for M_LI $\leq$ 6.0, $M_L=M_w$, for $M_b \leq 5.0$, $M_b=M_w$ and for $6.0 \leq M_s \leq 8.0$, $M_s=M_w$. In other situations, Ambraseys and Free relation (1997) could be used for converting M_s to M_w.

Focal depth

The focal depths of earthquakes may vary from shallow to deep in the whole study area of all seismic sources. The range of focal depths may be a particular challenge with respect to the choice of GMPEs to be used in the hazard calculations. This is why the depth distribution of the earthquakes in the catalogue shall be analyzed. An example histogram of focal depth distribution of earthquakes is drawn on Figure2. In this example, 10 km (the clear peak in the distribution) could be chosen as an average focal depth of earthquakes, at least for area sources.

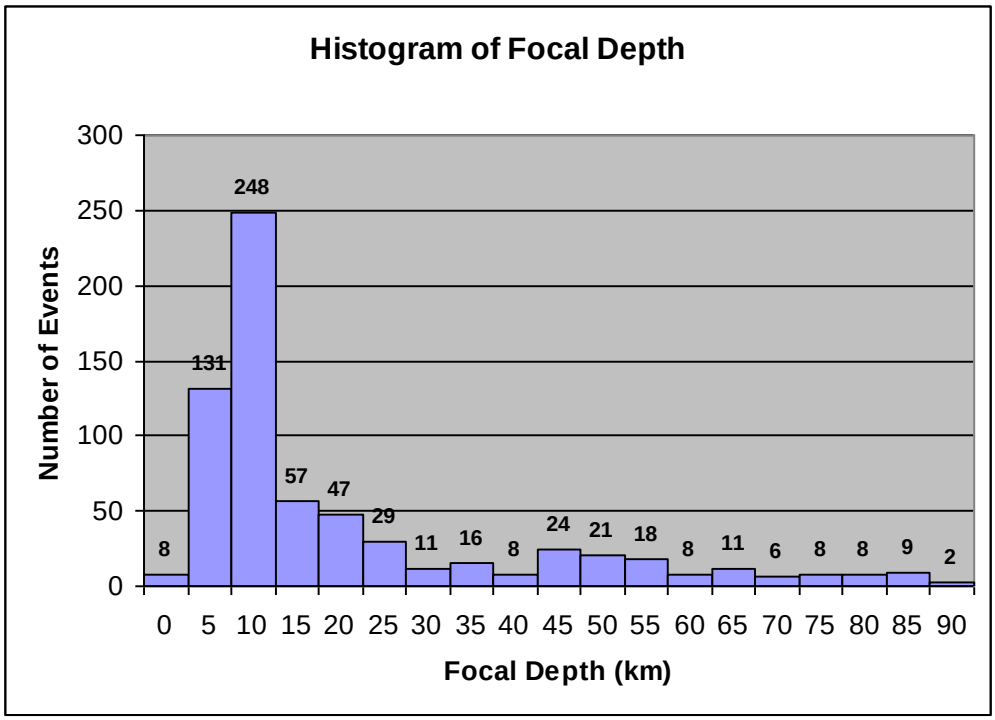

Figure 2 - Example of histogram of focal depth of earthquakes

Removing foreshocks and aftershocks

The spatial and temporal distribution of earthquakes in an extensive region is usually conspicuously inhomogeneous. Events occur in *'seismic clusters'*, being grouped spatially and temporally. The event with the highest magnitude is regarded as *'main shock'*. *'Aftershocks'* are events that follow the main shock within an appropriate spatial window, centered on the main event within a time interval counted from the beginning of the sequence. Events that precede the main event are retrospectively termed *'foreshocks'* or *'precursors'*.

The frequency of occurrence of the aftershocks follows a probability distribution different from the sequence of main events. The occurrence of seismic events in any region is generally modeled as a *Poissonian* stochastic process, a memory-less process, the characteristics of which are as follows:

- number of occurrences in a single time interval are independent of the number that occurs in any other time interval;
- the probability of occurrence during a very short time interval is proportional to length of the time interval;
- the probability of more than one occurrence during a very short time interval is negligible.

Typical earthquake catalogues are non-*Poissonian* if they are mixtures of two populations, aftershocks clusters which are not *Poissonian* and main sequence events which may or may not be (Gardner and Knopoff, 1974). Hence the need to remove foreshocks and aftershocks from the seismicity catalogue.

The suggested algorithm employed for eliminating foreshocks and aftershocks (or "declustering" the catalogue) is the one developed by Reasenberg (1985) for central California. This software has been provided by USGS as CLUSTER2000; it recognizes clusters in space-time in an earthquake

catalogue. All the events (foreshocks and aftershocks) with epicenters falling within the defined spatial and temporal window are removed with the exception of events whose magnitude is the same or very close to the main event.

Completeness analysis

As one goes backward in time the earthquake catalogue gets sparser and the uncertainty of its content increases. Earthquakes in the ancient times have not been recorded in written documents unless they were large and destructive. This illustrates the incompleteness of a catalogue and that an appropriate process must account for incompleteness in the statistical procedure of seismic hazard analysis.

Catalogue incompleteness can be defined as recorded seismicity that differs from the real seismicity (Mulargia et al., 1987). Different techniques are used to account for catalogue incompleteness. We recommend a simple, graphical procedure known as the 'Visual Cumulative Method' (CUVI Method) formulated by Mulargia et al. (1985) to estimate the period of completeness of the catalogue. The procedure to assess completeness is applied after removal of foreshocks and aftershocks and is described in attached Appendix A. The completeness analysis should deliver a completeness interval for each magnitude class.

Table 2 illustrates a result of completeness analysis for an entire earthquake catalogue.

Table 2- An example of completeness analysis

Magnitude Class	Year of Completeness
≥ 6.0	1900
5.5-6.0	1924
5.0-5.5	1950
4.5-5.0	1965
4.0-4.5	1983

Deliverables for stage 1

- The seismicity catalogue (delivered under electronic format)
- A draft chapter for the final report (delivered under electronic format) describing:
    - The spatial limits of the catalogue (at least 300 km around the project site);
    - The sources and references used;
    - The history of seismic survey networks in the vicinity of the project site and at the regional scale;
    - The criteria for choosing the properties for events reported in several catalogues;
    - The conversion formulae from original magnitudes to unified magnitude;

- The method for checking catalogue completeness and its results: table showing the date from which the catalogue can be considered complete, for the various magnitude classes;
- The method used for filtering foreshocks and aftershocks, and statistics related to this filtering (percentage of events suppressed for the various magnitude classes); and
- An analysis of the most powerful earthquakes registered in the vicinity of the site (less than 50 km) and an analysis of the whole seismic activity observed in the closest 10 km to the site.

These elements will be validated by the Client.

Stage 2: Seismic sources models

A go-ahead given by the client is required to start this stage.

Tectonic setting of the studied area

The definition of earthquake sources is essential. Sources may range from small faults to large seismotectonic provinces with uniform seismicity. The reliability of the seismic hazard assessment depends upon the coherence of strains at every scale, from that of plate tectonics to that of seismic scarp.

A regional seismotectonic scheme will be determined within a 300 km radius around the site, through a review of existing documents (e.g. scientific articles and maps), supplemented by satellite pictures and a Digital Elevation Model (DEM). In particular data provided by the Institute of Earthquake Engineering and Seismology of Dushanbe will be verified and may be discussed with the Institute.

The scheme will be used as a basis for the segmentation of the area into seismotectonic zones and seismic sources for the probabilistic seismic hazard assessment (PSHA).

If necessary, in order to achieve a local seismotectonic study, the presence of potential active faults within a 30 km radius around the site should be screened thanks to seismological data (location of epicentres and focal depth, if any) and satellite data combined with the DEM.

Situation of the region in the framework of plate tectonics

In order to obtain a view of the kinematics of deformation as well as a view of local stress patterns, major plates involved and relative movements at their nearest borders (global plate motion models) will be documented through available publications. Relative movements on the borders must be constrained.

Geological structure

In order to determine the most plausible mechanisms of active deformation, the inherited geological structure including the age of the continental bedrock, the type and strike of old faults likely to be reactivated by present day stresses, the type and thickness of sedimentary cover and the style of deformation has to be identified through both scientific articles and regional and geological maps.

Catalogues of seismicity

The analysis of the tectonic setting will make use of the seismicity catalogue established in stage 1, in order to clearly establish the manner in which current movements are taking place.

Seismotectonic zoning

The synthesis of information should allow the proposal of a model of active deformation, from which a seismotectonic map shall be drawn. Based on this map, several seismotectonic units (specifically domains, structural systems and structures) shall be identified. Seismotectonic units are considered geologically, geophysically and seismologically homogeneous (= sources).

Seismotectonic analysis and seismic activity parameters

The spatial distribution of seismic sources will be determined through:

- identifying faults and volumetric zones that will be the sources of future seismic activity In the region around the site; and
- characterizing the uncertainty in the spatial description of each source.

The geological and seismological information is used to define models for the potential earthquake sources that influence hazard at the site. The main aspects of the source characterization are:

- modeling of area sources based on the geological history of the region in general and on earthquake occurrence statistics (historical and contemporary seismicity catalogues), in particular; and
- modeling of fault-specific sources with 3-dimensional geometry, if such detailed information is available.

After finalizing active faults characterizations by seismotectonic studies, based on defined parameters for each fault, a background zone could be provided around them.

Methodology of regional seismic hazard assessment

Using a deterministic approach, ascribing the maximum historical earthquake to each fault or source area is too conservative. A traditional probabilistic approach with area seismic sources will lead to a dilution of the hazard since:

- the earthquake sampling is not significant for major crustal movement;
- sources areas are too large with respect to the earthquake density; and
- assuming the same probability for earthquake occurrence at any point of the source area is a rough approximation that can lead to hazard underestimation.

Most seismic hazard assessments are carried out using probabilistic and deterministic approaches. These methods are extensively applied where instrumental and historical earthquake catalogues (easily workable by software) are available. These approaches tend to assume: (i) an earthquake catalogue representative of crustal movements (in time and space), (ii) a homogeneous distribution of seismicity over large areas, and do not require a specific understanding of the regional geodynamics. Moreover, they do not allow for the identification of active faults crosscutting the site of interest.

However, rates of deformation along faults (few mm/yr) are less than rates of relative movements measured at plate boundaries. Consequently, the recurrence periods of major earthquakes for the fault systems in the study area may be significantly greater than the time span covered by earthquake catalogues. This implies that:

- a complete representation of the distribution of seismicity cannot be obtained in a short interval (a few centuries for historical seismicity); and
- it is necessary to incorporate low magnitude events (instrumental seismicity for the most recent period). Further problems then appear: (i) the location of low magnitude events is not well defined; and (ii) it is not certain that low magnitude events are representative for major crustal movements.

Consequently, taking into account:

- the short time of seismic instrumental records (a few decades);
- the incompleteness of data and the dubious reliability of most of the catalogues of historical seismicity;
- the inadequate geometry or number of stations of most local seismological networks, which prevents accurate localization of moderate seismicity; and
- the likely long recurrence period for strong earthquakes along the fault systems in the area (probably a few centuries);

the seismic hazard analysis should not be based only on instrumental and/or historical seismicity.

Since only large faults are capable of generating large magnitude earthquakes, considering that an earthquake may occur everywhere with the same probability seems to be a rough approximation. Moreover, if seismic activity recorded along a fault attests for its seismogenic character, the lack of recorded seismic activity, in the absence of other approaches, **does not** prove its inactivity.

Therefore we recommend the use of a mixed approach for estimating seismic hazard based on:

- identification and characterization of active faults; and
- time independent (*i.e.* probabilistic) seismic behavior of each identified fault.

Description of the hazard model

A seismic source represents a portion of the earth's crust with a potential to generate future earthquakes. Within a seismic source, the probability of earthquake occurrence and the size of the maximum magnitude are generally considered invariant. Seismic sources include faults with a potential to affect the site. Seismic sources also depict volumetric zones, in which future earthquakes may occur but specific faults are not identified.

In identifying and characterizing seismic sources, the scale of features to be considered and the level of investigation vary with distance from the site. Because ground motion decreases as distance between the source and the site increases, earthquake size must increase to produce significant ground motion at the site. The size of an earthquake that a feature can generate is related to its physical dimensions. Thus, as one gets farther from the site, larger faults are required for a significant ground motion potential to exist at the site.

Each seismic source shall be evaluated to provide its:

- spatial description, including variability in that description (two-dimensional zone of diffused seismicity or three-dimensional faults);
- probability of activity, which expresses the likelihood that the source is seismogenic and is based on the evidence of its activity during the Quaternary period; and
- dependency on other seismic sources.

Alternate interpretations of the spatial description of a seismic source permitted by the available data may be weighted according to their ability to explain the data. The spatial description of a seismic source includes an evaluation of the depth of earthquakes associated with the source.

Earthquake recurrence model

The seismicity recurrence characteristics for each source zone shall then be defined. Each source is characterized by an earthquake probability distribution or recurrence relationship. The recurrence relationship describes the relative frequency of occurrence of the stronger and less frequent earthquakes with respect to the weaker and more frequent earthquakes. The frequency-magnitude relationship shall be determined for each seismogenic zone after identifying the epicenters lying within their boundaries. The Gutenberg-Richter (1954) recurrence relationship postulates the existence of an exponential correlation between the mean annual rate of exceedance of an earthquake of specified magnitude and the magnitude itself. This law is a simple mathematical statement that larger events are less frequent than weaker events and that the difference in relative terms follows an exponential law.

The recurrence parameters could be defined either for area sources, active faults or area sources associated with an active fault.

- **Recurrence parameters for area sources:** the Weichert (1980) methodology described in attached Appendix B may be used.
- **Recurrence parameters for active faults:** the Anderson and Luco (1983) methodology described in attached Appendix C may be used.
- **Recurrence parameters for area sources associated with active faults:** these zones are background areas where seismicity between 4.5 and 5.0 is distributed in the whole area. The hypothesis is that main active faults concentrate the seismic activity of strong earthquakes. For moderate earthquakes (less than 5) activity can be due to other poorly known small faults. Area source model may then be used to take into account this kind of seismicity. Annual rate of earthquake between 4.5 and 5.0 should be calculated from the real observed activity in the catalogue.

For active faults, the characteristic model should be an alternative to the exponential magnitude distribution and will be analyzed when treating epistemic uncertainties.

Deliverables for stage 2

A draft chapter for the final report (delivered under electronic format), supported by an up-to-date literature review, describing:

- The situation of the region in the geodynamical context at the scale of tectonic plates;
- The main seismotectonic provinces in a radius of at least 300 km around the site, with structural geology and known active deformation data;

- A summary of each main active fault showing:
    - Its name;
    - A morphostructural interpretation based on satellite picture data;
    - The expected mechanisms;
    - Its length, segmenting and seismogenic capabilities;
    - Its dip;
    - The Maximum Credible Earthquake (MCE) and associated rupture area, based on empirical relationships such as Wells and Coppersmith (1994);
    - Its annual slip rate;
    - Return periods for major eathquakes, if provided in the literature; and
    - The associated instrumental or historical seismicity, from the seismicity catalogue or literature references.
- An analysis of active faults close to the project site, with careful attention to faults and associated events likely to directly concern the site.
- The criteria for choosing the seismic sources and justifying the description as fault or area sources;
- The methods used for seismic activity parameters (depth, maximum magnitude, λ, β) and associated uncertainties; and
- An analysis of the resulting map and table of the seismic sources zoning.

Stage 3: Probabilistic Seismic Hazard Assessment

A go-ahead given by the client is required to start this stage.

Assessment preparation

The seismic hazard is defined as the annual probability of exceeding a given ground parameter (displacement, pseudo-velocity or acceleration) due to the activity of surrounded seismic sources.

In PSHA studies, the basic methodology assumes that the seismicity within a source area is a non-memory process phenomenon characterized by a Poisson distribution. The concept of seismic source, in order to represent the seismicity activity by the probabilistic approach was introduced by Cornell (1968). The method used in this study will be based on a Cornell-McGuire type method that permits to estimate peak ground accelerations (PGA) and spectral accelerations for a site.

A recent and flexible tool of analysis must be used to perform this PSHA. We recommend using CRISIS version 2003 or 2007 (see below). As input of the tool different parameters have to be defined in this stage 4 of the study. They are described below.

Minimum magnitude

Magnitude thresholds can be different in each seismotectonic zone. Parameters *a* and *b*-value from Gutenberg-Richter relationships can be calculated using the minimum magnitude equal to the magnitude threshold.

The PSHA requires selection of minimum magnitude m_{min}. The same for all seismic zone sources shall be considered, with a value for which building and structure damages can occur (for instance magnitude greater or equal than 4.0 or 4.5).

Maximum magnitude

The maximum magnitude is defined between two values, in order to take into account uncertainties on this parameter. For instance the lowest value could be the maximum observed magnitude plus 0.5 and the greatest value the maximal observed magnitude plus 1. In high hazard regions, maximum magnitude could also be estimated using seismotectonic analysis (see stage 2).

Depth

Depth is a very important parameter that can control the levels obtained. It will be defined between two limits, in order to take into account its uncertainty.

Ground Motion Prediction Equations (GMPEs)

The range of earthquake sizes considered requires a family of earthquake attenuation or ground motion curves, each relating to a ground motion parameter, such as peak acceleration and distance for an earthquake of a given size.

There is evidence that the decay rate of ground motions is dependent on the magnitude of the causative earthquake (e.g. Douglas, 2003), and the decay rate also changes systematically with distance. Geometrical spreading is dependent on wave type, where in general, body waves spread spherically and surface waves cylindrically, while an elastic attenuation is wavelength (frequency) dependent. As hypocentral distance increases, the up going ray impinges at a shallower angle on the interfaces, reflecting increasing amount of energy downwards, thereby reducing the energy transmitted to the surface. For moderate and large earthquakes, the source can no longer be considered a point source and therefore the decay rate will be less than for smaller events. Therefore, for large events, the closest distance to the rupture area or the closest distance to the projection of the fault plane to surface (Joyner-Boore distance) are usually used instead of epicentral or hypocentral distance.

One of the most important sources of uncertainty in PSHA is the variability or scatter in the ground motion (attenuation) models, which is an aleatory uncertainty usually expressed through the sigma (σ) value of the log-normal distribution, which is often of the order of 0.7 in natural logarithms, corresponding to about 0.3 in base 10 units. This variability, which is often both magnitude and frequency dependent, is mainly expressing a basic randomness in nature and therefore cannot be significantly reduced with more data or knowledge. In PSHA this variability is integrated over, which is directly influencing the seismic hazard results.

By comparing and studying recent models, 4 or 5 robust GMPEs that are applicable for all magnitudes and distances considered in the PSHA have to be selected. Articles such as that by Bommer et al. (2010) on the selection of GMPEs should be consulted when making this choice.

Reference return period selection

Return periods corresponding respectively to the OBE, and MDE have to be considered. This means, according to ICOLD 2010:

- 145 years for OBE (50% exceedance probability in 100 years);
- 10 000 years for MDE (1% exceedance probability in 100 years);

Moreover the following return periods could be considered, according to Comité Français des Grands Barrages (November 2010):

- 200 years for OBE (40% exceedance probability in 100 years);
- 5 000 years for MDE (1.98% exceedance probability in 100 years).

The return period of 475 years (10% exceedance probability in 50 years) must also be considered because it is a general reference return period for PSHA globally.

Uncertainties

When a probabilistic hazard assessment is performed uncertainties must always be identified and they also must be propagated in models in order to find seismic motions.

Because of large uncertainties on seismological and geological data, for a same site, several seismotectonic and GMPEs could be identified: for instance GMPEs determined by different expert teams can diverge significantly.

That is the reason why two types of uncertainties must be considered. These uncertainties are called “epistemic” uncertainties and “aleatory” variability:

- « Epistemic » uncertainties: they are related to incomplete knowledge about phenomena of concern and inadequate matching of available databases to the case under assessment, etc. They can come from incomplete (or lack of) knowledge about fundamental phenomena. With time (e.g., additional observations) these uncertainties can be reduced and the true value ascertained.

    - In this category we can find the delimitation of source zones of a seismotectonic model, GMPE definition and definition of maximum magnitude.

- « Aleatory » uncertainties / variability: this can be called irreducible because they are due to the intrinsic randomness of nature. Indeed, several quantities can only be defined through probability distributions. They can be treated by well-established methods, e.g. propagated through the analysis by Monte Carlo simulation. These uncertainties can vary from a seismotectonic context to another.

In a PSHA study, uncertainties (epistemic and/or aleatory) mainly concern:

- Conceptual models (by zone or by smoothing);
- Seismotectonic models (fault, zones);
- Seismicity data;
- Parameters of reference earthquakes in the source zone : magnitude and depth;
- Parameters characterizing the distribution of activity : number of earthquakes/magnitude relation, return period; and
- GMPEs.

Tools for propagation of uncertainties

The recommended method uses a mix between logic tree techniques and the Monte-Carlo method. The logic tree is used in order to propagate the epistemic uncertainties whereas Monte-Carlo method is used in order to propagate aleatory variabilities.

In a PSHA study it is possible to propagate epistemic uncertainties using a logic tree with the following parameters: GMPE and regional seismological model. Each hypothesis made will be shown as a specific branch of the logic tree. The level of confidence for each hypothesis will be represented by a weight factor on the branch. The final result is the weighted sum of all results on the branches.

In addition we suggest propagating aleatory variabilities using a Monte-Carlo method on the following parameters:

- (*a, b, λ*, *β*) parameters of the Gutenberg-Richter relationship;
- Maximum magnitude; and
- Depth of considered earthquakes.

Independently of the choice of the GMPEs, their variabilities are also represented by a normal distribution with a standard deviation (σ) and are directly taken into account in the code. Other uncertainties (*λ* and *β* parameters, depth, and maximum magnitude) should be represented as probability distribution functions. Each parameter is associated to a distribution function (as normal, uniform or triangular distributions) that shows the uncertainty. An aleatory run would be done in order to obtain a sample of values of these parameters that must be introduced in the PSHA calculation. This run is done a great number of times in order to obtain a representative sample of the distribution function: for instance 100 or more runs would be performed for each parameter. A statistical processing of results permits to obtain an estimation of the uncertainty on the PSHA calculation represented as a median and percentiles values.

Ground motions on horizontal rock

Probabilistic seismic hazard assessment

It is well known that uncertainties are essential in the definition of all elements that go into seismic hazard analysis. Uncertainties often drive the results, and increasingly so for low exceedance probabilities. As it might be anticipated, this can sometimes lead to difficult choices for decision makers. Rational solutions to dilemmas posed by uncertainty can be based on the use of some form of probabilistic seismic hazard assessment. In contrast to the typical deterministic analysis, which (in its simplest form) makes use of discrete single-valued events or models to arrive at the required description of earthquakes hazard, the probabilistic analysis allows the use of multi valued or continuous model parameters. It is of utmost importance to include in the analysis the occurrence probability of earthquakes of various magnitudes or intensities. Another advantage of probabilistic seismic hazard assessment is that it results in an estimation of the likelihood of earthquake ground motions or other damage measures occurring at the location of interest. This allows for a more sophisticated incorporation of seismic hazard in seismic risk estimates; probabilistic seismic hazard estimates can be expanded to define seismic risk.

The methodology used in most probabilistic seismic hazard analyses was first defined by Cornell (1968). A description of this method is presented in attached Appendix D.

While the standard practice for a long time was to present the results of seismic hazard assessment in terms of a single best-estimate hazard curve, the growing awareness of the importance of parametric variability, and the trend to consult expert opinion in matters of scientific doubt, led later to the formulation of Bayesian models of hazard analysis (Mortgat and Shah, 1979), which try to quantify uncertainty in parameter assignment in probabilistic terms.

In the present work the CRISIS software will be used for seismic hazard assessment (Ordaz et al., 2003). The code accommodates uncertainty in a number of the seismicity model parameters, and has a user-friendly interface. It accepts polygon-dipping areas as well as fault sources, and also facilitates characteristic earthquake recurrence models.

Seismic hazard assessment results

Based on the above mentioned methodology, it is recommended to perform the analysis considering the final model of seismic source, including area sources and active faults, for at least 10 spectral periods, at least five return periods (145, 200, 475, 5000 and 10000 years for instance) and with 4 or 5 GMPEs (at least 3).

Hazard curves

The relationship between a range of ground motion levels and the associated annual exceedance probability constitute the hazard curve. The hazard curve for each GMPE as well as the mean hazard curve will be prepared (see example in Figure 1).

Uniform spectra

An essential element of the earthquake hazard assessment methodology is that seismic loading criteria may be evaluated in terms of equal-probability (equal hazard) spectra. This means that each frequency is evaluated independently, with its own uncertainty estimate.

The seismic loading criteria shall be specifically developed for bedrock outcrop (site with no soil). Design response spectra for the required annual exceedance probabilities based on the PGA values will be drawn, in certain cases accompanied by sets of real time histories (earthquake recordings) appropriately scaled to match the spectra.

The uniform hazard spectra for horizontal spectral ordinates have to be determined for various return periods. A uniform spectrum of a site for a 475 years return period has been illustrated in Figure 2 as a sample.

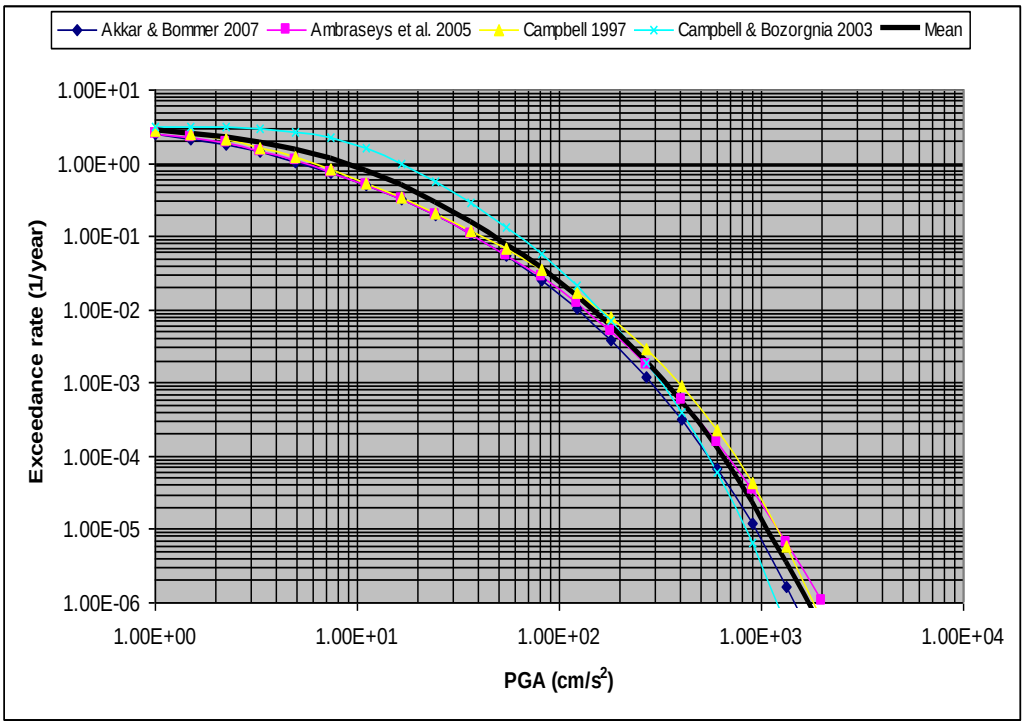

Figure 1 - Example of hazard curves

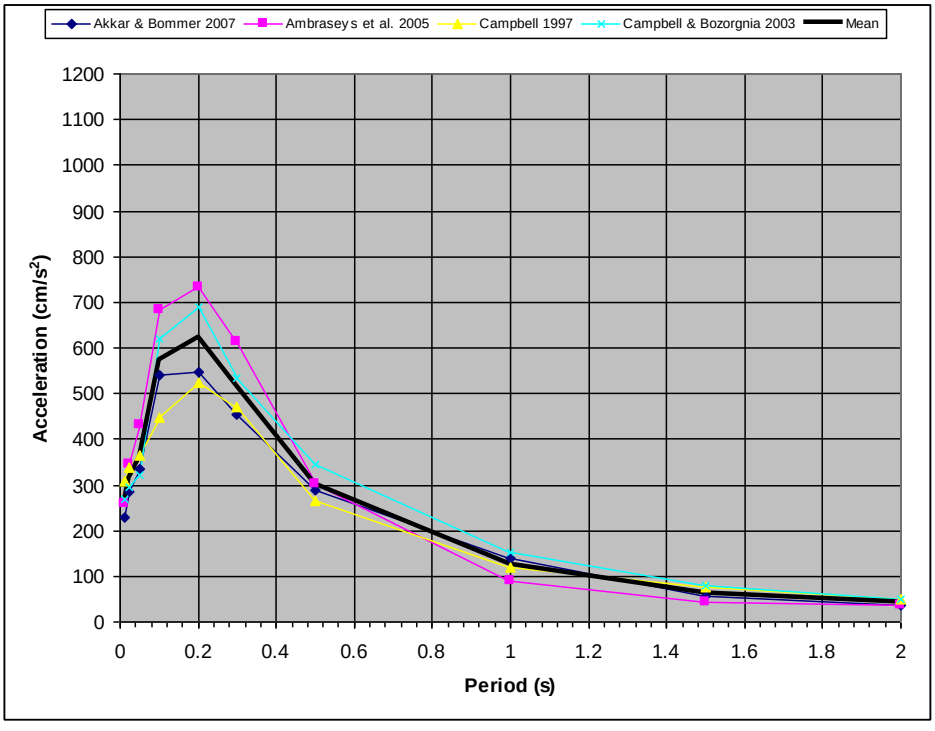

Figure 2 - Uniform spectra of a site for a 475 years return period

Disaggregation

The PSHA method aggregates ground motion contributions from various earthquake magnitudes and distances to the site. As such, the PSHA results are not representative of a single earthquake. However, engineering models and computer codes generally require observed or synthetic earthquake acceleration time series as input to dynamic analyses. Specific magnitudes and distances are also often required in slope stability and liquefaction analyses. An issue, then, is the selection of representative earthquake time acceleration series given a probabilistic uniform hazard response spectrum. A procedure called disaggregation has been developed to examine the spatial and magnitude dependence of PSHA hazard results. It can give an improved understanding of the results. Considerable attention has been focused on PSHA disaggregation in recent research literature (*e.g.*, Bazzurro and Cornell, 1999).

The PSHA results shall be disaggregated to determine the magnitudes and distances that contribute to the calculated exceedance frequencies (*i.e.*, the hazard) at a given return period and at structural periods of engineering interest. In this process, the hazard for a given return period and at a specified ground motion spectral period should be partitioned into selected magnitude and distance bins; the relative contribution to the hazard of each bin is calculated by dividing the bin exceedance frequency by the total exceedance frequency of all bins. The bins with the largest relative contributions — the modes — would identify those earthquakes that contribute the most to the total hazard. If there are no clear modes, the controlling or design earthquakes would be typically defined by the mean magnitude and mean distance.

Disaggregation results should be displayed as histograms giving, as a function of magnitude and distance, the percent contribution to the hazard of those earthquakes that are capable of causing ground motions equal to or greater than that corresponding to this hazard (see Figure 5 and Figure 6). The histogram will be provided for PGA and for spectral accelerations corresponding to varying structural periods, because of the difference in the way these spectral values scale with magnitude and distance. The relative frequencies specified by these histograms can be used to develop mean estimates of magnitude and distance, or to identify the modal contributions to the site hazard. A set of controlling or design earthquakes corresponding to the specified structural periods and return periods will then be defined. These design earthquakes can then be used as bases to select or construct input time histories for use in a dynamic site-response analysis or for ground failure evaluation.

The expected (median) ground motion amplitude corresponding to the disaggregated mean or modal magnitude and distance can be calculated by substituting these values into the GMPEs that were used in the PSHA.

The disaggregation results of a site for a 475 years return period for a specific GMPE relation is illustrated in Figure 5 and Figure 6 as an example. For PGA (Figure 5), main contributions come from moderate magnitude (Mw ~5.5) at very short distance (10-20 km). For a 1 second period (Figure 6), main contributions come from more distant and larger magnitude sources (30-40 km and Mw ~6.5).

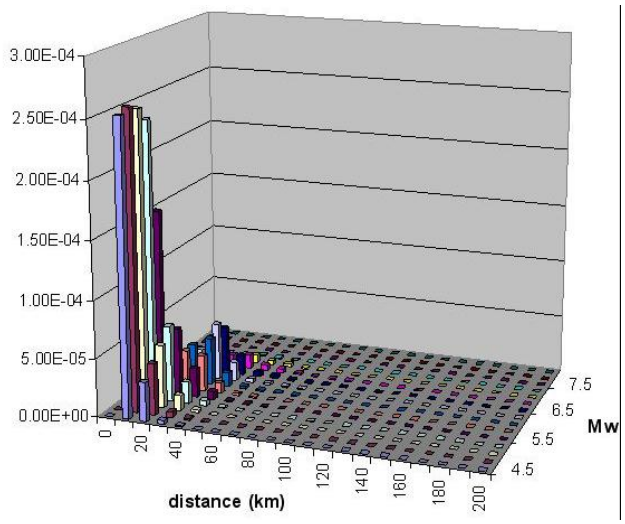

Figure 5 - Disaggregation analysis for a site for a 475 years return period – PGA

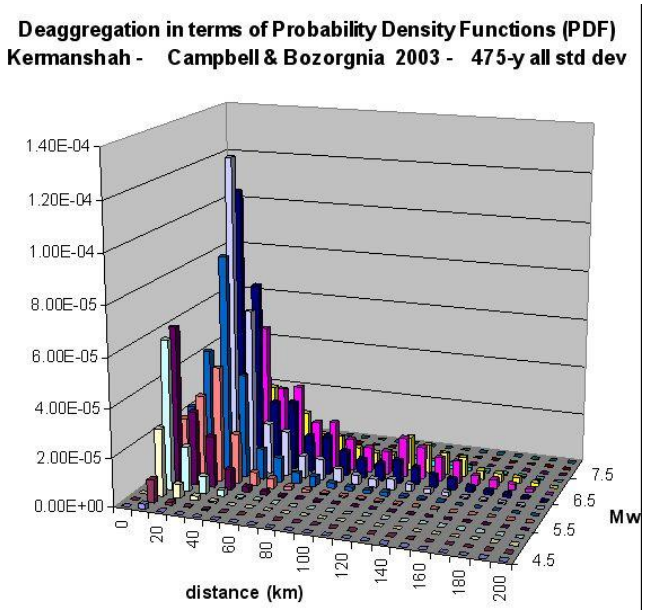

Figure 6 - Disaggregation analysis for a site for a 475 years return period – Spectral Period 1 s

Sensitivity analysis

A sensitivity analysis will be carried out to identify the input parameters that have the greatest impact on hazard assessment and its uncertainty. These tests will show the relative influence of epistemic and random uncertainties on the results. For this purpose, a reference set of parameters should be defined, from which the parameters could be varied one at a time: GMPE, Mmax, depth and activity rates (λ, β) and so forth.

The findings from this analysis may serve as a useful guide to facilitate further work on the seismic hazard assessment, because they discriminate parameters that have little or no effect on seismic hazard from parameters of great influence. A meticulous study of the latter parameters will lead to the reduction of uncertainties in future assessments.

Selection and modification of acceleration time-histories

A first set of several (at least 3) natural accelerograms (of three orthogonal components: two horizontal and one vertical) will be selected for at least two return periods. Preference will be given to independent accelerograms (e.g. those obtained during various earthquakes at different stations) so that the variability in possible ground motions is not underestimated. The selection of the accelerograms will be based on the match between the spectra (particularly within the period range 0.0 to 0.6s) and the magnitude and distance of the earthquake scenarios. The selected accelerograms would be linearly scaled so that their peak ground accelerations match those of the spectra.

In the second step, a second set of other accelerograms (at least 3) could be modified by the addition of wavelets using for instance the program RSPMatch2005 (Hancock et al., 2006) so that their elastic response spectra exactly match the spectra.

Deliverables for stage 3

A draft final report (delivered under electronic format) of the Seismic Hazard Assessment which includes:

- The chapters written during stage 1 and stage 2 and validated by the client at those stages.
- A description of the method used to elaborate the PSHA:
    - The list of GMPEs chosen, with their description and selection criteria. There should be at least three different GMPEs, whose validity domains are consistent with the seismotectonic context of the sources and the magnitude type consistent with the scale of the seismicity catalogue.
    - The PSHA computing and analysis (disaggregation) tools to be used, including:
        - The PSHA computation methodology taking into account parameter randomness and epistemic uncertainty.
        - Description of the input parameters (e.g. minimum magnitude taken into account, maximum distance to sources, spectral periods and truncation of the GMPE distribution)
        - Description of the expected outputs (e.g. return periods, uniform hazard spectra, median, mean and percentile values)
    - The logic tree considered for representing epistemic uncertainty, with justification of this choice and of the weighing of each hypothesis.
    - Distribution functions used for parameters in order to propagate aleatory variabilities.
- A synthesis of the results of the PSHA:
    - Hazard curves and UHS spectra;
    - Disaggregation analysis of the hazard curve and graphs for spectral periods 0.2 s and 1.0 s for the selected return periods;
    - Description of seismic design parameters associated to reference earthquakes, as shown by the disaggregation analysis; and
    - Sensitivity analysis and associated graphs. The selection and modification procedure followed and providing details of the chosen accelerograms;
    - Comparison to previous studies conducted at the site; and

- Identification of potential active faults at the site and potential surface displacements.

Stage 4: Review of the PSHA

The validation of the final report will be performed through a review by an independent expert chosen by the customer.

The final report will be delivered at the end of this stage.

Appendices

Appendix A: Mulargia (1987) methodology for catalogue completeness analysis

Events are divided into magnitude classes, as incompleteness is known to be a function of magnitude (Mulargia et al., 1987). Either the subdivisions could be intervals (where ΔM_c is between 0.5 and 1.0 for instance) or cumulative, containing all the events of magnitude exceeding the lower bound of a chosen interval.

An appropriate time interval depending on the coverage of the catalogue is adopted and for every magnitude class, a chart is constructed with time in years from the beginning of the catalogue as the abscissa and the cumulative number of events as the ordinate. The cumulative number of events in each magnitude class is computed by summing the number of events in a given interval with the number of events in the previous interval.

The catalogue is considered to be complete from the time when the trend of the data stabilizes to approximate a straight line. The approach is based on the fact that the slope coincides with the seismicity and a straight line or a *'constant average slope'* indicates a constant average rate of occurrence. It implies that from the identified period, the available data in the catalogue are substantially complete. The *'completeness interval'* is the number of years from the beginning to the period to the last year of occurrence in the catalogue.

A few important aspects of the problem at hand emerge when the procedure is applied.

- An abrupt change of slope is noticed from the point the catalogue is considered to be complete. If the catalogue had been considered to be complete from a period before this point, then it would result in grossly underestimating the occurrence rate of events in the corresponding magnitude class.
- The completeness interval for the higher magnitude classes would be relatively difficult to determine. The graph would exhibit a stepped behavior due to the fact that stronger events tend to be separated by relatively long time intervals and sometimes occur within a short period, both owing to the physical nature of earthquakes in a seismogenic zone.
- For the highest class of magnitudes, a certain degree of arbitrariness would be present in determining the period of completeness. Generally, the entire length of the catalogue years is considered with a degree of conservativeness, in order that large earthquakes in the early period of the catalogue are not ignored.

Appendix B: Recurrence parameters for area sources: Weichert (1980) methodology

Weichert (1980) methodology is a maximum likelihood estimation of the earthquake parameters in the relation $\lambda = \lambda 0 \exp(-\beta m)$ generalized to unequal observational periods. In this relation, λ is the annual rate of earthquakes above magnitude m, β is related to the b-value of the Gutenberg-Richter (1954) recurrence relationship: $\beta = \ln(10) \times$ (b-value).

This method is well adapted to zones where the completeness period is different for each range of magnitude.

In this method, β parameter is obtained iteratively by solving the following equation using Newton method:

$$\frac{\sum_i t_i m_i \exp(-\beta m_i)}{\sum_j t_j \exp(-\beta m_j)} = \frac{\sum n_i m_i}{N} = \overline{m}$$

Where in our case:

N = the sum of earthquake events

n_i = number of earthquake events in a certain interval

m_i = central magnitude

t_i = observation period

β = ln(10) × (b-value)

The annual event rate λ0 at or above magnitude m0 is given by:

$$\lambda 0 = N \frac{\sum_i \exp(-\beta m_i)}{\sum_j t_j \exp(-\beta m_j)}$$

Observation period t_j for each class of magnitude is deduced from completeness study of the catalogue.

Appendix C: Recurrence parameters for active faults: Anderson and Luco (1983) methodology

The seismic parameters that characterize each area are defined by the frequency distribution law or recurrence curve for the different sizes of earthquakes in each area. This distribution was defined by Gutenberg and Richter (1954) and assumes that the number of earthquakes (N) decreases exponentially with its magnitudes (M), according to the following formula:

$$\log_{10} N(M) = a - bM$$

where N(M) is the number of earthquakes greater than M, "10^a" the annual earthquake rate of a magnitude greater than 0 in the region, and "b" is the value which defines the proportion of major earthquakes compared with small earthquakes. This equation assumes that all earthquakes are independent of space and time, i.e. it has the properties of a Poisson model.

The seismic moment, M_o, is the most physically meaningful parameter to describe the size of an earthquake in terms of static fault parameters according to below equation:

$$M_o = \mu \Sigma D$$

where μ is the rigidity or shear modules (usually taken to be about 3×10^{11} dyne/cm²), Σ is the rupture area on the fault plane undergoing slip during the earthquake, and D is the average displacement over the slip surface. The total seismic moment rate M_0^T or the rate of seismic energy release along a fault is estimated by:

$$M_0^T = \mu \Sigma S$$

where S is the average slip rate along the fault, and Σ is the total fault plane area. The seismic moment rate provides an important link between geologic and seismicity data. Seismic moment is translated to earthquake magnitude according to Hanks & Kanamori (1979) relation as below:

$$\log M_0 = 1.5m + 16.1$$

that M_o is in dyne-centimeter.

Once the fault slip rate is used to constrain the seismic moment rate on the fault, a model must be assumed in which the rate of released moment is distributed to earthquakes of various magnitudes. Several authors have developed relationships between earthquake recurrence parameters and fault or crustal deformation rates, assuming an exponential magnitude distribution.

The link between fault slip rate and earthquake rates is made through the use of seismic moment. The total rate of seismic moment can be related to earthquake occurrence rate by the below expression:

$$M_0^T = \int_{-\infty}^{M_0} n(M) M_0(m) d_m \qquad (1)$$

Where n(m) is the density function for earthquake occurrence rate and may be expressed according to Youngs and Coppersmith (1985) as:

$$n(m) = \frac{N(m^o)\beta \exp(-\beta(m - m^0)}{1 - \exp(-\beta(m^u - m^0))} \qquad \text{for } m \le m^u$$

$N(m^o)$ is the normalized number of events per unit time, m^u is the upper bound magnitude (n(m) = 0 for $m > m^u$), m^o is some arbitrary reference magnitude, $\beta = b \times \ln 10$ with b from the Gutenberg-Richter exponential frequency magnitude relationship log N(m) = a - b× m, when n(m) is the cumulative number of earthquake of magnitude greater than m, and a and b are constants.

Integrating equation (1), the reference magnitude is obtained corresponding to a given return period as function of the upper bound magnitude m^u, the associated upper bound seismic moment, the slip-rate assumed along the fault, the chosen period of return, the b-value from the Gutenberg-Richter exponential frequency magnitude relationship, and the total fault plane area.

$$\mu \Sigma s = \frac{bN(m^o) M_0^u \exp(-\beta(m^u - m^o))}{(c - b)(1 - \exp(-\beta(m^u - m^o)))} \qquad (2)$$

This is equivalent to the relationship developed by Anderson (1979) and the type 2 relationship presented by Anderson and Luco (1983). The term M_0^u is the moment for the upper bound magnitude m^u. By assuming the slip rate, S, on a fault is known, equation (2) provides a constraint on the three parameters of the recurrence relationship $N(m^o)$, b, and m^u.

The constraint imposed by fault slip rate allows the development of fault-specific recurrence relationships in regions where the historical seismicity data are only sufficient to establish the regional recurrence rate for small to moderate size earthquakes. For each fault in the region,

estimates of the upper bound magnitude, m^u, can be made using fault characteristics. The historical seismicity data can be used to determine a regional b-value. Assuming the individual faults have all a b-value equal to the regional b-value, the earthquake activity rate for each fault, $N(m^o)$, can be computed from the estimated slip rate for the fault using equation (2).

Then it can be estimated the reference magnitudes along each identified active faults taking into account the period of return of the reference earthquakes ($N(m^o) = 1/T(m^o)$, the slip-rate along the faults (S), the maximum seismogenic capability of the faults (Σ) and the b-value.

$$m^o = m^u - \frac{1}{\beta}\ln\left[1+\frac{N(m^0)\beta M_0^u}{(\delta-\beta)\mu\Sigma S}\right] \qquad (3)$$

Where M_0^u is the seismic moment corresponding to the maximum credible magnitude (MCE) along a given fault, δ=ln(10)×b.

$$N(m^o) = \frac{(\exp(\beta(m^u - m^o)) - 1)\mu\Sigma S}{M_0^u\left(\frac{\beta}{\delta-\beta}\right)} \qquad (4)$$

From equation (4) it is able to calculate seismic activity parameter of the fault:

- Slip rate S and maximum seismogenic surface Σ are estimated from the fault study
- m^u is the MCE from the fault
- M_0^u is calculated from the MCE with Hanks & Kanamori (1979) formula
- b-value on the fault is equal to the b-value estimated for the area source zone containing this fault

Appendix D: Cornell (1968) for probabilistic seismic hazard assessment

According to Cornell (1968) there are four basic steps for assessment of PSHA:

- Step 1 is the definition of earthquake sources. Sources may range from small faults to large seismotectonic provinces with uniform seismicity.
- Step 2 is the definition of seismicity recurrence characteristic for the sources, where each source is described by an earthquake probability distribution, or recurrence relationship. A recurrence relationship indicates the chance of an earthquake of a given size to occur anywhere inside the source during a specified period of time. A maximum or upper bound earthquake is chosen for each source, which represents the maximum event to be considered. Because these earthquakes are assumed to occur anywhere within the earthquake source, distances from all possible location within that source to the site must be considered.
- Step 3 is the estimation of the earthquake effects which is similar to the deterministic procedure except that in the probabilistic analysis, the range of earthquake sizes considered requires a family of earthquake attenuation or ground motion curves, each relating to a ground motion parameter, such as peak acceleration and distance for an earthquake of a given size.

- Step 4 is the determination of the hazard at the site, which is substantially dissimilar from the procedure used in arriving at the deterministic hazard. In this case, the effects of all the earthquakes of different sizes occurring at different locations in different earthquake sources at different probabilities of occurrence are integrated into one curve that shows the probability of exceeding different levels of ground motion level (such as peak acceleration) at the site during a specified period of time. With some assumptions this can be written as:

$$E(z) = \sum_{i=1}^{N} \alpha_i \int_{m_0}^{m_a} \int_{r=0} f_i(m) f_r(r) P(Z > z \mid m, r) d_r d_m$$

where E(Z) is the expected number of exceedance of ground motion level z during a specified time period t, α_i is the mean rate of occurrence of earthquakes between lower and upper bound magnitudes (m_o and m_u), $f_i(m)$ is the probability density distribution of magnitude within the source i, $f_r(r)$ is the probability density distribution of epicentral distance between the various locations within source i and the site for which the hazard is being estimated, and P(Z>z | m,r) is the probability that a given earthquake of magnitude m and epicentral distance r will exceed ground motion level z.

It is usually assumed to carry out the probabilistic seismic hazard analysis when earthquakes are Poisson-distributed and therefore have no memory; implying that each earthquake occurs independently of any other earthquake.

One of the most important of the recent developments within PSHA has been in seismic source modeling. Originally, seismic sources were crudely represented as line sources (Cornell, 1968) and later area zones, which could be narrowed to represent the surface outcrop of faults as in McGuire's (1976) computer program EQRISK. An improved scheme, which included the effects of fault rupture, was proposed by Der Kiureghian and Ang (1977), and in a modified form implemented by McGuire (1978) in his fault modeling program FRISK, written as a supplement to his earlier and very popular EQRISK area source program. While the standard practice for a long time was to present the results of seismic hazard analyses in terms of a single best-estimate hazard curve, the growing awareness of the importance of parametric variability and the trend to consult expert opinion in matters of scientific doubt, led later to the formulation of Bayesian models of hazard analysis (Mortgat and Shah, 1979) which seek to quantify uncertainty in parameter assignment in probabilistic terms.

For the present work, **it is recommended to use the CRISIS computer code for seismic hazard assessment** (Ordaz et al., 2003). The code accommodates uncertainty in a number of the seismicity model parameters, and has a user-friendly interface. It accepts polygon-dipping areas as well as fault sources and also facilitates characteristic earthquake recurrence models.

Theoretical framework

In the original Esteva (1970) - Cornell (1968) approach, the territory under study is first divided into seismic sources according to geotectonic considerations; in most cases, it is assumed that, within a seismic source, an independent earthquake occurrence process is taking place. For each seismic source, magnitude exceedance rates, N(M), are estimated by means of statistical analysis of earthquake catalogues. These rates are the number of earthquakes, per unit time, in which magnitude M is exceeded, and they characterize the seismicity of the source.

Seismic sources are usually lines, areas or volumes, so a spatial integration process is carried out to account for all possible focal locations. Usually, it is assumed that, within a seismic source, all

points are equally likely to be an earthquake focus. In this case, acceleration exceedance rates due to a single source – the i[th] - are computed with the following expression:

$$V_i(a) = \sum_j w_{ij} \int_{M_0}^{M_u} \left(-\frac{d\lambda_i(M)}{dM}\right) \Pr(A > a \mid M, Rij)\, dM$$

Where M_0 and M_u are the smallest and largest magnitudes considered in the analysis, respectively, Pr (A>a|M,R_{ij})) is the probability that acceleration exceeds the value "a" at the site, when an earthquake of magnitude M at distance R_{ij} originates. R_{ij} is the distance between the site and the sub elements which the source has been divided. The weight w_{ij} has been assigned to each sub elements, and the above mentioned expression assumes that $\Sigma Sw_{ij}=1$. Finally, the contributions of all the sources (N) to earthquake hazard at the site are added:

$$V(a) = \sum_{i=1}^{N} v_i(a)$$

Seismicity models that could be used in this study

Earthquake occurrence model used for seismic sources is the Poisson model. In this case, the earthquake magnitude exceedance rate is given by:

$$\lambda(M) = \lambda_o \frac{\exp(-\beta M) - \exp(-\beta M_u)}{\exp(-\beta M_o) - \exp(-\beta M_u)} \qquad M_o \le M \le M_u$$

Where λ_0 is the exceedance rate of magnitude M_0, β is a parameter equivalent to the "b-value" for the source (except that it is given in terms of the natural logarithm) and M_u is the maximum magnitude for the source.

The probability density of the earthquake magnitude is given by:

$$p(M) = -\frac{d\lambda(M)}{dM} = \lambda_o \beta \frac{\exp(-\beta M)}{\exp(-\beta M_o) - \exp(-\beta M_u)} \qquad M_o \le M \le M_u$$

CRISIS can account for uncertainty in both β and M_u. In this case, the user must give the coefficient of variation and the standard deviation of β and M_u, respectively.

Probabilistic interpretation of attenuation relations

In general, for a given magnitude and distance, intensity A is assumed to be a random variable with lognormal distribution, with median Am(M,R) given by the attenuation table for the appropriate combination of magnitude and distance, and standard deviation of the natural logarithm (s).

The probability of exceeding a specified acceleration "a" is given by:

$$\Pr(A > a \mid M, R) = 1 - \Phi\left[\frac{1}{\sigma} \ln \frac{a}{Am(M,R)}\right] \qquad a \ge 0$$

that Φ is a cumulative normal distribution.

With CRISIS, it is possible to truncate the probability distribution to a limited number of standard deviations.

References

Ambraseys, N. N. and Free, M. W. (1997), Surface-wave magnitude calibration for European region earthquakes, Journal of Earthquake Engineering, 1(1), 1-22.

Anderson, J. G. (1979), Estimating the seismicity from geological structure for seismic-risk studies, Bulletin of the Seismological Society of America, 69, 827- 843.

Anderson, J. G. and Luco, J. E. (1983), Consequences of slip rate constraints on earthquake occurrence relations, Bulletin of the Seismological Society of America, 73, 471-496

Bazzurro, P., and Cornell, C.A. (1999), Disaggregation of Seismic Hazard. Bulletin of Seismological Society of America, 89(2), 501-520.

Bommer, J. J., Douglas, J., Scherbaum, F., Cotton, F., Bungum, H. and Fäh, D. (2010), On the selection of ground-motion prediction equations for seismic hazard analysis, Seismological Research Letters, 81(5), 783-793. DOI: 10.1785/gssrl.81.5.783

Cornell, C.A. (1968), Engineering seismic risk analysis, Bulletin of the Seismological Society of America, 58, 1583-1606.

Der Kiureghian, A., and Ang, A. H.-S. (1977), A fault-rupture model for seismic risk analysis. Bulletin of the Seismological Society of America, 67(4), 1173-1194.

Douglas, J. (2003), Earthquake ground motion estimation using strong-motion records: A review of equations for the estimation of peak ground acceleration and response spectral ordinates. Earth-Science Reviews, 61(1–2), 43–104.

Esteva, L. (1970), Seismic Risk and Seismic Design Decisions, Seismic Design of Nuclear Power Plants, in R.J. Hansen (Ed.), MIT Press, Cambridge

Gardner, J. K. and Knopoff, L. (1974), Is the sequence of earthquakes in Southern California, with aftershocks removed, Poissonian? Bulletin of the Seismological Society of America, 64, 1363-1367.

Gutenberg, B. and Richter, C.F. (1954), Seismicity of the Earth and Associated Phenomena, 2nd ed. (Princeton, N.J.: Princeton University Press).

Hancock, J., Watson-Lamprey, J., Abrahamson, N. A., Bommer, J. J., Markatis, A., McCoy, E. and Mendis, R. (2006), An improved method of matching response spectra of recorded earthquake ground motion using wavelets, Journal of Earthquake Engineering, 10(Special issue 1), 67-89.

Hanks, T. C. and Kanamori, H. (1979), Moment magnitude scale, Journal of Geophysical Research, 84 (B5), 2348–2350

Heaton, T.H., Tajima. F., and Mori, A.W., (1986), Estimating ground motions using recorded accelerograms, Surveys in Geophysics, V. 8, pp 25-83.

ICOLD (2010). Selecting seismic parameters for large dams: guidelines. Bulletin 148 (Bulletin 72, 2010 revision), International Commission on Large Dams.

Kanamori, H. (1977), The energy release in great earthquakes, Journal of Geophysical Research, 82(20), 2981–2876

McGuire, R. K. (1976), Fortran program for seismic risk analysis. U.S. Geological Survey Open-File Report 76–67,

McGuire, R. K. (1978), FRISK: computer program for seismic risk analysis using faults as earthquake sources. U.S. Geological Survey Open-File Report, 78–1007.

Mortgat, C. P. and Shah, H.C. (1979), A Bayesian model for seismic hazard mapping. Bulletin of the Seismological Society of America, 69, 1237-1251.

Mulargia, F., S. Tinti and E. Boschi (1985), A statistical analysis of flank eruptions on Etna volcano. J. Volcanol. Geotherm. Res. 23, pp. 263–272.

Mulargia, F., Gasperini, P. and Tinti, S. (1987), Contour mapping of Italian seismicity, Tectonophysics, 142, 203-216.

Ordaz, M., Aguilar A., and Arboleda J. (2003), Crisis 2003. Program for computing seismic Hazard, Ver. 3.01.

Reasenberg, P. (1985), Second-order moment of central California seismicity, 1969-82, Journal of Geophysical Research, 90, 5479-5495.

Wells, D.L and Coppersmith, K.J., (1994), New empirical relationships among Magnitude, Rupture Length, Rupture Width, Rupture Area, and Surface Displacement, Bulletin of the Seismological Society of America, 84(4), 974-1002.

Weichert, D. H. (1980), Estimation of the earthquake recurrence parameters from unequal observation periods for different magnitudes, Bulletin of the Seismological Society of America, 70, 1337-1346.

Youngs, R. R., and Coppersmith, K. (1985), Implications of fault slip rates and earthquake recurrence models to probabilistic seismic hazard estimates, Bulletin of the Seismological Society of America, 58, 939–964.